

Badger Engineers

Lunar Flagpole



EMA 469: Senior Design
Engineering Mechanics and Aerospace Engineering
Department of Mechanical Engineering
University of Wisconsin – Madison

Authors

Emmett Peters
Chase Orvis
Brian Jerominski
Kaden Reybrock
Olivia Janson

Supervisors

Sonny Nimityongskul
Travis Sheperd
Nino Miosi

December 12, 2023



Lunar Flagpole

Collapsed Configuration



Extended Configuration



Executive Summary

NASA's Artemis missions aim to return humans to lunar terrain, providing a significant opportunity to advance methodologies and designs utilized in the Apollo missions. One such opportunity lies in the deployment and design of a lunar flag that is to be planted on the Moon's surface. The contents of this report contain the details pertaining to the design of a lunar flagpole proposed by the Badger Engineers using NASA's Micro-G NExT Lunar Flag competition.

The Micro-G NExT Lunar Flag competition presents teams with the challenge of designing and developing a dependable, stable, and ergonomically friendly flag for deployment on the lunar surface. To achieve this, the flag must be able to withstand a force applied vertically upward and another applied horizontally from the top of the flagpole without yielding or buckling to a safety factor of at least 1.25. Additionally, the flag must remain under a weight limit of 10 lb and telescope out to a height of 8-10 ft while fitting within a compact volume of 48 inches (4 ft) in length, 12 inches in width, and 8 inches in height when in its stowed configuration. Assembly and deployment of the flag must be completed in no more than 10 minutes.

The approach taken to tackle this challenge began by splitting the flagpole design into 3 subsections: how the flag would telescope, how it would be anchored to the lunar surface, and how the flag would be mounted. Several possible designs for each subsection were created and decision matrices were created to evaluate the extent to which each design met the product design specifications and to determine the preliminary design that would act as the basis for the final design. It was determined that complexity should be added in the form of a ratchet driving mechanism to stand out amongst competitors, and preliminary models were created for each part in SOLIDWORKS. Analysis was conducted on each of the distinct components to determine the feasibility of the current design and to drive the corresponding dimensions of each respective part. The design was then modified and updated with acceptable dimensions, allowing the parts required to create a prototype of the final design to be determined and ordered. Parts were machined and assembled in the UW-Madison TEAM Lab and upon completion, the prototype was tested in a pseudo-lunar environment. Drawings of all parts and assemblies were made up to ANSI standards. Deployment instructions were created and observations of the project in its entirety were made while areas of potential improvement were identified.

The Badger Engineers have successfully designed a flagpole for lunar applications, adhering to the standards and specifications put forth by NASA's Micro-G NExT Lunar Flag competition. The prototype of the lunar flagpole telescopes to a height of 9 ft, stows within a 48 in x 8 in x 12 in space, can hold a 5 ft x 3 ft flag and weighs 9.928 lb. Additionally, the flagpole features a ratcheting mechanism that enables easier deployment by simplifying the process by which the auger is driven into the ground. Supports are also included to aid the auger in preventing failure due to the defined loads and it was determined through in-depth analyses that the final design auger and support poles will prevent pull-out failure. Furthermore, the entire design was analyzed and found to prevent buckling and yielding to a factor of safety of 1.25.

Members of the Artemis missions can be confident that the presented lunar flag design fully adheres to their specifications, is designed to be easily deployed by a fully suited astronaut and is an innovative solution to their challenge that matches or exceeds the desired level of dependability, stability, and ergonomic ability.



1	Introduction	6
1.1	Problem Statement	6
2	Product Design Specifications	7
2.1	Review of Competition	7
2.2	Foldable Portable Flagpole Patent	9
2.3	Standards	10
2.4	Performance	11
2.5	Size and Weight	11
2.6	Environment	12
2.7	Maintenance	12
2.8	Materials	12
2.9	Product Life Span	12
2.10	Ergonomics and Human Factors	13
2.11	Testing	13
2.12	Other Impacts	13
2.12.1	Safety, Public Health, and Human Welfare	13
2.12.2	Economic, Cultural, Social Factors	14
2.12.3	Environmental Impact	14
2.13	Critical Design Specifications	14
3	Concept Design	15
3.1	Preliminary Concepts	15
3.1.1	Telescoping System	15
3.1.2	Anchoring System	18
3.1.3	Flag Mount	21
3.2	Final Concept Selection	22
4	Analysis of Assembly	26
4.1	Pole Analysis	26
4.2	Supports Analysis	36
4.3	Collar Analysis	45
4.4	Auger Assembly Analysis	50
4.4.1	Auger Analysis	50
4.4.2	Auger Fastener Torque Analysis	57
4.5	Ratchet and Pawl Analysis	58
4.6	Spring Selection	64
5	Prototype	65
5.1	Prototype Design	65
5.1.1	Top Pole Assembly	65
5.1.2	Middle Pole Assembly	67
5.1.3	Bottom Pole Assembly	67



5.1.4	Lunar Flagpole Full Assembly	70
5.2	Manufacturing	71
5.2.1	Part Simplifications	71
5.2.2	Part Manufacturing Methods	73
5.2.3	Assembly Simplifications	74
5.3	Results and Observations	75
5.3.1	Prototype Results	75
5.3.2	Observations and Refinements	79
5.4	Operation Procedure	80
6	Conclusion	83
7	References	86
8	Appendix A – Product Design Specifications	89
9	Appendix B – Pole Analysis	92
10	Appendix C – Support Pole, Support Pin, and Collar Analysis	97
11	Appendix D – Auger Analysis	100



1 Introduction

Over the last decade, space exploration has seen a growth in public interest paired with an increase in privatized companies specializing in this sector of the workforce. The Space Report 2022 is an authoritative report on space published by the nonprofit advocate, Space Foundation. The report highlights increased interest in space, stating “the space economy grew 9% since 2020” and notes a “6.4% growth the commercial space sector” [1]. This led to the creation of the Artemis missions: NASA’s plan to put humans back on the moon for the first time since December 19, 1972 [2]. As stated by NASA on their official Artemis website, “With Artemis missions, NASA will land the first woman and first person of color on the Moon, using innovative technologies to explore more of the lunar surface than ever before. We will collaborate with commercial and international partners and establish the first long-term presence on the Moon. Then, we will use what we learn on and around the Moon to take the next giant leap: sending the first astronauts to Mars” [3]. This mission presents a great expanse of opportunities for innovation, with one such opportunity lying in the flag to be planted by the astronauts that victoriously land on the lunar surface.

Flags can represent freedom or control, danger, or safety. They are best known as national symbols — and are used to air a country's past, present, and future vision all rolled into one. Planting and flying a flag signifies the completion of a task, symbolizing the pride, strength, sacrifice, and resilience it took to achieve the task. NASA has presented this opportunity to undergraduate students through their Micro-G NExT Lunar Flag competition to be a part of the innovation brought about by the Artemis mission. This competition tasks teams with designing a lunar flag, flagpole, and anchoring system that can be deployed on the lunar surface [4].

1.1 Problem Statement

NASA is returning to the moon for the Artemis missions. The goal is to design and develop a dependable, stable, and ergonomically friendly flag for deployment on the lunar surface during the Artemis III missions. The current challenge lies in improving upon the design of flags deployed during the Apollo missions, which were effective but lacked certain key attributes. Specifically, the issues include the flag's height, stability, collapsibility, ease of deployment, and overall ergonomics, all while ensuring it remains visually striking and symbolic. A superior design is crucial to enhance the Artemis missions; moreover, it represents a unique opportunity to advance lunar flag technology and further the goals of human exploration beyond Earth [4].



2 Product Design Specifications

The product design specifications section reviews competing designs and clearly defines what the product must include. A review of the competition is included first. Then, the standards that are useful for this project are included. Next, the list of specifications in the following categories: performance, size and weight, environment, maintenance, materials, life span, ergonomics and human factors, testing, and other impacts. To conclude the section, a list of critical design specifications defines the most important specifications for the final product.

2.1 Review of Competition

The primary customer for this project is NASA, with a specific focus on creating a working prototype that can serve as a model for potential replication in other lunar missions. This is the first iteration of NASA's lunar flagpole competition, coming at a time when the organization is planning a new mission, Artemis, that will take astronauts back to the moon. While mass production capabilities may not be required, the paramount goal is to ensure that the flag always remains visible during the mission. This emphasis on visibility underscores the importance of the flag as a symbol of the mission's success and its representation of NASA's achievements in lunar exploration.

The historical context of competing, existing, and past designs for lunar flags provides valuable insights into the challenges and successes of lunar missions. The first flag on the moon was from the United States NASA Apollo missions. During the Apollo missions, the flag assembly had to be deployed within a 10-minute timeframe, withstand forces on the moon's surface, and endure engine blasts during takeoff [5]. The design, shown in **Figure 2.1.1**, consisted of gold-anodized aluminum poles that telescoped out during assembly and a hardened steel point similar to a garden stake [6]. A hemmed pocket was sewn into the top of a standard 3 ft by 5 flag and a horizontal pole was ran through it to mount it to the pole. The entire assembly was mounted on the Lunar Module ladder in a heat protected capsule during travel, where it was exposed to extreme temperatures from the harsh space environment [7]. The telescoping poles presented difficulties for the crews, and the lower portion of the flagpole could only be driven 6 to 9 inches into the lunar ground [5]. Despite the challenges, most of the Apollo flags remained standing years later, albeit bleached white by the sun [8].



Figure 2.1.1: US lunar flagpole assembly [7].

China recently brought a flag to the moon as well but took a different approach. Their flag was deployed from the lander's body rather than planting it in the lunar soil, shown in **Figure 2.1.2**. The specifications of the moon, including its temperature, gravity, and surface pressure, were important considerations for both the US and China. The flag measured approximately 6.5 ft wide and 3 ft tall and weighed about 2.2 lb. The fabric that China used for the flag was designed to maintain color within a wide temperature range and is expected to last on the moon for a substantial amount of time [9].

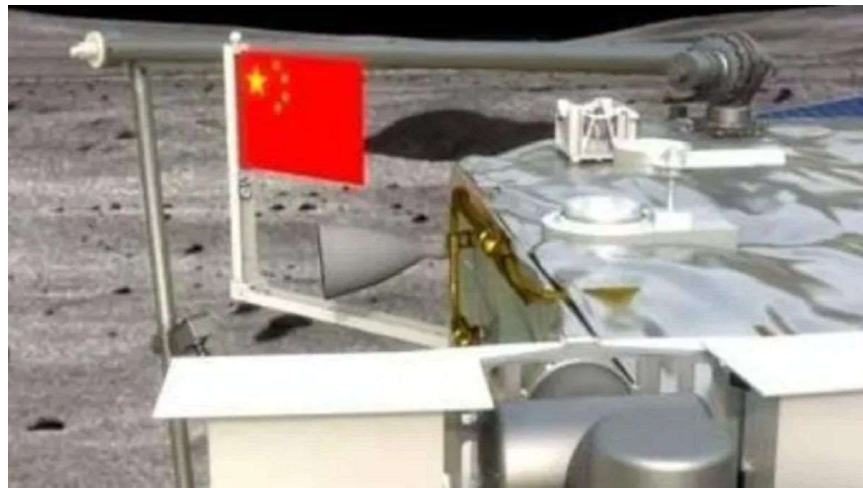


Figure 2.1.2: China's lunar flag deployed from the lander's body [9].

Importantly, the flags planted on the moon served as symbolic gestures of national pride, and there were no formal complaints from other nations regarding this practice. These historical insights provide valuable context for the design and objectives of the current project, emphasizing the importance of meeting NASA specifications, ensuring flag visibility, and considering the long-term presence of the flag on the lunar surface [5].

2.2 Foldable Portable Flagpole Patent

Sichuan Technology and Business University boasts a patent for a foldable portable flagpole shown in **Figure 2.2.1**. This design consists of two primary components: a telescoping shaft and collapsible base. The shaft is comprised of two poles, noted on the figure as callouts 2 and 3, which upon extending the smaller upper shaft from the larger lower shaft engages a locking spring and ball mechanism. The second component, the base, uses an extending Y configuration where the two outward angled segments fold onto each other, aligning in parallel, and retracting into the larger foundational support segment noted on the figure by callout 4. The resulting collapsed segment then pivots upwards, aligning itself alongside the folded base pole [10].

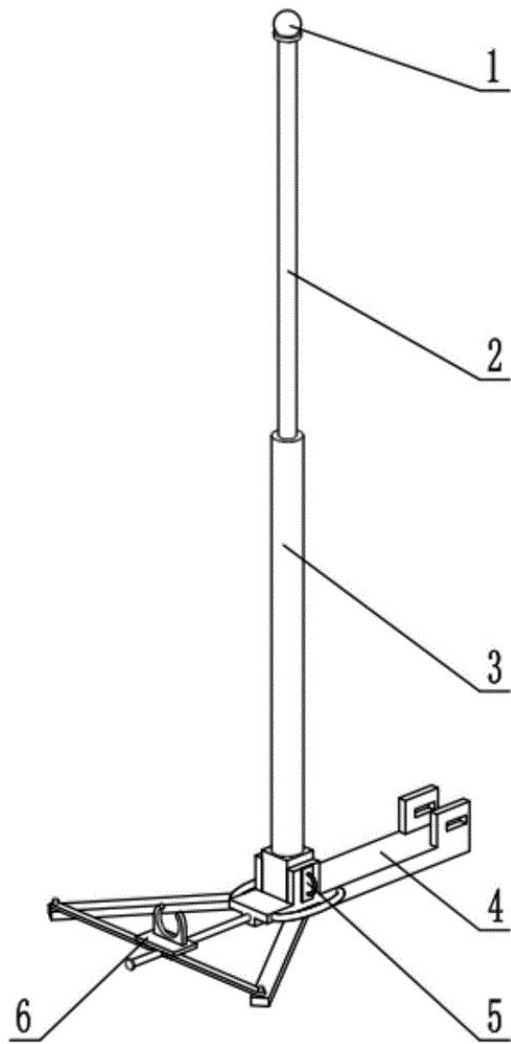


Figure 2.2.1: Sichuan Technology and Business University portable flagpole patent design [10].

2.3 Standards

As the flagpole is part of an official NASA competition, most of the technical specifications have been given within the problem statement. In addition to these specifications, the project will conform with relevant general NASA standards as given below.

- NASA-STD-6001 -> Flammability, Offgassing, and Compatibility requirements and test procedures [3]
This standard provides basic information on test procedures done by NASA that the design may have to comply to.
- NASA-STD-1008 -> Testing against dust [3]
This standard provides information on dust tolerance requirements and what tests the design may have to pass.
- NASA-STD-5006 -> General welding requirements for aerospace materials [3]
This standard provides information on welding requirements for aerospace parts. This will be important to consider as welding will be a part of the design process.
- NASA-STD-5017 -> Design and development requirements for mechanisms [3]
This standard provides the requirements for ordnance-actuated mechanical devices, quick-release pins, threaded interfaces designed to be actuated in service, and interfaces designed to release mechanical degrees of freedom that are subject to failure modes typical of mechanisms.
- NASA-HDBK-7009 -> NASA handbook for models and simulations [3]
This document provides technical processes, techniques, and examples for good modeling and simulation practices in NASA.
- NASA-STD-7001 -> Payload vibroacoustic test criteria [3]
This standard provides information on the acoustic and random vibration environments and test levels for the vibroacoustics that manifest throughout the payload.
- NASA-STD-7002 -> Payload test criteria [3]
This standard includes parameters for demonstration tests necessary to validate the capability of hardware to perform its intended function.
- NASA-STD-7009 -> Standard for models and simulations [3]
This standard, like NASA-HDBK-7009, establishes uniform practices in modeling and simulation to ensure essential requirements are applied to design, development, and use.
- AIAA S-110-2005 -> Standard for the design, analysis, material selection and characterization, fabrication, test, and inspection of structural items in space systems [11]
- NBL Materials List -> Approved list of materials and coatings [12]
The design must comply with an approved materials list given from NASA NBL.



2.4 Performance

The performance requirements for the flagpole assembly include the ability to withstand a 10 lb axial force while preventing yielding or buckling. Additionally, it should withstand a 10 lb horizontal force applied at the top of the flagpole tip without yielding or buckling. **Figure 2.4.1** shows the application of the loads in an FBD. To ensure structural integrity, material properties such as stress/strain, buckling resistance, impact resistance, and resistance to vibrations need to be considered. The project guidelines specify a safety factor of 1.25, which is common in aerospace engineering applications [4].

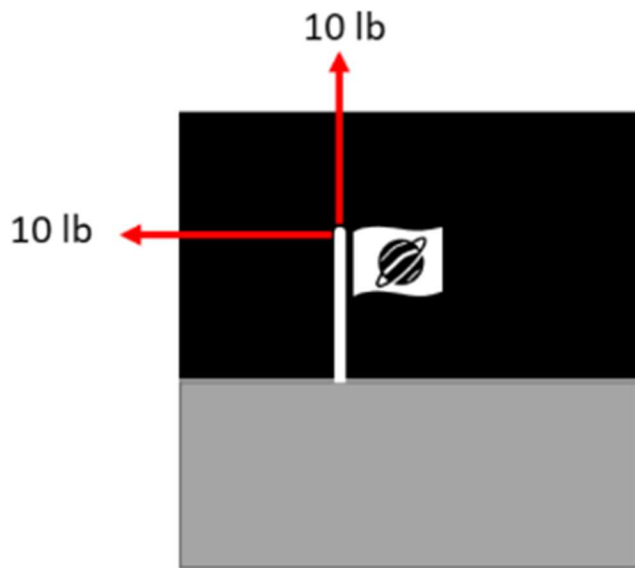


Figure 2.4.1: FBD of loads the flagpole must withstand [4].

Regardless of the mechanism used, whether it is a linear actuating mechanism (with a force requirement of ≤ 20 lb.) or a rotational mechanism (with a torque requirement of ≤ 30 in-lb.), the flagpole must transition from a stowed to an assembled position within a 10-minute timeframe, with deployment occurring only once. A tether loop would be incorporated at the top of the flagpole upon testing, and the flag must remain unfurled in the absence of wind, ensuring its continuous visibility and functionality. These design parameters collectively define the specifications and expectations for the flagpole assembly [4].

2.5 Size and Weight

The collapsed assembly is required to fit within a compact volume of 48 inches (4 ft) in length, 12 inches in width, and 8 inches in height, ensuring ease of storage and transport. When fully deployed, the flagpole should measure between 96 and 120 inches (8-10 ft) in height, providing flexibility in its final positioning while accommodating various display requirements. The flag itself should have dimensions of 3 ft by 5 ft and should not exceed a maximum weight of 10 lb (on Earth), ensuring manageability during setup and maintenance. These specifications define the size, weight, and dimensional constraints of the flagpole assembly, allowing for practical use and storage while meeting the desired display and functionality criteria [4].



2.6 Environment

The flagpole assembly must be designed to endure extreme temperature variations experienced on the moon, ranging from -298°F during the lunar night to 260°F in direct sunlight. Moreover, it should exhibit resistance to moon dust erosion, a critical consideration for long-term functionality. To address these challenges, the assembly should incorporate dust-tolerant features and materials to mitigate the effects of lunar dust. The flagpole assembly should withstand a combined rocket induced vibration and ignition overpressure range of 5 to 200 hertz applied by base excitation [13].

In addition to thermal concerns, the flagpole should be tested to perform reliably in conditions such as an 86°F testing pool with a depth of 40 ft, ensuring its resilience in aquatic environments. Furthermore, the assembly must withstand radiation exposure from space and the sun while also meeting sterilization requirements for spacecraft to prevent contamination of celestial bodies. Finally, offgassing in space must be minimized to maintain the integrity of the spacecraft and its components. These factors underscore the need for a robust and adaptable design for the flagpole assembly, capable of enduring the unique challenges of lunar missions [4].

2.7 Maintenance

The flagpole assembly is required to remain in a vertical position for extended periods, ensuring that the flag's display remains upright and visible throughout its mission duration. It is important to note that the deployment of the flagpole should be a one-time event, emphasizing the need for durability and reliability in maintaining its vertical orientation over time. These specifications emphasize the importance of designing a flagpole assembly that can provide a consistent and stable display without the need for frequent adjustments or interventions, contributing to the overall success of the mission.

2.8 Materials

The flagpole assembly must be constructed using materials that are listed in the approved material list from the Neutral Buoyancy Laboratory (NBL) [12]. Additionally, it should be compatible for underwater use during testing, reflecting the need for its functionality and integrity to be maintained even in aquatic environments. It is important to note that the use of regular PLA (Polylactic Acid) is not permitted, but tough PLA, as specified by NASA, is an acceptable material choice for the construction of the flagpole assembly. These requirements ensure that the materials used in the assembly adhere to safety and performance standards while accommodating the unique testing conditions associated with underwater evaluations [4].

2.9 Product Life Span

The primary objective is to maximize the longevity of the flag's display, aiming for an extended period of visibility. To assess and predict the flag and pole's durability, thorough fatigue analyses will be conducted. The parameters of the fatigue analysis will be determined later in the timeline of this project. These analyses will provide critical insights into the assembly's structural integrity over time, allowing for the determination of how long the flag and pole can effectively withstand the stresses and environmental factors they encounter during their mission. The results of these fatigue analyses will be instrumental in optimizing the design and materials used, ensuring that the flagpole assembly can remain operational and maintain its display for the desired duration.



2.10 Ergonomics and Human Factors

The flagpole assembly must be designed to be Extravehicular Activity (EVA) compatible, allowing astronauts to interact with it while wearing EVA gloves. There should be no sharp edges on any of its parts, minimizing the risk of injury during handling and operation. Manual power alone should be sufficient for deploying the flagpole, eliminating the need for additional mechanical assistance or power sources. Additionally, the design must exclude any holes or openings that could potentially lead to the entrapment of fingers, aligning with safety standards to prevent accidents or hazards during use. These specifications emphasize the importance of user-friendly, safe, and astronaut-accessible features for the flagpole assembly in a space mission context [4]. Another factor to consider is EVA glove traction on the pole. This will be considered when designing and testing the flagpole design.

2.11 Testing

The flagpole assembly will undergo testing in a controlled environment, situated at the bottom of a 40-ft-deep Neutral Buoyancy Laboratory (NBL) pool with a temperature maintained at 86°F. During these tests, the assembly will be immersed in a barrel of sand measuring 3 ft inches in diameter and 3 ft in depth, simulating lunar surface conditions. The loads that the flagpole is required to withstand will be applied. These include a 10 lb axial pole force and a 10 lb horizontal force applied at the top of the flagpole tip. It is worth noting that, if necessary, an EVA hammer can be employed for deployment, offering an additional option for ensuring the flagpole's proper installation and stability in the test environment. These testing parameters replicate the conditions the flagpole may experience during lunar missions, allowing for rigorous assessments of its functionality and durability [4].

2.12 Other Impacts

In the Other Impacts section, impacts that go beyond design specifications will be addressed. These include safety, public health, human welfare, economic, cultural, social factors, and environmental impact.

2.12.1 Safety, Public Health, and Human Welfare

The design of the flagpole assembly must prioritize astronaut safety by eliminating sharp edges or pieces that could potentially puncture an astronaut's spacesuit. For this to happen, the sharp edge that will drive into the ground could be detachable and removed prior to deployment. Edges can also be filed if needed to keep the astronauts safe while maintaining function. Additionally, the assembly should not feature any holes or openings that may lead to the entrapment of fingers, ensuring that it is safe and user-friendly for astronauts during deployment and handling. Furthermore, sterilization of the materials used is essential to prevent any organic matter from Earth from contacting the lunar surface, adhering to planetary protection protocols, and minimizing contamination risks during lunar missions. These design considerations collectively emphasize the importance of safety, hygiene, and adherence to space exploration protocols for the flagpole assembly [4].



2.12.2 Economic, Cultural, Social Factors

The storage and presentation of the flag must adhere to the United States Flag Code, ensuring proper handling and respect for the national flag [14]. During deployment and after being deployed, the flag must not contact the ground, maintaining its dignity and significance. It is crucial to recognize that the flag, along with its appearance, serves as a direct representation of NASA and the United States on a broader scale. Consequently, the success of this mission bears significant implications for NASA and the broader field of space exploration, underscoring the importance of meticulous planning, execution, and the utmost respect for the flag to uphold the nation's image and the agency's reputation in the realm of space exploration.

2.12.3 Environmental Impact

The flagpole assembly should be engineered to withstand the harsh lunar environment without experiencing degradation. It must also possess the capability to be sterilized and resist exposure to harsh chemicals, ensuring its integrity and functionality throughout the mission duration. The materials used should not contaminate the environment. This includes ensuring that plastics or paints do not break down or chip off.

Additionally, it is imperative to consider the environmental impact associated with the acquisition of raw materials used to create the flagpole. Sustainable and responsible sourcing of materials should be a priority, aligning with environmentally conscious practices to minimize any adverse ecological effects related to the project's material choices. These considerations underscore the importance of both durability and environmental responsibility in the design and execution of the flagpole assembly for lunar missions.

2.13 Critical Design Specifications

The most important specifications and must haves for the final product:

- Withstand 10 lb axial pole force.
- Withstand 10 lb horizontal force from flagpole tip.
- Flag assembly shall be collapsible into an EVA-compatible stowed configuration that fits within a volume of 48 x 12 x 8 inches.
- Goes from stowed to assembled in 10 minutes.
- The flagpole must be between 96 and 120 inches in height when fully deployed.
- Mass of the full flag assembly shall not exceed 10 lb in 1G Earth gravity.



3 Concept Design

During the initial conceptualization phase of the project, ideas were systematically categorized into three distinct components: the telescoping system, anchoring system, and flag mount. In the process of selecting the optimal design for each component, multiple design options were generated for every section. These designs were evaluated based on criteria such as ease of use, simplicity, weight, dust tolerance, durability, and collapsibility. Notably, dust tolerance was deemed irrelevant for the anchoring system and flag mount, and therefore, it was omitted as a metric for the evaluation of these two components. This structured approach allowed for a methodical assessment and selection of the most suitable designs for each facet of the lunar flagpole project.

3.1 Preliminary Concepts

This section covers the preliminary concepts for each component of the flagpole design.

3.1.1 Telescoping System

In the initial phase of design considerations, the focus was on the deployment system to transition the flagpole from its stowed configuration. The first design involved a straightforward screw mechanism, featuring a nested arrangement of poles that could be extended and then interlocked by screwing them together at their ends. The simplicity of this approach enables astronauts to manually execute the deployment by twisting the poles together with their hands. A hand drawing of this design is shown in **Figure 3.1.1**.

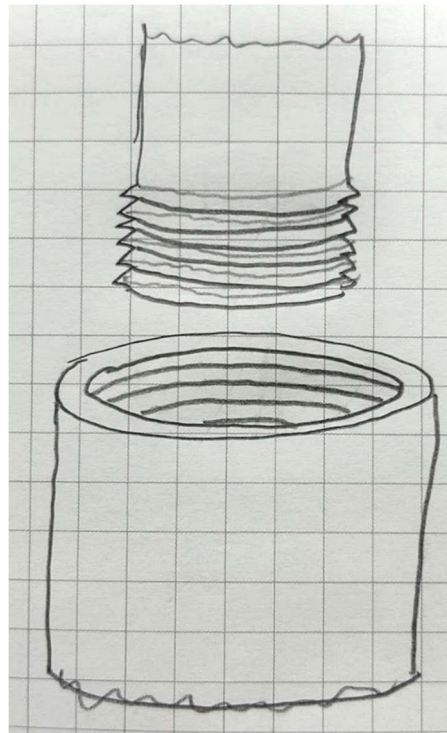


Figure 3.1.1: Preliminary design sketch of screw telescoping system.

The second conceptual approach involved a j-hook design. In this configuration, each flagpole's top section would feature a press-fit collar with a drilled j-slot. The nested pole would have a corresponding tab at its end, fitting securely into the j-slot. Compared to the screw design, the j-hook concept offers a simpler actuation process, requiring less precision from astronauts during deployment. This design enhancement aims to streamline the deployment procedure and enhance the overall ease of use. A hand drawing of this design is shown in **Figure 3.1.2**.

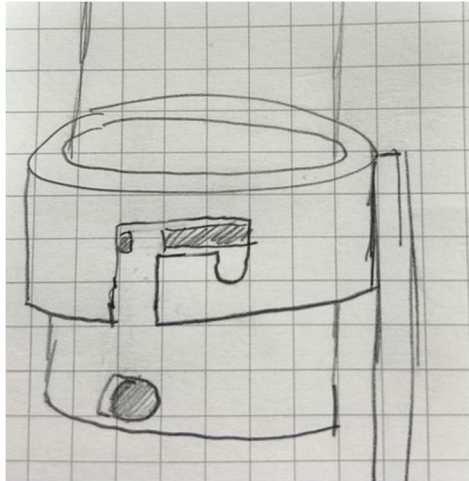


Figure 3.1.2: Preliminary design sketch of j-hook telescoping system.

The third conceptualization introduces a gear and rack design. In this setup, a gear is positioned inside the largest pole, while racks are affixed to each of the telescoping poles. Astronauts would utilize an external crank attached to the flagpole to rotate the gear, facilitating the extension of the poles into an upright position. It's important to note that this design necessitates carrying a crank to the mission site for flag deployment. The gear and rack mechanism offers a mechanical advantage, providing an alternative approach to the deployment process with considerations for ease of use and practicality in the mission context. A hand drawing of this design is shown in **Figure 3.1.3**.



Figure 3.1.3: Preliminary design sketch of the gear and rack telescoping system.

The fourth concept shown in **Figure 3.1.4** uses friction to keep the poles together once deployed. In this configuration, the nested poles are subtly tapered, creating interference between the top of one pole and the bottom of the next when fully deployed. To execute this design, two astronauts would be required to pull on both ends simultaneously, ensuring the complete deployment of the pole. The reliance on friction offers a unique mechanism for securing the poles in their extended state, presenting a distinctive approach to the flagpole's deployment.

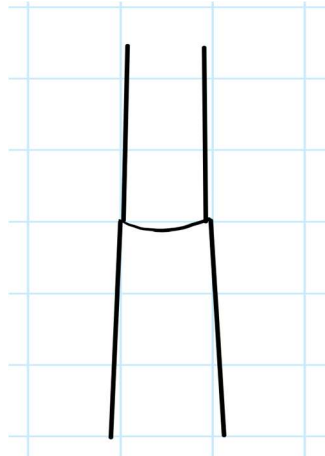


Figure 3.1.4: Preliminary sketch of friction design for telescoping poles.

The last concept, depicted in **Figure 3.1.5**, introduces the push-button design. In this configuration, holes are drilled into the tops of each nested pole, accompanied by matching spring-loaded pins on the inside of the next pole. During deployment, these pins would spring into the corresponding holes drilled in the larger pole, effectively locking the poles into place. Notably, this design eliminates the need for additional effort from astronauts, as the pins are preloaded in the stowed configuration. The push-button mechanism offers a straightforward and efficient means of securing the extended flagpole in place.

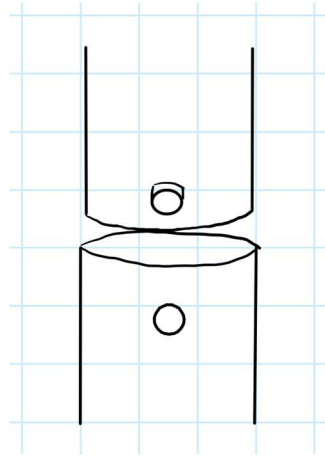


Figure 3.1.5: Preliminary sketch of push button telescoping system.

3.1.2 Anchoring System

Moving on to the anchoring system, the initial concept involved a screw or auger design, as illustrated in **Figure 3.1.6**. This design incorporates a conical spike with spiral ribs attached to the bottom of the pole. Once the auger is secured to the pole, it can be twisted into the moon's soil. The rationale behind opting for an auger rather than a simple spike lies in the consistent nature of the moon soil. Conventional spikes face challenges penetrating the moon soil effectively without additional assistance, making the auger design a more practical choice for secure anchoring.

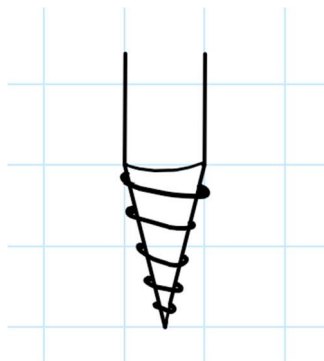


Figure 3.1.6: Preliminary sketch for auger anchoring system.

The second design under consideration involves a straightforward spike attached to the bottom of the flagpole. This design facilitates the pole being driven directly into the ground upon reaching the mission site. Following the competition rules, astronauts are permitted to utilize an EVA hammer to assist in the process of driving the flagpole into the lunar soil. This design echoes the methodology employed for anchoring the flag during the Apollo missions, drawing on a proven approach for securing the flagpole in place [6].

The third design expands upon the second by introducing pillar supports, as depicted in **Figure 3.1.7**, in conjunction with the spike. These supports would be hinged on the main body of the flagpole. Before driving the main spike into the ground, astronauts would retract the supports from the main body and then hammer both the supports and the main spike into the lunar soil simultaneously. This innovative approach offers a dynamic anchoring solution, providing additional stability during deployment. Furthermore, these supports can be effectively utilized in combination with other anchoring designs for enhanced versatility.

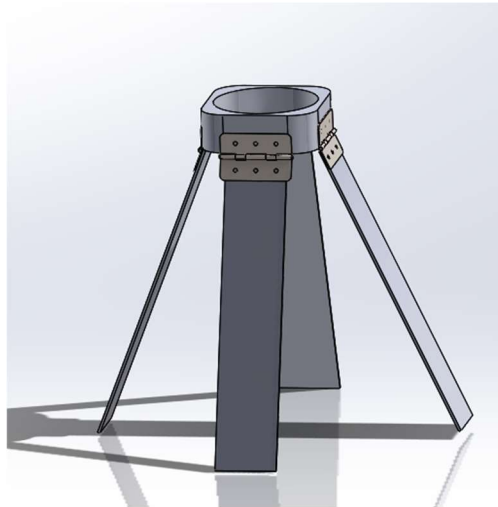


Figure 3.1.7: Preliminary model of support bars for anchor design.

Similar to the third design, the fourth concept, illustrated in **Figure 3.1.8**, enhances the spike by incorporating a stabilizing disk. Positioned flat on the ground, this disk addresses the spike's limitation in supporting high lateral forces on the tip of the flagpole once deployed. Notably, unlike the third design, astronauts would not need to deploy any additional components before driving the flagpole into the lunar soil, as the stabilizing disk would be pre-installed, streamlining the anchoring process. This modification aims to bolster the stability and lateral support of the flagpole once it is in position.

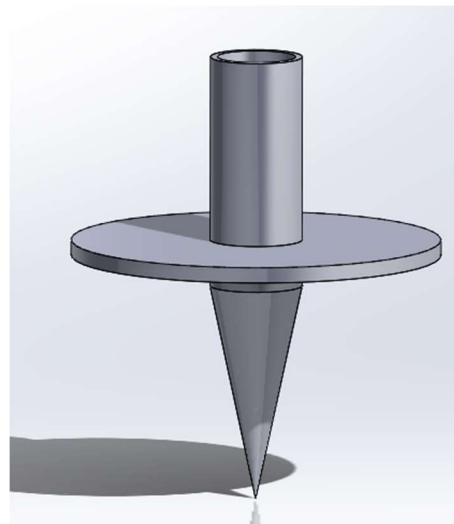


Figure 3.1.8: Spike and disk combination for anchor design.

The final concept in consideration for the anchoring system introduces guy wires, as depicted in **Figure 3.1.9**. These wires would be affixed to the main body of the flagpole. Operating akin to tent stakes, astronauts could pull each wire taut and then hammer it into the lunar soil to stabilize the flagpole. It's crucial to note that if this concept is chosen, it would need to be integrated with another anchoring design for the main body of the flagpole. Guy wires, while effective in stabilizing and keeping the flagpole upright, cannot independently provide sufficient anchoring to the lunar soil. Their role is complementary, enhancing stability rather than anchoring the flagpole itself.

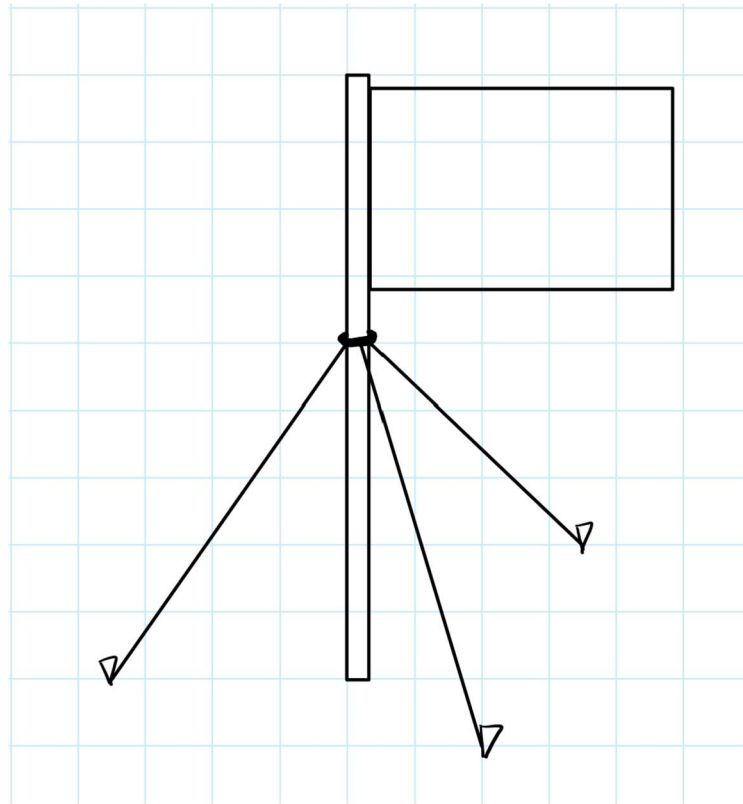


Figure 3.1.9: Preliminary drawing for guy wire design for anchoring system.

3.1.3 Flag Mount

The last system under consideration for the design focuses on mounting the flag to the pole. The initial concept involves a straightforward wire, as depicted in **Figure 3.1.10**, affixed to the top of the pole and running the length of the flag to maintain its upright position in the absence of lunar wind. This wire is designed to be spooled up when the flagpole is in its stowed configuration and can be straightened when astronauts are deploying the flag. The flag itself would feature a hemmed pocket along the top edge, allowing it to slide onto this wire for secure attachment. This uncomplicated yet effective design aims to ensure the flag's stability and proper display on the lunar surface.

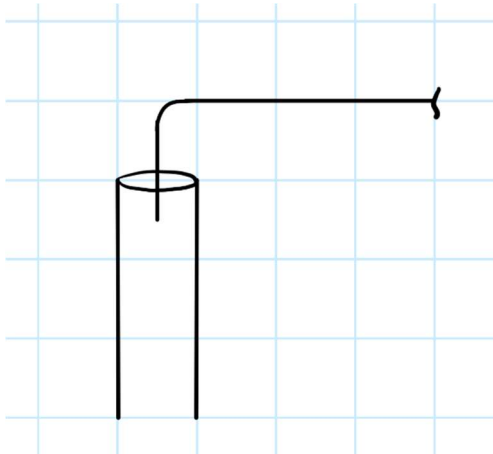


Figure 3.1.10: Preliminary sketch of wire flag mount design.

An alternative concept for supporting the flag on the pole involves hinge bracket. This would consist of a long piece of circular rod that hinges up into a defined space and is then locked in with a friction lid. This design offers a versatile and easily deployable solution for flag mounting, enhancing the efficiency of the overall system. A hand drawing of this design is shown in **Figure 3.1.11**.

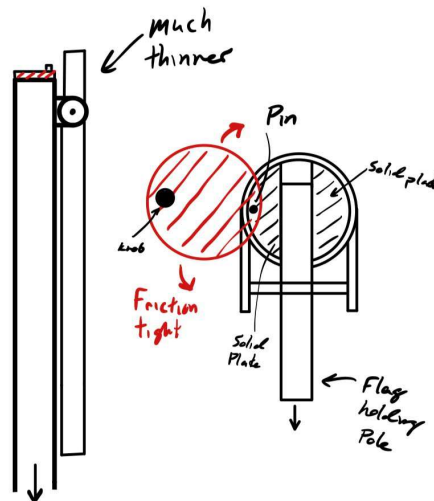


Figure 3.1.11: Preliminary sketch of bracket flag mount design.

3.2 Final Concept Selection

In the comparison of parameters detailed in **Section 3**, evaluation matrixes were created, incorporating weighted metrics. The highest weights were assigned to ease of use, durability, and collapsibility, deeming them the most critical aspects. Under ease of use, considerations included how easily the component could be used or assembled by astronauts. Durability focused on the component's resilience to applied loads and its overall lifespan. Collapsibility assessed the practicality of fitting the design within volume constraints. Each conceptual design received a score of 1, 3, or 5, with 1 denoting the least favorable and 5 indicating the most favorable performance. The total score for each design was computed by summing the scores, each multiplied by its respective weight. This systematic approach facilitated a comprehensive evaluation of each concept based on these key criteria. A decision matrix for each component was made and presented in the following tables. First, **Table 3.2.1** evaluates the telescoping system preliminary designs. Second, **Table 3.2.2** evaluates the anchoring system. Last, **Table 3.2.3** evaluates the flag mount system.

Table 3.2.1 Telescoping System Decision Matrix

Design Parameters	Parameter Weight	Telescoping System				
		Screw	J - Hook	Gear + Rack	Friction	Push Buttons
Ease of use	4	3	5	3	1	3
Simplicity	2	5	3	1	5	3
Weight	3	3	3	1	5	5
Dust Tolerance	2	5	5	3	1	3
Durability	5	5	1	1	3	5
Collapsibility	4	5	5	3	5	5
Totals		86	70	40	66	84

Upon thorough evaluation of the five designs in **Table 3.2.1**, the Gear + Rack concept lags behind primarily due to its complexity, leading to an associated increase in weight. Conversely, the screw and push-button concepts emerged as the top performers. After careful consideration between these two, the screw concept was chosen for its simpler implementation, without compromising its capacity to withstand the prescribed loads in the challenge. However, it's important to note that the screw design poses a challenge in terms of the dexterity required to grip both poles and screw them together. This challenge will necessitate further consideration and refinement before the completion of the prototype.



Table 3.2.2 Anchoring System Decision Matrix

Design Parameters	Parameter Weight	Anchoring System				
		Screw/Auger	Spike/Spikes	Spike + Supports	Disk + Spike	Guy wires
Ease of use	4	3	5	5	5	1
Simplicity	2	3	5	3	5	5
Weight	3	3	5	3	1	5
Durability	5	5	1	3	1	3
Collapsibility	4	5	5	5	3	3
Totals		72	70	70	50	56

Following the assessment of the five anchoring systems in **Table 3.2.2**, the auger, spike, and spike with supports all received similar grades. The choice of the auger design was influenced by its improved resistance to the vertical load of 10 lb. Acknowledging the potential need for additional support to prevent failure from the test force creating a bending moment, supports will be incorporated from the spike + supports design. This hybrid approach aims to integrate the auger idea with the supports, offering extra reinforcement against the horizontal 10 lb force at the top of the flagpole. In summary, the final anchoring system will amalgamate the strengths of both designs for optimal performance.

Table 3.2.3 Flag Mounting System Decision Matrix

Design Parameters	Parameter Weight	Flag Mount	
		Wire	Brackets
Ease of use	4	3	3
Mechanical Complexity	2	5	3
Weight	3	5	3
Load Resistance	5	3	5
Collapsibility	4	5	3
Totals		72	64

After evaluating both designs for the flag mount in **Table 3.2.3**, bracket design will be chosen, despite it receiving a lower score. The wire design, while very simple and still functional, is prone to bending over time. The bracket design aligns with the preference for longevity and risk reduction. The design's sturdiness and simplicity make it a better fit for ensuring the durability and reliability of the flag mounting system in diverse conditions.



The chosen design, illustrated in **Figure 3.2.1** and based on the evaluation matrices, integrates key features to facilitate efficient flag deployment. Callout 1 shows the bracket with a hinged attachment, while callouts 2, 3, and 4 highlight the telescoping poles that fit snugly within each other, incorporating screw locking mechanisms for secure alignment. The bottom pole, depicted in callout 4, connects to the auger, marked by callout 5. To fortify the auger against potential failure resulting from the test load creating a moment, additional support bars are introduced, as indicated in callout 6. This comprehensive design ensures stability, ease of use, and resilience under applied loads, ensuring the successful deployment of the flag.

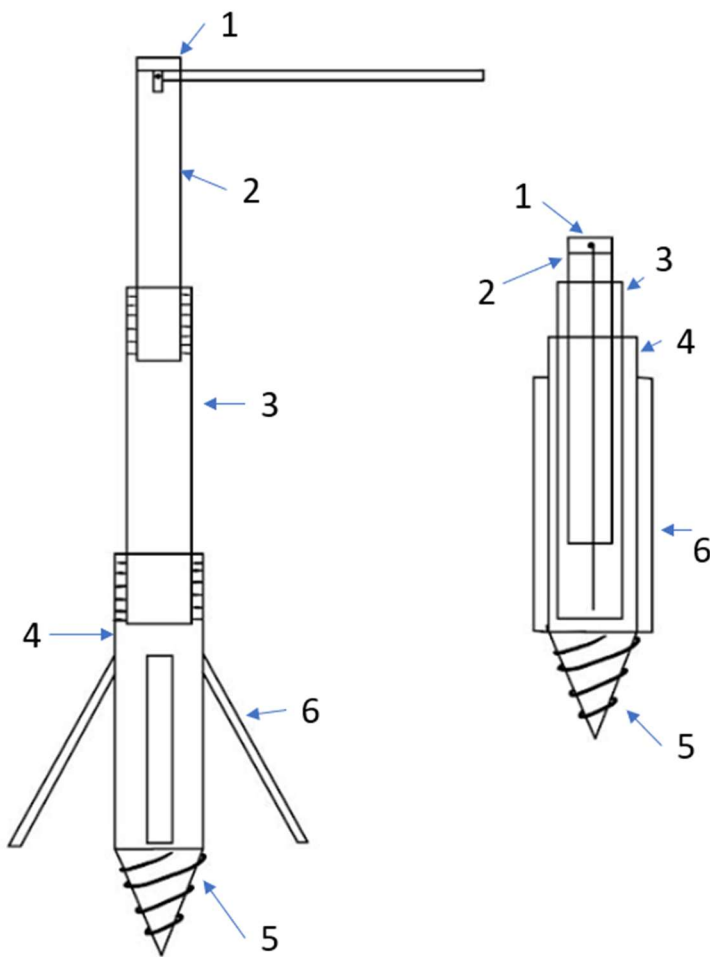


Figure 3.2.1: Sketch of the chosen preliminary concepts in assembled form and collapsed form.

The lower section with the desired construction methods is depicted in the preliminary CAD, made in SOLIDWORKS, shown in **Figure 3.2.2**. A gear-ratchet system wrapping around the exterior of the outer bottom shaft has been incorporated to assist in driving the auger into the ground. Four supports are attached to the ratchet system, serving a dual purpose as handles during deployment. This addition is designed to enhance the ease of use for astronauts, considering the limited mobility of a space suit. The gear-ratchet system and strategically positioned supports contribute to the overall efficiency and user-friendliness of the anchoring system in the challenging conditions of space exploration.

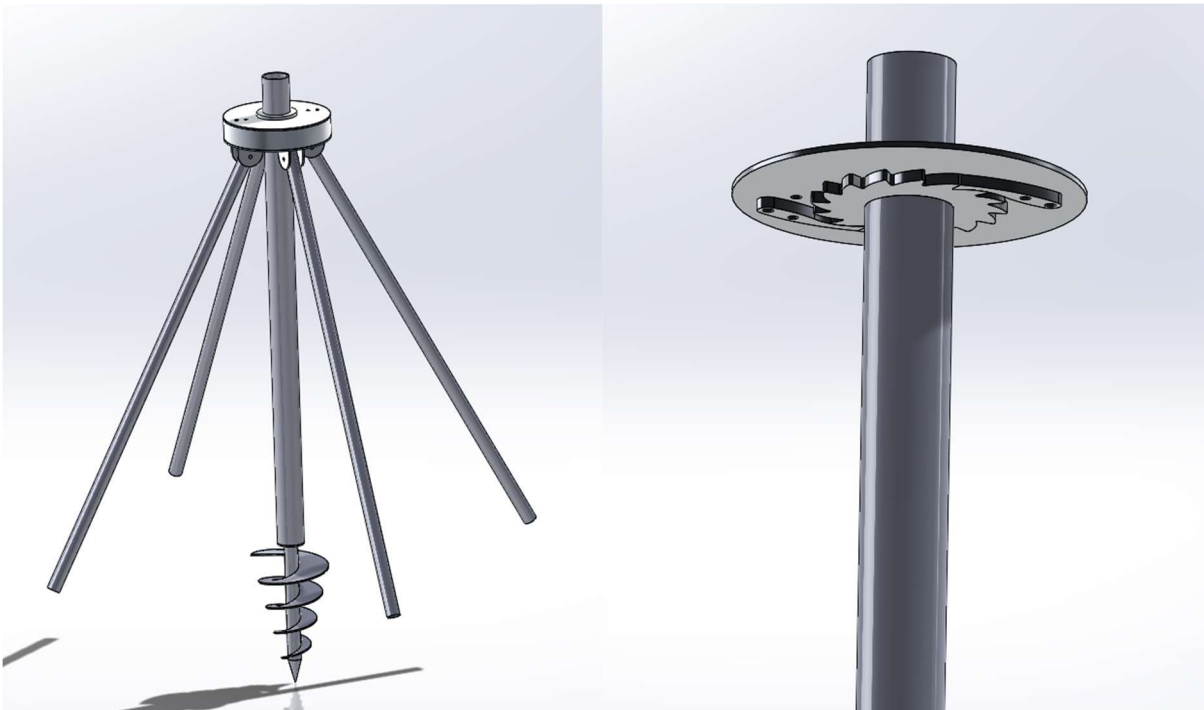


Figure 3.2.2: CAD model for chosen design and positioning of ratchet.

4 Analysis of Assembly

In the **Analysis of Assembly** Section, a comprehensive analysis will be conducted to analyze the various loads and conditions that the individual parts and the entire assembly may encounter. This includes analysis on the forces impacting the poles, supports, press-fitted collars, auger resistance to pull-out forces, and the mechanics of the ratchet and pawl. This detailed examination aims to uncover the key factors influencing the stability and functionality of the flagpole assembly and to determine the allowable values for various geometries.

4.1 Pole Analysis

In this section, an analysis of the loads applied to the flagpole assembly's pole will be conducted. The pole is segmented into three parts, each with equal length and wall thickness but varying outer diameters. This structural configuration poses a distinctive engineering challenge, warranting a detailed examination of the loads and stresses involved to ensure the pole's stability and durability. The forces acting upon each segment will be explored, and the impact of diameter variations on the stresses in the pole will be investigated. This in-depth analysis is a crucial aspect of the study, aiming to provide insights into the structural behavior of the flagpole under different loads. The MATLAB scripts used to analyze the pole are shown in **Appendix B – Pole Analysis**.

The material chosen for this pole is Aluminum 6061, selected for its excellent combination of strength, lightweight properties, and corrosion resistance. McMaster Carr and Grainger offers a wide range of pipe sizes in Aluminum 6061, providing a variety of options to suit different aerospace engineering needs [15]. As indicated in **Table 4.1.1**, Aluminum 6061 exhibits a tensile yield strength of 40 ksi, making it a suitable choice for withstanding the various loads and forces the pole will experience. Additionally, its low density of 0.0975 lb/in³ ensures that the pole remains lightweight, a crucial factor in aerospace applications. Moreover, its resistance to corrosion ensures the longevity of the pole, even when exposed to environmental elements.

Table 4.1.1 Material properties of Aluminum 6061 [16]

Property	Value
Modulus of Elasticity	10000 [ksi]
Shear Modulus	3770 [ksi]
Density	0.0975 [lb/in ³]
Yield Strength	40 [ksi]
Shear Strength	30 [ksi]



The pole is divided into three segments, which are depicted in **Figure 4.1.1**. The segments are denoted as Section 1, Section 2, and Section 3, with each section being of equal length, measuring 3 ft. This standardized length not only contributes to the desired height of the flagpole, but also ensures that it can be efficiently stowed within a compact case during launch.

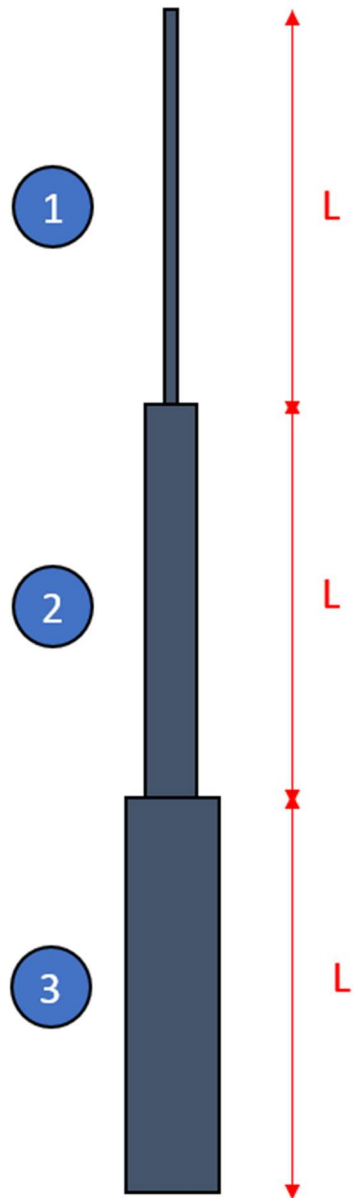


Figure 4.1.1: Diagram of the pole sections.

Aluminum tubing is sold at various lengths and wall thicknesses, but it is most available at a wall thickness of 0.065 inches. A uniform wall thickness, t , of 0.065 inches will be used throughout the entire length of the pole and provides structural integrity while maintaining a balance between weight and strength. **Figure 4.1.2** depicts the dimensions used to analyze the pole sections. D refers to the outer diameter and t is the wall thickness. The predetermined, chosen dimensions before the analysis are displayed in **Table 4.1.2**.

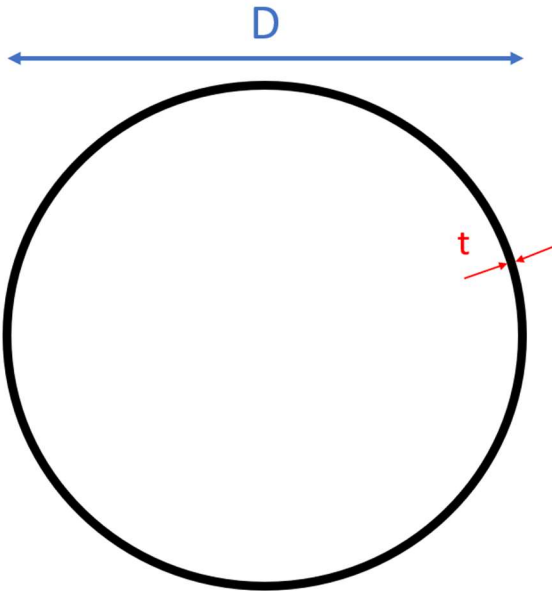


Figure 4.1.2: Dimensions used to analyze the pole sections.

Table 4.1.2 Predetermined Dimensions

Dimensions	Value
Pole Section Length, L	3 [ft]
Pole Wall Thickness, t	0.065 [in]

To perform proper analysis on the pole, the geometric properties of the flag pole's cross sections must be found. These parameters are crucial for understanding axial stress, resistance to bending, and torsional rigidity. The inner diameter d in terms of the outer diameter D and wall thickness t are defined by,

$$d = D - 2t.$$

The cross-sectional area of each section is found using,

$$A = \frac{\pi}{4}(D^2 - d^2). \quad (4.1.1)$$

The area moment of inertia is found using,

$$I = \frac{\pi}{64}(D^4 - d^4). \quad (4.1.2)$$

The polar moment of inertia is calculated from,

$$J = \frac{\pi}{32}(D^4 - d^4) = 2I. \quad (4.1.3)$$

The two test loads defined by the problem statement are a vertical force of 10 lb and a horizontal force of 10 lb, both applied at the uppermost section. These loads are shown in [Figure 4.1.3](#), where R is the reaction force(s) at the base of the pole.

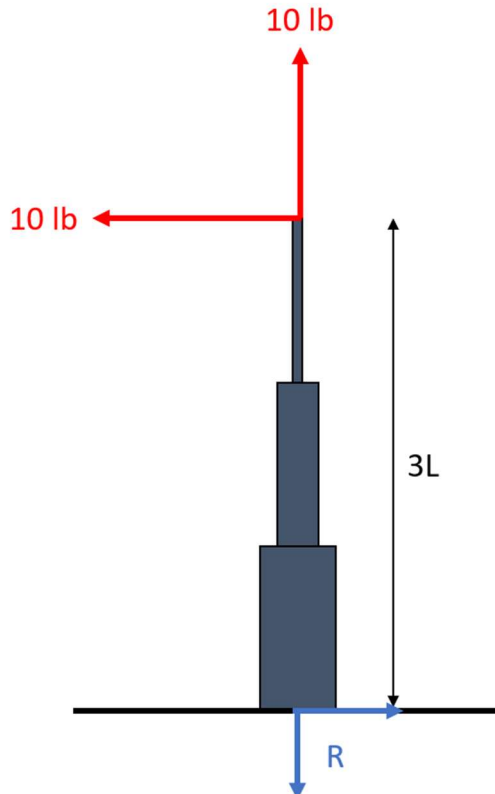


Figure 4.1.3: FBD of test loads applied to assembly.



To evaluate the stresses induced by these loads, refer to **Figure 4.1.4**, which displays the stress distribution along a pole's cross section. The maximum stress occurs along the outside edge of the cross section that experiences tension.

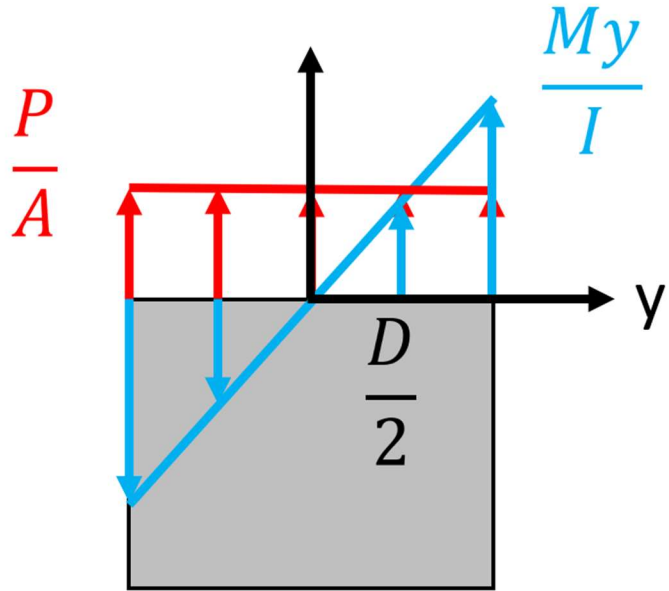


Figure 4.1.4: FBD of the stresses at a pole cross section.

The stress due to the tensile load and moment can be calculated using,

$$\sigma_{test} = \frac{P}{A} + \frac{My}{I}.$$

The maximum stress occurs at $y = \frac{D}{2}$ and the moment at each section is $M_i = i * LP$, where i is the section number and P is the test load. Using Equation (4.1.1) for the cross-section area and (4.1.2) for the area moment of inertia, the maximum stress at each cross section is given by,

$$\sigma_{test} = \frac{P}{\pi t(D_i - t)} + \frac{32D_i L_i P}{\pi [D_i^4 - (D_i - 2t)^4]}. \quad (4.1.4)$$

Since the length and loads are known, the stress is a function of the outer diameter of the pole. Based on the given yield stress and a factor of safety of 1.25, the minimum outer diameters for each section can be solved for.

Figure 4.1.5 presents a graphical representation of the maximum (total) test stress within each section of the pole as a function of the outer diameter, generated using MATLAB. The maximum allowable stress is indicated by the horizontal black line and is equal to the yield strength divided by the factor of safety, $\frac{\sigma_y}{SF}$.



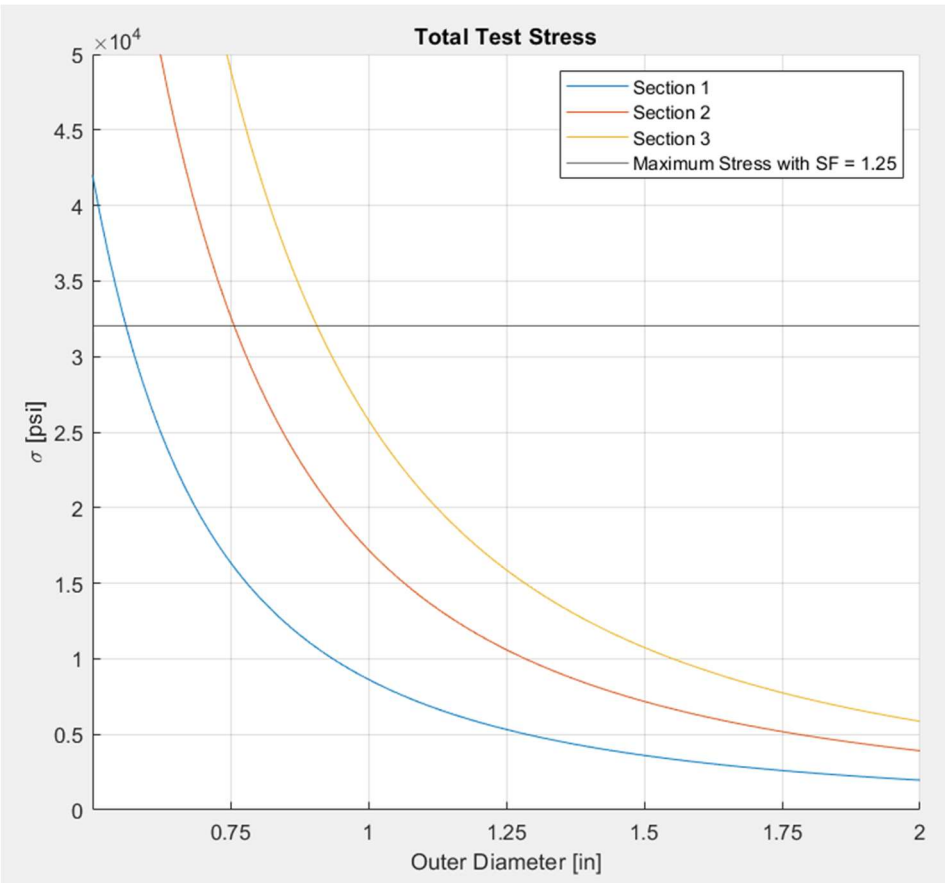


Figure 4.1.5: Total test stress (y-axis) vs outer diameter (x-axis).

Table 4.1.3 provides the results obtained by Equation (4.1.4) for the minimum outer diameters in each section.

Table 4.1.3 Minimum Outer Diameters

Section Number	Minimum Outer Diameter [in]
1	0.561
2	0.757
3	0.907

Upon determining the minimum outer diameters for each section of the flagpole, the next step is to assess the impact of the flagpole's use on the lunar surface. This evaluation includes two key factors: a downward force of 20 lb and a torque of 540 in-lb, both applied to pole Section 3. These loads are illustrated in **Figure 4.1.6**.

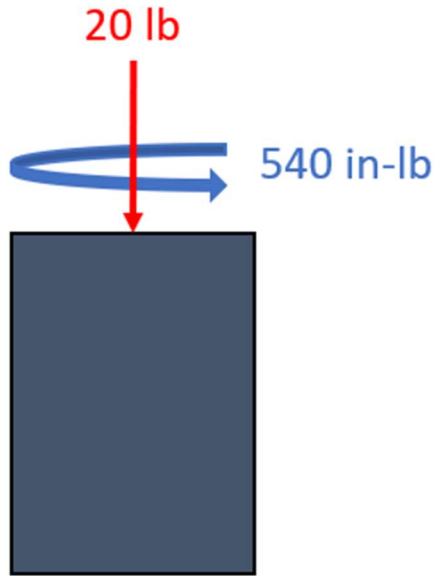


Figure 4.1.6: FBD of application loads applied to section 3.

Utilizing the geometric properties specific to this section, the loads will be examined to ensure that they do not exceed the structural limits and, thereby, guarantee the flagpole's reliability and safety during application. The normal and shear stresses due to the application loads are defined by,

$$\sigma_A = \frac{F}{A_3} = \frac{F}{\pi t(D_3 - t)} \text{ and} \quad (4.1.5)$$

$$\tau_A = \frac{TD_3/2}{J} = \frac{16D_3T}{\pi[D_3^4 - (D_3 - 2t)^4]}. \quad (4.1.6)$$

Where, F is the applied load, T is the applied torque, and J is the polar moment of inertia which is calculated from Equation (4.1.3).



The maximum normal and shear stresses in Section 3 due to the application are shown in **Table 4.1.4**. These results were obtained by solving Equations (4.1.5) and (4.1.6) using MATLAB. The structural analysis demonstrates that the flagpole can safely withstand the imposed forces, confirming its suitability.

Table 4.1.4 Maximum Normal and Shear Stresses

	Normal Stress [psi]	Shear Stress [psi]
Maximum Stress with SF = 1.25	32000	24000
Application Maximum Stress	116	7988

Furthermore, it's important to determine the weight of the pole, which can be calculated using

$$W = \rho L \sum_i^3 A_i, \quad (4.1.7)$$

resulting in a weight of 1.455 lb with the minimum diameters each pole section. It's worth noting that this weight comfortably falls within the 10-lb limit, allowing for the allocation of additional mass to create more intricate components in the remaining parts of the assembly.

Although the optimized minimum outer diameters result in very low weight and are strong enough to resist the loads, there must be enough clearance for proper telescoping. Furthermore, the flag and mount must fit inside the poles, and the ratchet assembly needs to properly integrate with section 3, leading to an increase in outer diameters. To allow for this to happen, the outer diameters of the pole sections will be 1, 1.5, and 2 inches. Section 3 will have an outer diameter of 2 inches, a deliberate design choice made to accommodate the ratchet and auger mechanism, ensuring the flag is secure attachment during launch and deployment. Using Equation (4.1.7) with the new outer diameters of 1, 1.5, and 2 inches yields a weight of 3.08 lb, which remains an acceptably low weight.



The cross sections of the optimized poles and the new diameters are shown in **Figure 4.1.7**. Before increasing the diameters, there is not enough room for the poles to properly fit inside each other. After increasing, there is enough clearance between each section to allow for parts to fit inside and telescope.

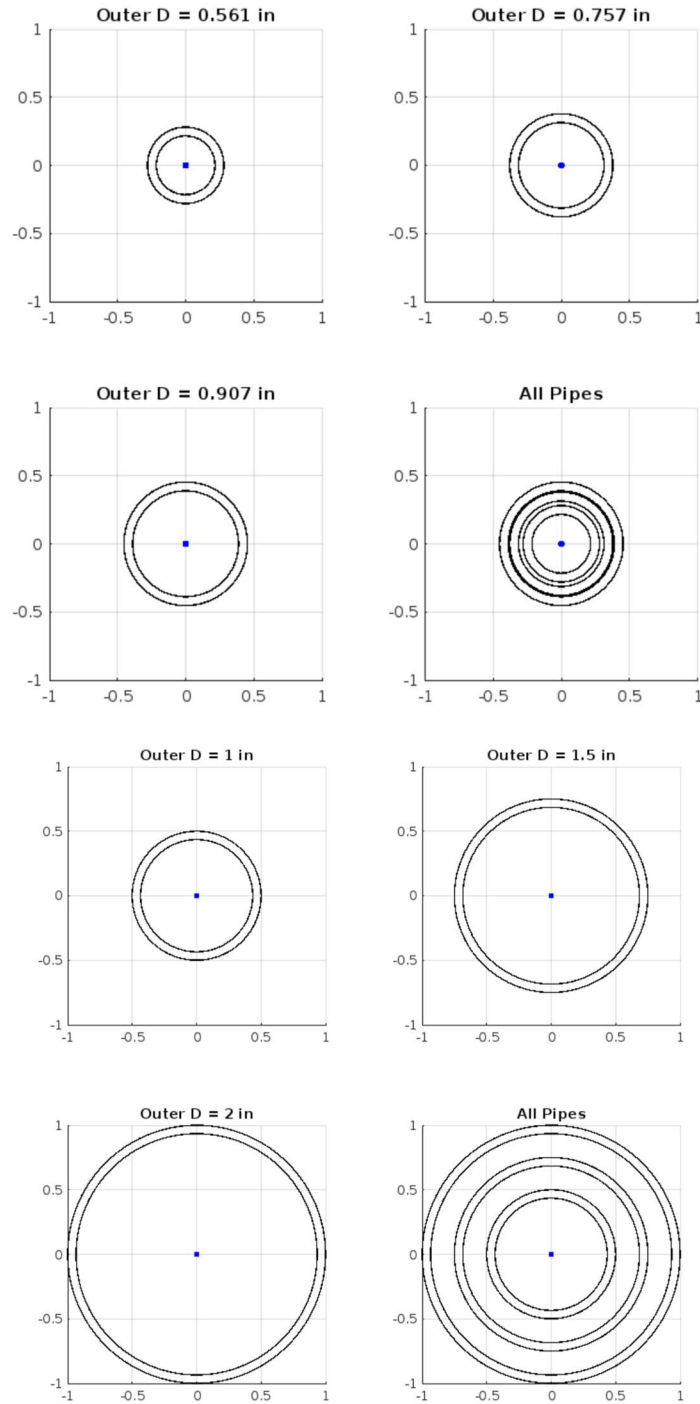


Figure 4.1.7: Cross sections of the optimized pole sections (top) and the new sections (bot).



In conclusion, the analysis of the flagpole's structural integrity, geometric properties, and its response to applied loads has yielded valuable insights crucial to its success. By solving for the minimum outer diameters for each section and assessing the normal and shear stresses under varying loads, the structural poles have been designed to maintain structural integrity during application. With new outer diameters that are greater than the minimum required ones, the pole will be strong enough to resist the expected loads as well as any unpredicted conditions. The use of MATLAB in plotting data and solving key equations has greatly facilitated this analysis. The results clearly demonstrate that the flagpole can safely endure the applied forces, ensuring its reliability during lunar operations. **Table 4.1.5** shows a summary of the pole analysis.

Table 4.1.5 Pole Analysis Results

	Minimum Outer Diameter [in]	Outer Diameter [in]
Pole 1	0.561	1
Pole 2	0.757	1.5
Pole 3	0.907	2
Total Weight [lb]	Wall Thickness [in]	Length [ft]
3.08	0.065	3



4.2 Supports Analysis

The supports of the flagpole are designed to resist the 10 lb horizontal force acting on the top of the flagpole shown in **Figure 4.2.1**. Some assumptions were made while completing this analysis. First, each support was analyzed in the worst-case scenario where a single support pole supports the entire horizontal force. Additionally, to leave room for the ratchet system above the support and the anchor for the support itself, each support was taken to be 3 ft long and attached 2.5 ft above the bottom of the lowest flagpole segment as shown in **Figure 4.2.1**.

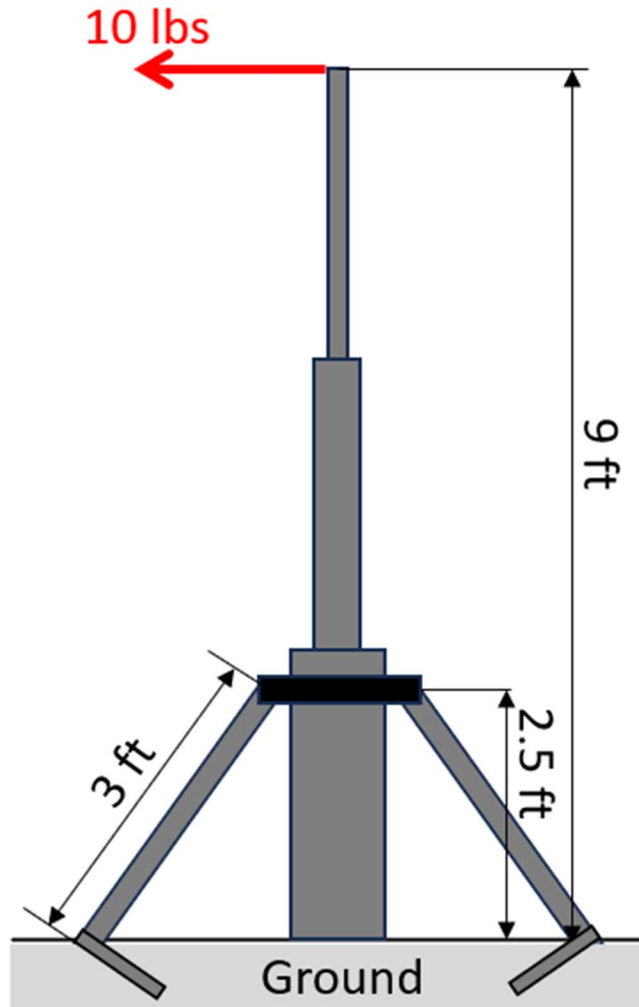


Figure 4.2.1: FBD of the applied load and geometry of supports used for analysis.

Furthermore, the modes of failure likely to occur in the support must be examined. For the support itself, which is akin to a cantilever beam, failure is likely to occur in the form of beam buckling or yield. Additionally, these supports will be affixed to the main flag body using a form of bolt or pin and thus another potential area of failure is the bearing failure of the support as well as shear failure of the pin.

The first area of analysis is buckling and yield in the support. **Figure 4.2.2** is used to better visualize the forces acting on the support.

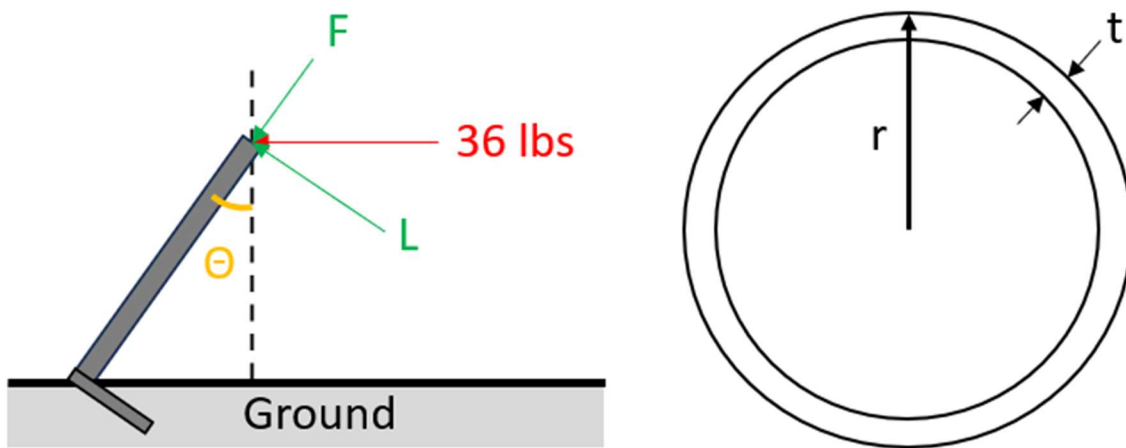


Figure 4.2.2: Depiction of the loading analyzed on the support and its cross section.

From **Figure 4.2.2**, r is the outer radius of the support and t is the wall thickness. The length of the flagpole was taken to be 9 ft, and thus when the 10 lb horizontal force was moved down to the support, the equivalent force was calculated to be 36 lb. Additionally, from the geometry shown in **Figure 4.2.2**, both the axial and horizontal force on the support can be calculated. [Using the geometry from Figure 4.2.1 and Figure 4.2.2 in the equations](#)

$$\theta = \cos^{-1} \frac{2.5}{3},$$

$$F = 36 * \sin(\theta),$$

force F was calculated to be 19.901 lb. Similarly, using

$$L = 36 * \cos(\theta),$$

force L was calculated to be 30 lb. The critical force that induces buckling in the support was calculated using,

$$P_{cr} = \frac{\pi^2 EI}{L_{eff}^2} [17].$$

Where E is the Elastic Modulus, found in [Table 4.1.1](#) and L_{eff} is the effective length of the support, given as $0.8L_{support}$ for a fixed-pinned beam [17]. The area moment of inertia, I , is found by

$$I = \frac{\pi}{4} * (r^4 - (r - t)^4).$$



From these equations, many critical forces can be found using a range of different radii and thicknesses. The results of the critical force calculations are shown in **Figure 4.2.3**.

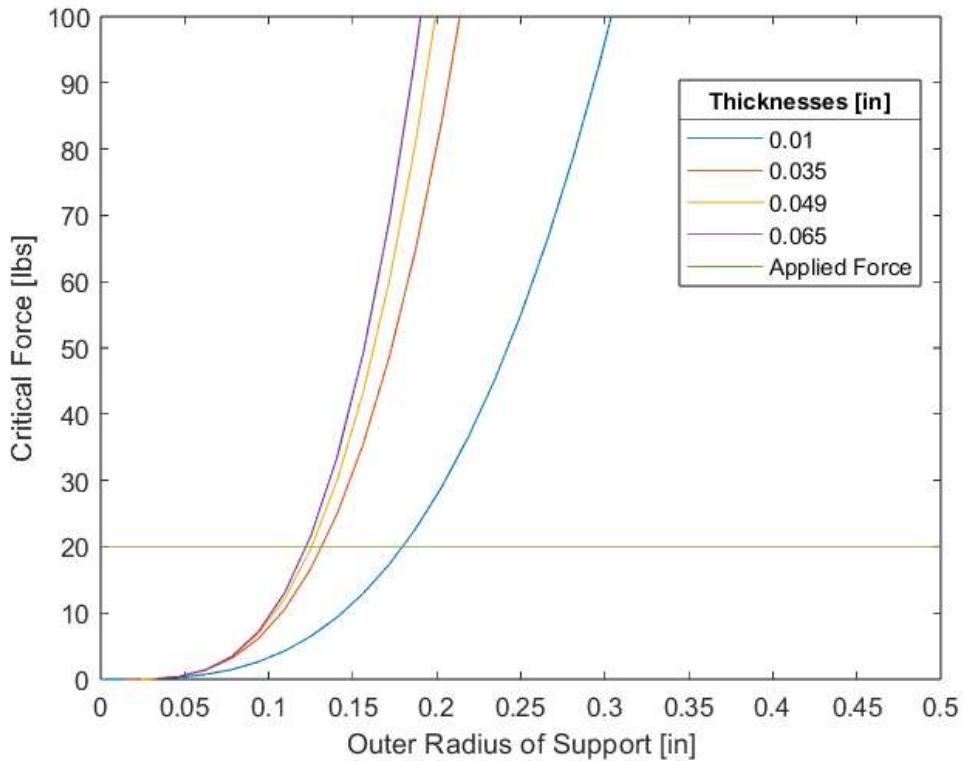


Figure 4.2.3: Plot of the critical force for various r and t of the support.

The green line in **Figure 4.2.3** is the force that the support is experiencing; therefore, a critical force above this line for the support geometry is desired. As the radius of the support increases, so does the critical force. The same relation is true for the thickness of the support; however, there is a larger jump in the critical force for an increase in radius than an increase in thickness. For the final prototype, the support geometry must lie somewhere above the green line while also maximizing cost effectiveness for the geometry.



Next, the maximum stress state in the supports must be calculated to ensure that the supports do not yield. The normal stress from an axial force was found using,

$$\sigma_a = \frac{P}{A}, \quad (4.2.1)$$

with A corresponding to the area calculated by

$$A = \pi * [r^2 - (r - t)^2].$$

The normal stress resulting from the moment was found using,

$$\sigma_b = \frac{My}{I} = \frac{Mr}{I}. \quad (4.2.2)$$

The moment M in (4.2.2) is given by moving the force L down to the end of the support, thus causing the moment to be maximized. M can be found by multiplying the force L by the length of the support (3 ft). Because the maximum value of normal stress is of interest, the y in Equation (4.2.2) is simplified to r . Additionally, the support experiences shear stress due to force M , but because the support is a long and slender beam, the stress due to shear will be much lower than that due to bending and/or normal forces and therefore can be ignored. Because the supports will be made from a ductile material, the Von Mises failure criteria can be used to calculate failure points [17]. First, the principal stresses must be found by finding the roots of

$$\sigma^3 - I_1\sigma^2 - I_2\sigma - I_3 = 0.$$

Where $\sigma_1 \geq \sigma_2 \geq \sigma_3$. I_1, I_2, I_3 are given by,

$$I_1 = \sigma_{xx} + \sigma_{yy} + \sigma_{zz}$$

$$I_2 = -(\sigma_{xx}\sigma_{yy} + \sigma_{yy}\sigma_{zz} + \sigma_{zz}\sigma_{xx}) + \sigma_{xy}^2 + \sigma_{yz}^2 + \sigma_{zx}^2$$

$$I_3 = \begin{vmatrix} \sigma_{xx} & \sigma_{xy} & \sigma_{xz} \\ \sigma_{yx} & \sigma_{yy} & \sigma_{yz} \\ \sigma_{zx} & \sigma_{zy} & \sigma_{zz} \end{vmatrix} [17].$$

Because the normal stress from forces P and L are aligned in the same direction, the stress matrix gets reduced to only $\sigma_{xx} = \sigma_a + \sigma_b$ from (4.2.1) and (4.2.2)

Von Mises stress can then be calculated using,

$$\frac{\sigma_Y}{FS} = \frac{1}{\sqrt{2}}[(\sigma_1 - \sigma_2)^2 + (\sigma_2 - \sigma_3)^2 + (\sigma_3 - \sigma_1)^2]^{1/2} [17].$$

Where the right side of the equation gives the Von Mises equivalent stress, and the left side of the equation gives the maximum stress calculated from the yield stress of aluminum from **Table 4.1.1** and the factor of safety (1.25). **Figure 4.2.4** shows the trend in Von Mises equivalent stress as the thickness and radius of the support are varied.



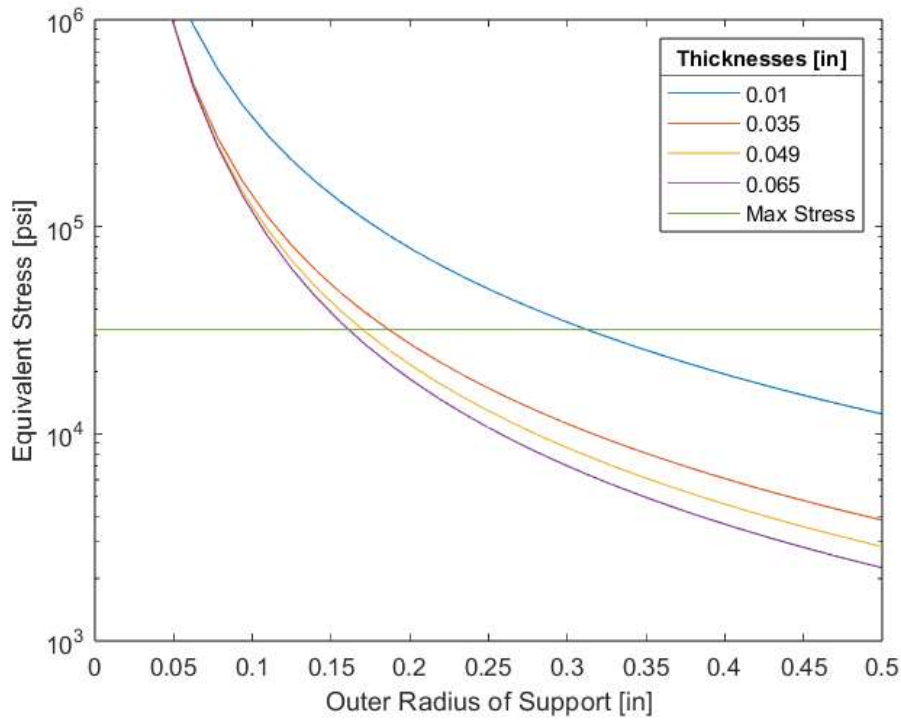


Figure 4.2.4: Equivalent stress in the support for various r and t .

In comparison to the critical force to induce buckling, the Von Mises stress for the supports is much more restrictive in the usable geometry. The support geometry must lie below the max stress line to pass the maximum equivalent stress restriction. This graph is only meant to show trends as outer radius and thickness vary because the geometry of the support becomes unphysical as thickness becomes larger than the outer radius. [From both Figure 4.2.3 and Figure 4.2.4, the optimal size of the support poles can be determined.](#) Because the thickness of the support poles will be quite thin, it will be more cost effective to buy them from a manufacturer as extruded or drawn tubes rather than buying four billets of material and machining the poles down. Because of this, the radius and thickness come in a finite set of values. This means the lowest radius used must be 0.25 in. With this radius, the lowest thickness used by manufacturers for extruded tubes is 0.035 in. This geometry works for both the critical buckling load as well as the maximum stress restriction.

Additionally, the bearing stress on the supports from the support pins must be calculated. The horizontal force on the top of the flagpole will be transmitted into the supports through the support pins, thus the bearing stress on this contact point must be calculated. [Figure 4.2.6 and Figure 4.2.6](#) show the location of interest from the CAD model and the simplified geometry respectively.



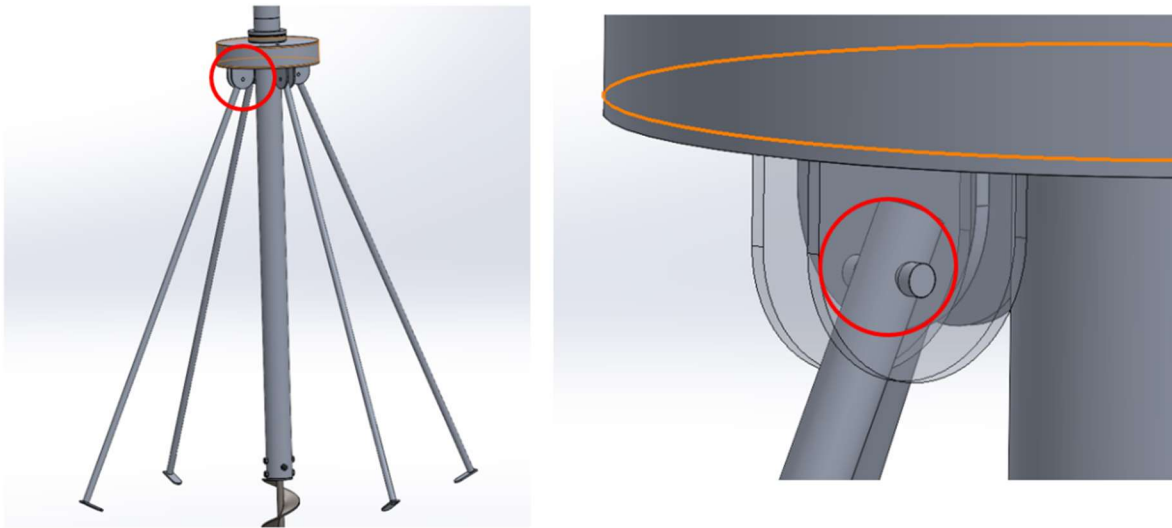


Figure 4.2.5: Pin location in CAD model.

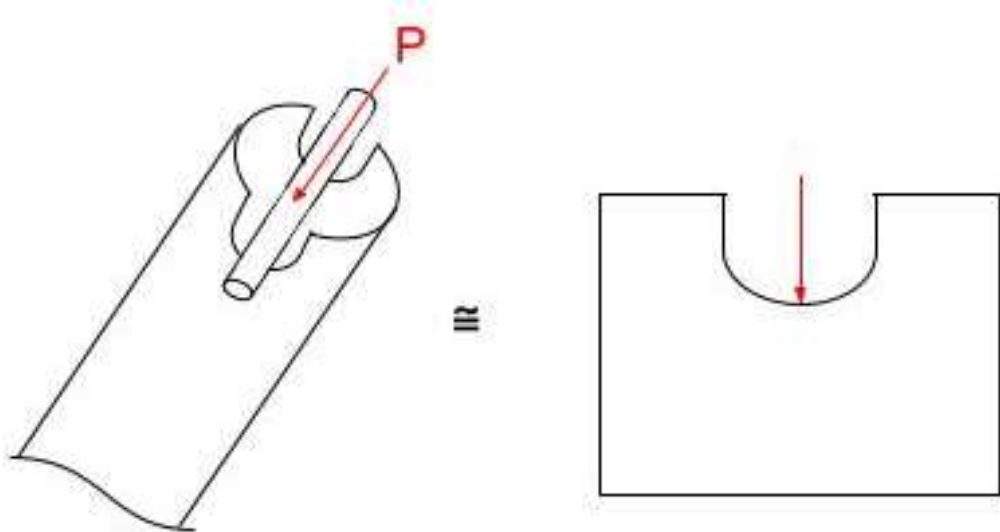


Figure 4.2.6: Simplified geometry for support and collar pin interaction.

The bearing stress was calculated using,

$$\sigma_{br} = \frac{P}{A_{br}},$$

where P is the 36 lb force from **Figure 4.2.2**. The area was calculated from the support pin diameter, D_{pin} , using:

$$A_{br} \approx 2D_{pin}t.$$

In a similar fashion, the bearing stress equation can be iterated through a variety of different pin diameters and thicknesses to see various trends in the equations and get a bound for the geometry of the support. Additionally, these results can be compared to the yield stress of aluminum from **Table 4.1.1** divided by the factor of safety (1.25). **Figure 4.2.7** shows the results of these calculations.

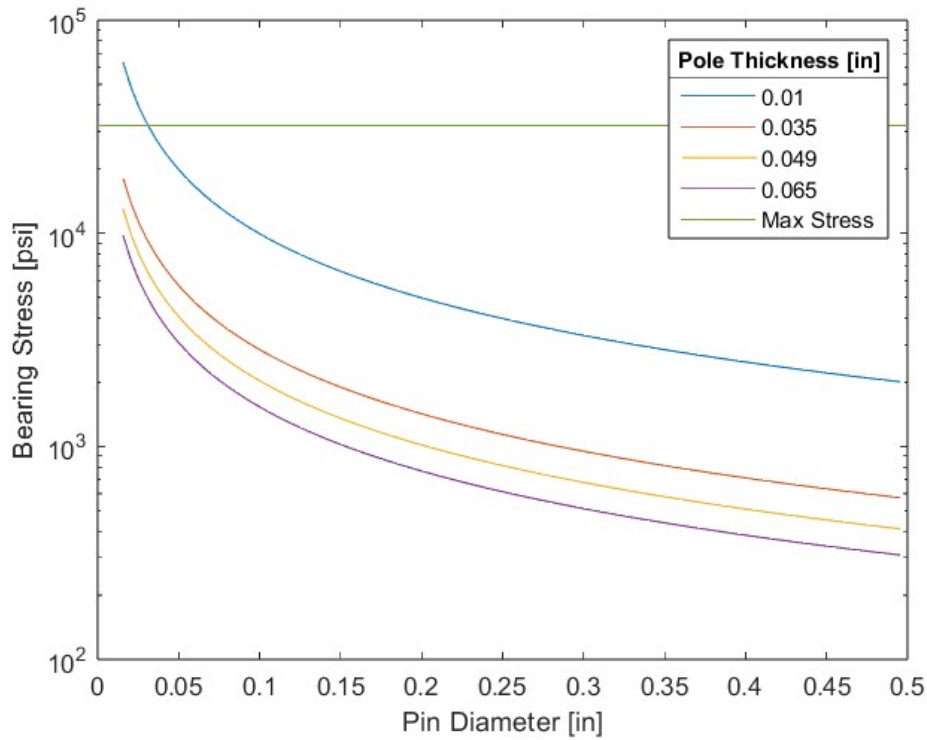


Figure 4.2.7: Bearing stress calculations.

As the pin radius and support thickness increase, the bearing stress on the support decreases. This graph can be used to minimize the size of the pin that the support needs. To be safe from bearing failure, the geometry of the pin and support must remain below the green line shown in the graph. The green line represents the yield stress for aluminum from **Table 4.1.1** divided by the factor of safety (1.25). An additional consideration when consulting this figure is the support radius. For this figure to remain true, the pin diameter must be less than twice the support radius, [otherwise the pin would be larger than the support it needs to hold](#).

The final consideration for failure would be shear failure of the support pins themselves. These pins must be able to transmit all the horizontal force to the supports without shearing. **Figure 4.2.8** shows the setup of the pins and how they would end up shearing.

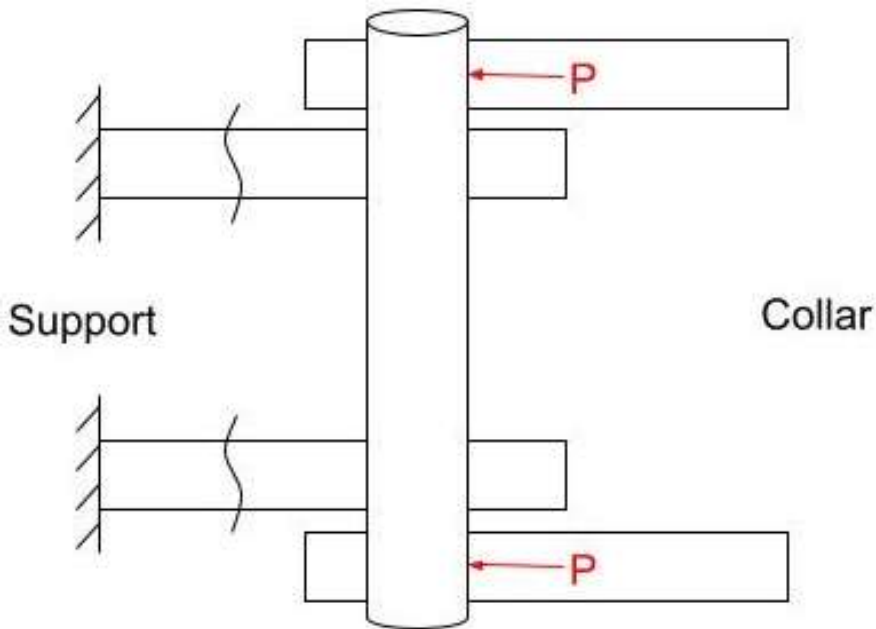


Figure 4.2.8: Geometry of the ratchet collar pins in shear.

To calculate the shear stress in the supports, the force and area of shear must be found. Because the pins need to be able to transmit the entire 10 lb horizontal force from the top of the flagpole, the total force on the pin is 36 lb. Additionally, because the pin is in a state of double shear, the area of one side can be multiplied by two. The shearing stress in the pins was thus calculated by,

$$\tau = \frac{36}{2*\pi/4 D_{pin}^2}.$$

By varying the pin thickness and using this equation, the shear stress in the pins can be calculated. The value from the equation can then be compared to the max shear strength of aluminum from **Table 4.1.1** divided by the factor of safety (1.25). This allowable shear stress is calculated as 24000 psi.

Figure 4.2.9 shows the shear stress in the support pin as pin thickness varies.

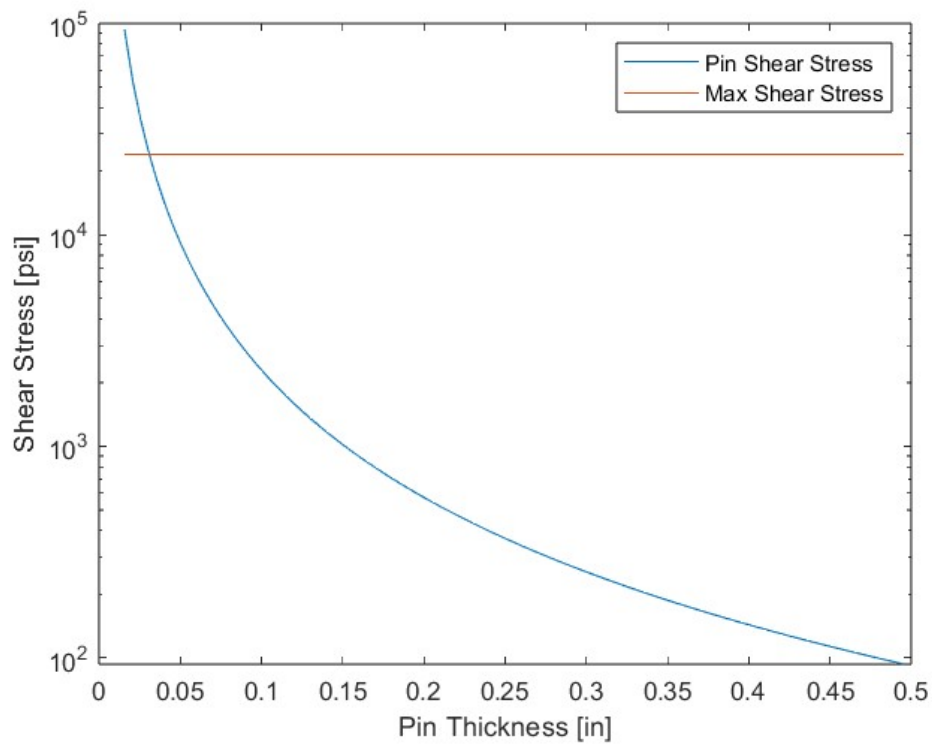


Figure 4.2.9: Shear stress in the support pin as pin radius varies.

For the geometry of the prototype to not fail, the geometry of the pins must fall below the max shear stress line. Using both **Figure 4.2.7** and **Figure 4.2.9**, the geometry of the pins can be determined. Due to a large range of pin thicknesses passing both the bearing stress and shear restrictions, a pin diameter of 0.25 in was chosen to facilitate easier manufacturing and assembly. MATLAB code for both the support pole and support pin analysis can be found in **Appendix C – Support Pole, Support Pin, and Collar Analysis**.



4.3 Collar Analysis

The collars between each of the main flagpole body segments are designed to press fit into the pole segment itself and then subsequently thread into the mating collar in the smaller flagpole segment. Because these collars are not designed to move around once affixed on the pole, they must be interference fit on the pole segment. Due to the thickness of the main pole body being very small, a FN1 interference fit is chosen [18]. Because of the ranges of diameter of the main flagpole assemblies, multiple different interference calculations must be run to ensure that the collars will not get pulled out of the main segments. **Figure 4.3.1** shows a view of one collar and its main flagpole segment in CAD.

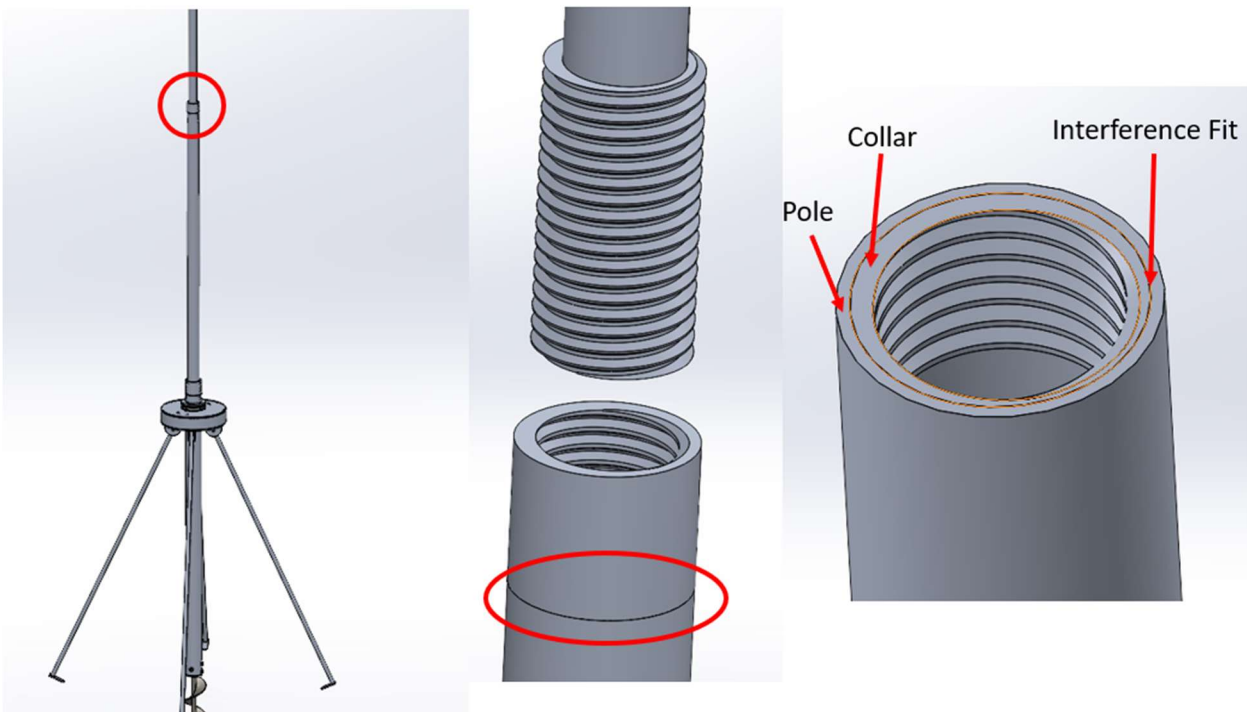


Figure 4.3.1: Location of a collar and its interference fit in the CAD model.

The pressure resulting from the interference of two cylindrical members must be calculated for each of the three ranges of fits using,

$$p_c = \frac{E\Delta}{2c^3} \frac{(a^2 - c^2)(c^2 - b^2)}{(a^2 - b^2)} \quad [17].$$

The definitions of a, b, and c are shown in **Figure 4.3.2**. The contact pressure can then be used to calculate the force normalized by the length of interference needed to pull the collar out of the interference fit.

The geometry of the shrink fit and corresponding variables are given in **Table 4.3.1**. The pull-out force is then found using,

$$\frac{P_{po}}{L} = 2\mu_s p_c \pi c.$$

Where μ_s = Coefficient of static friction which is 0.5 for aluminum [19].

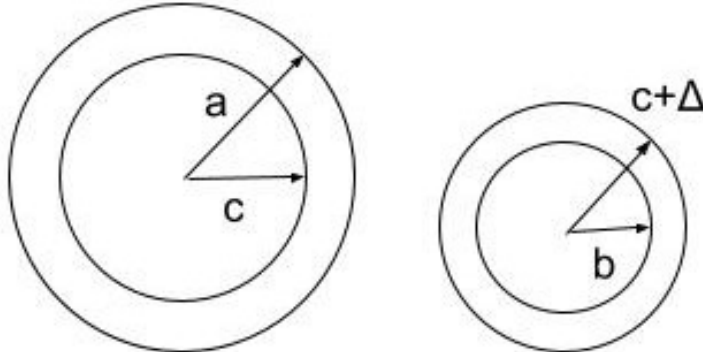


Figure 4.3.2: Collar shrink fit geometry.

From the FN1 interference fit, there are a range of values given for the nominal diameter, c , and the interference itself, Δ . These values are listed in **Table 4.3.1**.

Table 4.3.1 FN1 Interference Fits [18]

Nominal Diameter (c) [in]	FN1 (Δ) [10^{-3} in]
1.19 - 1.58	0.3 - 1.3
1.58 - 1.97	0.4 - 1.4
1.97 - 2.56	0.6 - 1.8

For the three different ranges of nominal diameters that the main flagpole segments lie within, there are three different ranges of FN1 fits. Because of this, the pull-out force calculation must be run three different times for each diameter range to ensure that none of the collars will fall out of the segments. By using these values and the associated equations, plots of the normalized pull-out force can be obtained. These then need to be compared to the axial force exerted on the flagpole to ensure that the collars do not come out.

Figure 4.3.3, Figure 4.3.4, and Figure 4.3.5 show the pull-out force per unit length vs radius of contact.

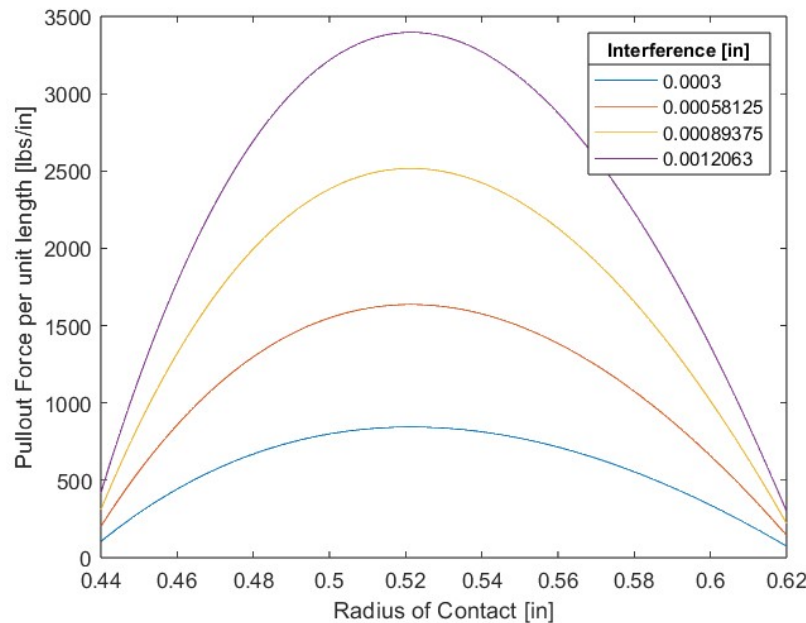


Figure 4.3.3: Normalized pull-out force per fit parameters.

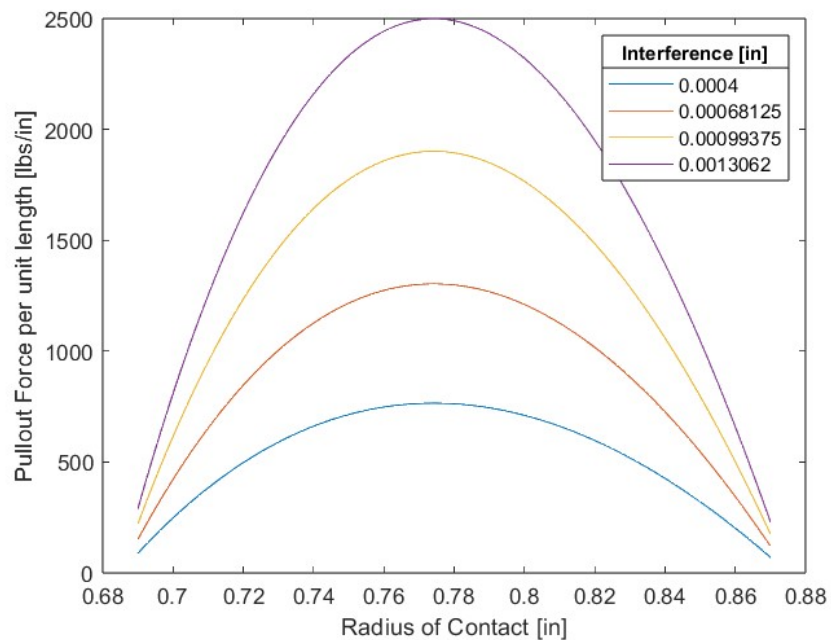


Figure 4.3.4: Normalized pull-out force per fit parameters.



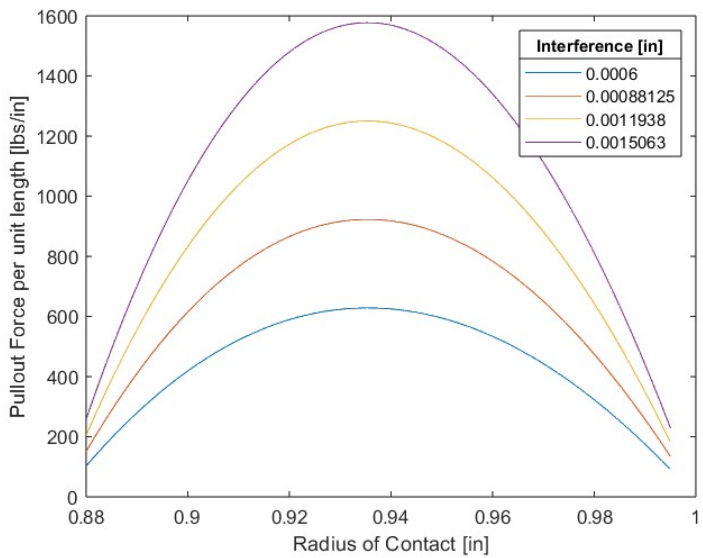


Figure 4.3.5: Normalized pull-out force per fit parameters.

Figure 4.3.3, Figure 4.3.4, and Figure 4.3.5 show similar findings for all ranges of fits. The normalized pull-out force follows a parabolic path as the radius of contact increases and increases as the interference increases. From all graphs, the interference of the fit has a much higher correlation to the magnitude of the normalized pull-out force than the radius of contact. These figures also allow the calculation of exact length of the collar that must be in an interference fit with the main flagpole segment. By reducing the length of the collar, the material cost can be lowered. This calculation was run using Aluminum 6061 for both the collar and the flagpole segment; however, a similar calculation can be run if the collars are made of a different material. [For the prototype, the inner/outer radius of the main flagpole segments can be found and then used with these figures to find the exact value of interference needed to keep the collars in each tube.](#)



In addition to the interference fit, there must be some consideration made for the type of thread used in the collars. Because the collars will be made from a non-steel metal, the threads should be designated as UNC [20]. Additionally, the astronauts putting the flagpole together will have limited dexterity, thus having coarse threads makes them easier to screw together. In addition to the designation of thread, the geometry of the collar "shaft" can be considered. The threads on the collars need to be designed to be as easy to put together as possible due to the limited dexterity of the astronauts. From this, the geometry of the collar can be changed, as in a conical shape for instance, to facilitate ease of assembly. As an additional regulation on the length of the collars, the length of the threaded surface can be considered. In the case of aluminum and plastic, the length of the threaded face should be at least twice the nominal diameter of the threads [20]. Due to this restriction and the average diameters of top and middle, and the bottom and middle pipes being 1.25 in and 1.75 in respectively, the collars will be 2.5 in and 3.5 in long for the top and bottom collar pairs respectively. Half of the length of each collar was then specified to have an interference fit with the poles, as from [Figure 4.3.3 - Figure 4.3.5](#), for the smallest interference, these lengths of interference provide more than the necessary pull-out force. [Figure 4.3.6](#) shows the CAD models of two collars for reference. MATLAB code for all calculations in this section can be found in [Appendix C – Support Pole, Support Pin, and Collar Analysis](#).

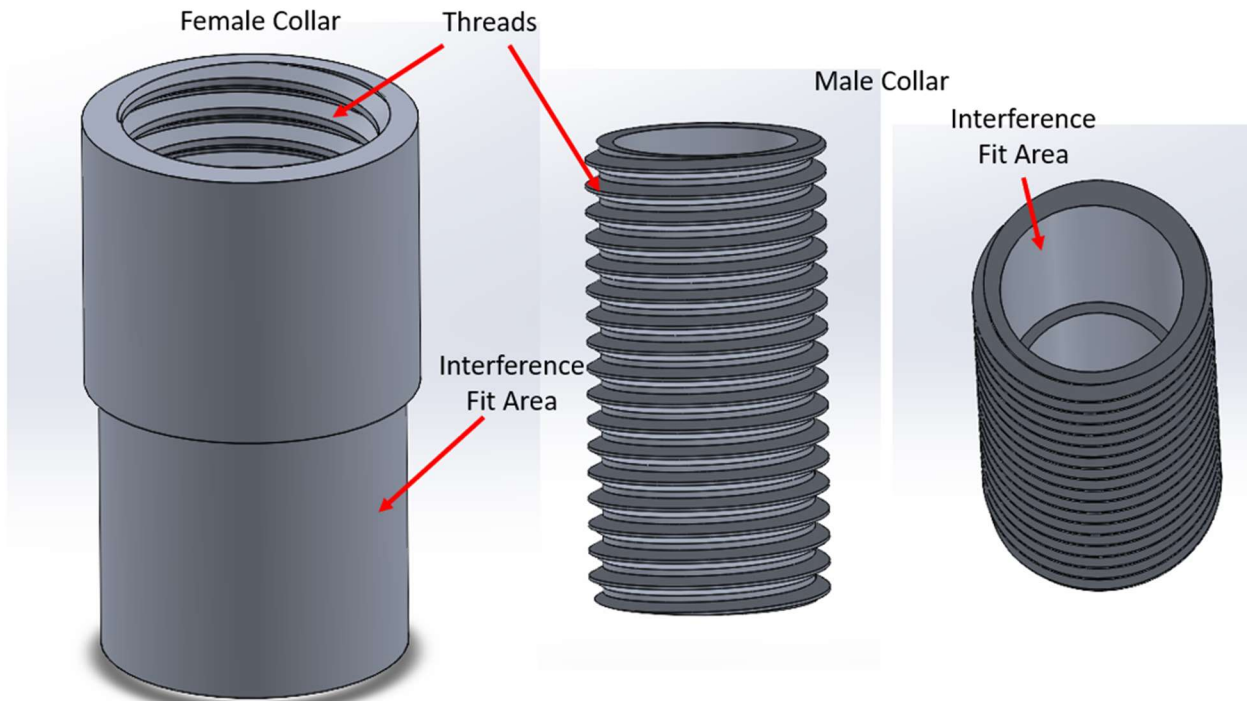


Figure 4.3.6: CAD models of one male and one female collar for reference.

4.4 Auger Assembly Analysis

The auger assembly was analyzed in two distinct parts. First, the auger itself will be analyzed to determine the shape necessary to prevent pull-out due to the predetermined loads. Following this, the nuts and bolts that connect the auger to the bottom pole will be analyzed to determine the maximum torque specification on these bolts to prevent the torque from causing buckling of the bottom pipe.

4.4.1 Auger Analysis

In designing the auger shape and specifications, the pull-out force was used as the sole method of failure. This failure comes from the lunar soil pulling itself apart, preventing the auger from holding the flagpole upright. The pull-out force required by the auger must be no less than 12.5 lb as determined by the vertical force of 10 lb and a factor of safety of 1.25, each defined respectively in the problem statement. It should be noted that the analysis of the auger does not consider the 10 lb horizontal force's contribution to pulling the auger out of the ground. This decision was made as the support poles were designed to carry this moment force and the vertical force will have a much greater effect on pull-out than a moment arm due to the much greater distance from the ground to the top of the pole than that of the ground and the bottom of the auger. In essence, with the auger in the ground, the horizontal load acts as a lever with its fulcrum at the ground. While there will be increased force on the ground and the auger (yet resisted by the support poles), the distance the top of the pole must travel to rotate the auger out of the ground is extreme as the entire pole would need to be nearly horizontal for the auger to be pulled free of the soil. Thus, any resistance the auger provides against pull-out failure due to bending is purely an additional bonus and the horizontal force's contribution to pull-out can be neglected. The pull-out force for a screw is shown in **Figure 4.4.1** and is given by the equation,

$$F = S_s * \pi * D_p * L, \quad (4.4.1)$$

where F is the pull-out force and is defined by the shear stress S_s , the pitch diameter D_p , and the axial length of full thread engagement L . For the purposes of this analysis, it was assumed that the entire 12 inches allocated to the auger's length past the bottom pole by the design is fully threaded and thus equivalent to the axial length of full thread engagement L . Notably, the pull-out force is a function of shear stress [21].



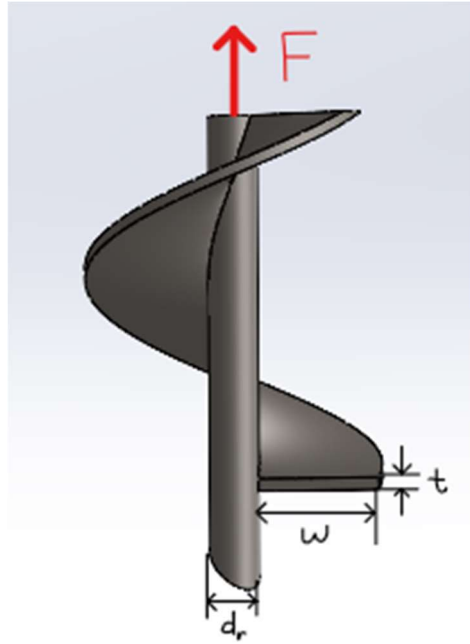


Figure 4.4.1: Pull-out force and general auger dimension definitions.

The pitch diameter is defined as the average thread diameter,

$$D_p = \frac{(D_{major} + D_{minor})}{2}.$$

D_{major} is the maximum diameter of the auger and D_{minor} is the diameter of the auger's rod which is also the minimum diameter. As shown in Equation (4.4.2), the major and minor diameters can be rewritten in terms of the dimensions d_r and w to give,

$$D_p = \frac{((d_r + 2 * w) + (d_r))}{2} = d_r + w, \quad (4.4.2)$$

where d_r and w will be utilized throughout the extent of this analysis.

To optimize the design of the auger, maximum pull-out force is desired, meaning the shearing stress should be maximized. As stated by the American Society of Mechanical Engineers in the excerpt, *Properties and mechanics of the lunar regolith*, the shear strength of lunar regolith, defined as the maximum value of shear stress the material can withstand, can be determined using,

$$\tau = c + p * \tan(\phi), \quad (4.4.3)$$

where c is the cohesive component of the material (in this case lunar regolith), p is the stress perpendicular to the surface of failure, and ϕ is the soil friction angle [22].

The same document provides ranges of values for both the cohesive component c and the soil friction angle ϕ of lunar regolith, found from studies during the Surveyor mission. These studies determined that lunar regolith has a cohesive component that ranges from 0.35 kPa and 0.70 kPa, whereas the soil friction angle ranges from $35^\circ - 37^\circ$ [22].

To determine the stress perpendicular to the surface of failure p , the surface of failure must first be defined. In these calculations, the assumption was made that the surface of failure can be approximated by a cylindrical surface around the screw. Due to this assumption, the stress perpendicular to the surface is purely due to bending along the threads. To calculate the stress due to bending, it was assumed that each thread had the same width and thickness and that the threads were evenly spaced. Bending stress was calculated by using the basic mechanics of materials computation,

$$p = \sigma_{bending} = \frac{M * y}{I}, \quad (4.4.4)$$

with $\sigma_{bending}$ representing the normal stress due to bending, M is the moment acting on the desired location, y is the distance from the desired location to the neutral axis, and I is the moment of inertia. To analyze the bending stress upon the threads of the auger, the threads can be “unwrapped” from the inner diameter to model it as a beam with a distributed load across the entire surface.

This model is shown in **Figure 4.4.2**, where w is the width of the threads from a single side, t is the thickness of the threads, n_t is the number of threads, and d_r is the root diameter of the auger. It also shows the location of interest, which is the location at which the bending stress is greatest.

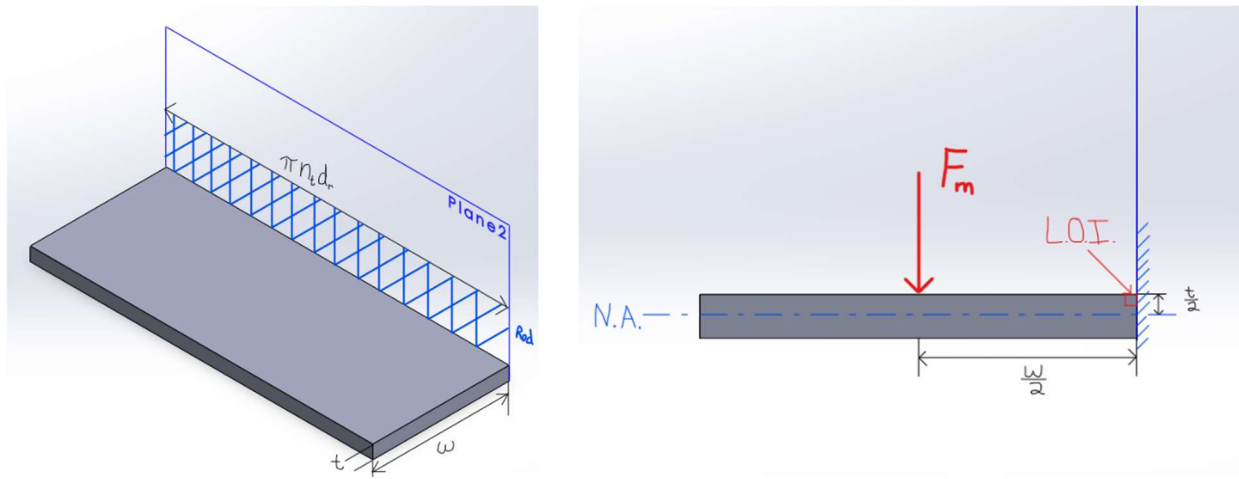


Figure 4.4.2: “Unwrapped” auger geometry with dimensions (left) and front view defining the neutral axis, location of interest, and force causing moment (right).

The neutral axis of a rectangular beam is defined as the line of symmetry perpendicular to the applied load, in this case being,

$$y = \frac{t}{2}, \quad (4.4.5)$$

as labeled in **Figure 4.4.2**. The moment of inertia of the threads can be approximated by that of a rectangular beam,

$$I = \frac{1}{12} * b * h^3,$$

where b is the base and h is the height of the beam, oriented such that the force is parallel to the height and perpendicular to the base. For the unwrapped threads,

$$b = n_t * \pi * d_r \text{ and } h = t.$$

The moment of inertia is then,

$$I = \frac{1}{12} * n_t * \pi * d_r * t^3. \quad (4.4.6)$$



The moment causing bending stress can be described by the applied force and its distance from the location of interest,

$$M = F_m * \frac{w}{2}. \quad (4.4.7)$$

Combining Equations (4.4.5), (4.4.6), and (4.4.7) produces the equation for the stress perpendicular to the surface of failure,

$$p = \frac{3 * F_m * w}{\pi * d_r * n_t * t^2}. \quad (4.4.8)$$

The force F_m causing the moment is, in this case, the weight of the lunar regolith distributed evenly over the upper threaded surfaces. This distributed surface load, exerted on the screw by the lunar regolith, is equivalent to a distributed line load force located halfway between the inner and outer edges of the threads. The magnitude of this force is the product of the density of lunar regolith ρ_{reg} , the volume \mathbb{V} of regolith that sits upon the threads, and the moon's gravity ($g_{moon} = 1.62 \frac{m}{s^2}$),

$$F_m = \rho_{reg} * \mathbb{V} * g_{moon}. \quad (4.4.9)$$

The volume of regolith upon the threads is the cylindrical volume the auger occupies,

$$\mathbb{V} = \pi * \left(\frac{d_r}{2} + w \right)^2 * L,$$

and by substituting this relation into Equation (4.4.9) produces the full relation for the force causing moment,

$$F_m = \rho_{reg} * \pi * \left(\frac{d_r}{2} + w \right)^2 * L * g_{moon}. \quad (4.4.10)$$

For the purposes of these analyses, the density of lunar regolith was taken to be constant. The density of lunar regolith (ρ_{reg}) can be determined from data retrieved from the Apollo missions, where the relative density was experimentally determined for a range of depths [22]. For depths of approximately 30 cm or 1 ft, the relative density of lunar regolith is approximately 90% of the maximum. The maximum density ρ_{max} of lunar regolith was experimentally determined to be $1.89 \frac{g}{cm^3}$, and as such the density of lunar regolith can be calculated to be,

$$\rho_{reg} = \rho_{max} * 0.90 = 1.701 \frac{g}{cm^3}.$$



Combining and simplifying Equations (4.4.1), (4.4.2), (4.4.3), (4.4.8), and (4.4.10) the fully derived equation for the pull-out force becomes,

$$F = \pi L(d_r + w)[c + \frac{3w g_{moon} (\rho_{reg} (\frac{d_r}{2} + w)^2 L)}{d_r n_t t^2} \tan(\emptyset)]. \quad (4.4.11)$$

This equation takes the known values of cohesive component c , soil friction angle \emptyset , density of regolith ρ_{reg} , axial length of thread engagement L , and desired pull-out force F and has 4 degrees of freedom consisting of root diameter d_r , thread width w , number of engaged threads n_t , and thickness t . To determine the minimum parameter values, the desired pull-out force was set to 12.5 lb and Equation (4.4.11) was solved while varying each of the free parameters individually.

To create a table of the unknown minimum parameters that satisfied Equation (4.4.11), several constraints were placed on the auger's properties. The thickness was allowed to be one of four commonly occurring thickness measurements: namely $[\frac{1}{16}, \frac{1}{8}, \frac{3}{16}, \frac{1}{4}]$ inches. The root diameter was constrained to be either $\frac{1}{2}$ or 1 inch, and the number of teeth were varied between 1 and 10 by $\frac{1}{2}$. Additionally, the total width of the auger may not exceed 8" as per the competition's standards [4]. By constraining these parameters to reasonable values, Equation (4.4.11) was solved using MATLAB, as shown in **Appendix D – Auger Analysis**. A table was created using the MATLAB code that listed all the values of the minimum parameters that satisfied Equation (4.4.11).



After looking at augers available for purchase, the resulting table shown in **Table 4.4.1** was narrowed down to values of n_t of 1 to 2 and d_r of $\frac{1}{2}$ inches, which correlates to typical numbers for the chosen length.

Table 4.4.1 Calculated Values for Augers Within Specifications

Number of Threads	Width of Threads [in]	Thread Thickness [in]
1	0.0156	1/16
1	0.0471	1/8
1	0.0806	3/16
1	0.1128	1/4
1.5	0.0221	1/16
1.5	0.0622	1/8
1.5	0.1025	3/16
1.5	0.1401	1/4
2	0.0279	1/16
2	0.0749	1/8
2	0.1203	3/16
2	0.1619	1/4

As shown in **Table 4.4.1**, for any given thickness, the calculated width of the threads needed for a pull-out force that withstands the axial force within a safety factor of 1.25 is substantially smaller than typical marketed augers and ground screws. The augers found online had thread widths varying from 1.1875 to 1.5 inches. It is reasonable to assume that a larger width will increase the pull-out force required due to the greater amount of friction from more surface interaction between the lunar regolith and the auger's blade; furthermore, Equation (4.4.11) shows that the pull-out force will greatly increase with any increase in width. Therefore, the values calculated from Equation (4.4.1) are minimum values required to ensure that the flagpole will remain upright after deployment. A thread width of 1.25 inches with 1.5 threads can be chosen to obtain a pre-manufactured auger to streamline the machining process of the entire assembly.



4.4.2 Auger Fastener Torque Analysis

The auger assembly includes several nuts and bolts that attach the auger to the bottom pole. These bolts must be tightened to an extent that prevents rattling or falling off while experiencing vibrations while inside the rocket during flight. In addition, the bolts must not be overly tight to the point at which yielding of the bottom pole occurs as this would increase the likelihood of buckling. To determine the torque specifications required for these bolts, they can be modeled as an unstiffened pipe resting in saddle supports, where there are high local stresses that do not exceed

$$\sigma_{max} = k \frac{P}{t^2} \ln \frac{R}{t},$$

where P is the total saddle reaction or in this case twice the applied force since there are 2 bolts applying force to the pole, t is the thickness of the pipe, R is the radius of the pipe, and k is the coefficient with a value of 0.029 [23]. Setting the maximum stress to the yielding stress of aluminum from **Table 4.1.1**, a force of 1066 lb is found for each bolt.

To determine the torque that corresponds to this force, the torque-tension relationship model can be utilized, where

$$T = KFD.$$

Taking K to be the nut factor ratio - found to be 0.20 for steel, F to be the force each bolt applies, and D the diameter of the nut head, the torque becomes 53.3 in-lb [24]. Applying the 1.25 factor of safety gives a value of 42.64 in-lb. This is the maximum allowable torque value that should be used on the nuts and bolts that connect the auger to the bottom pole.



4.5 Ratchet and Pawl Analysis

When designing the ratchet gear and pawl system, careful consideration of a variety of variables was taken to ensure a ratchet system that would provide safe performance while also allowing for easy machining. All calculations will be based on aluminum 6061-T6 whose material properties are listed in **Table 4.1.1**.

The lunar flagpole will utilize a two-pawl system with the pawls being 180 degrees from each other, which allows for increased load capacity and enhanced reliability. Increased loading capacity is a necessary factor to add to the design as it can help consider any impulses of a high torque application on the pole if a regolith is encountered. With a dual pawl system, if a pawl were to unexpectedly, its counterpart would still be able to help the astronaut plant the flag.

15 lb was selected as a baseline force applied to opposite supports, at 18 inches from the center of the assembly when upright. Therefore, the resulting magnitude of the moment is 540 in-lb. Due to size constraints, a diameter of 3.1 inches for the ratchet was adopted, with each tooth being 0.25 inches long and the center of each tooth being 1.50 inches from center. Using the center distance, the moment, and two pawls distributing the force, the resulting force on a tooth face from this moment was calculated to be 180 lb. **Figure 4.5.1** is the resulting FBD on the ratchet and pawl pin because of the applied moment, where the force on the tooth face and on the pin are equal and opposite. Due to the curved nature of the ratchet teeth, the contact patch between pawl and gear is approximately 0.25 inches tall.

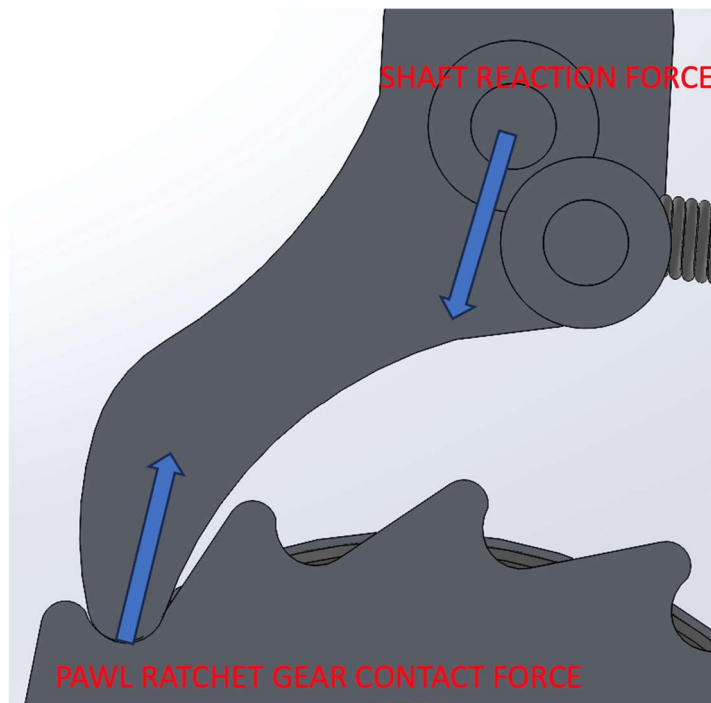


Figure 4.5.1: FBD of Pawl and Ratchet under illustrated moment.

Using,

$$\sigma_{shear\ (Maximum\ Circular)} = \frac{4V}{3A},$$

where $\sigma_{shear\ (Maximum\ Circular)}$ is the shear stress in psi, V is the force in lb, and A is the area in in², the smallest allowable pawl shaft area, 0.008 in², a minimum diameter of approximately 0.101 inches was found for Aluminum 6061-T6 with a shear strength of 30000 psi. From,

$$\sigma_{bend\ (Maximum\ Circular)} = \frac{32Fd}{\pi D^3},$$

where $\sigma_{bend\ (Maximum\ Circular)}$ is the bending (normal) stress in psi, F is the force in lb, d is the distance from pawl center along shaft to the shaft base in inches, and D is the diameter of shaft in inches, the distance the center of the pawl would need to be from the base of the pawl shaft to fail using the calculated minimum diameter was found to be 0.0225 inches for a tensile strength of 40000 psi. This shaft diameter and distance to pawl center along the shaft can be easily accepted as too small and unrealistic to machine and could easily fail under increased torque impulses. To protect the shaft of the pawl, a shaft diameter of 0.25 inches has been selected, which results in a bending stress failure location 0.341 inches away from the pawl shaft base if that were to be the location where the force is applied.

Under the conditions of a 0.25-inch diameter dowel, the experienced shear stress due to the moment was 4889.24 psi, and the bending stress was 26401.90 psi when the pawl is 0.225 inches along the pawl shaft. Utilizing

$$\sigma_{avg} = \frac{\sigma_x + \sigma_y}{2},$$

where σ_{avg} is the average normal stress, σ_x is the normal stress in the X-direction, and σ_y is the normal stress in the Y-direction. A value of 13200.95 psi was found for the center of the Mohr's circle as Y-stress was equal to 0 and X-stress was equal to the bending stress. The radius of the Mohr's circle is calculated using,

$$R = \sqrt{\sigma_{avg}^2 + \tau^2},$$

where σ_{avg} is the average normal stress and τ is the shear stress. From this, the radius was determined to be 14077.28 psi. Utilizing the 2D circle geometry and calculated values to find the maximum shear and normal stress using Mohr's circle, values of 14077.28 psi and 27278.23 psi were found respectively. Both values are well under the acceptable values of 30000 psi and 40000 psi respectively for Aluminum 6061.



Because the dowl is a three-dimensional object, the Z-direction must be accounted for; however, because the Z-direction is in plane stress, the third principal stress is zero. This means that the maximum shear and tensile stress previously found are still the appropriate values. [Figure 4.5.2](#) depicts the geometry of the 2D and 3D Mohr's circle.

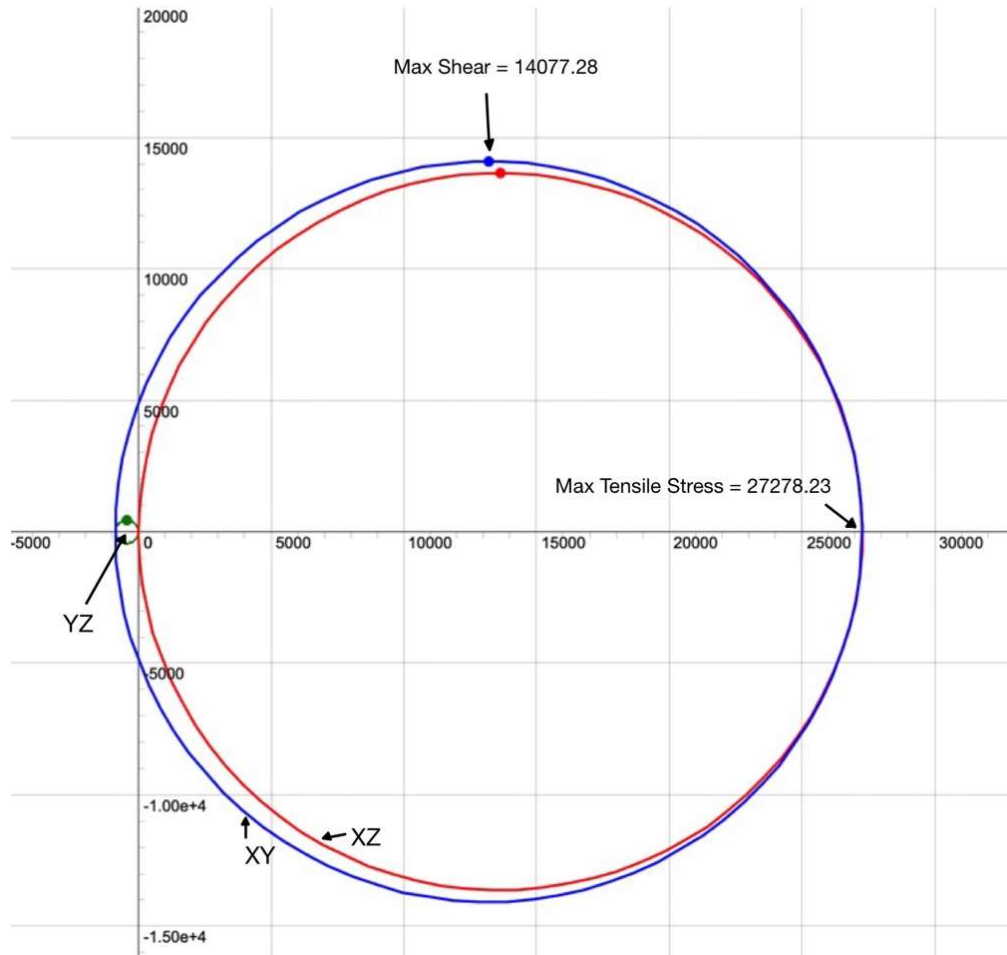


Figure 4.5.2: 3D Mohr's circle with principle and maximum stresses.

To elucidate the response of the ratchet gear under anticipated conditions, it is imperative that parameters pertaining to the geometry of the ratchet are well-defined. These parameters shall be utilized in,

$$\sigma_{safe} = (SF)(0.5) \frac{MF}{LNP^2}, \quad (4.5.1)$$

where σ_{safe} is safe stress, SF is the desired safety factor, M is the moment in in-lb, F is the ratchet factor of value, N is the number of teeth, L is the thickness, and P is the circular pitch in inches. This will allow for the systematic examination of safe stress as a function of the geometry and conditions [25]. For this case, the thickness of the ratchet along with the number of teeth will be altered to see the response.

The ratchet factor of value is defined as 50 for ratchet gears with 12 teeth or less, 35 for ratchet gear comprising of 12 to 20 teeth, and 20 for ratchet gear over 20 teeth. A range of 12 to 20 teeth was selected as that comprises of a uniform F , but it also allows for each gear to utilize a range of 30 to 18 degrees, respectively. This allows for easier machining practices compared to a high tooth count, and accurate ratchet adjustments that would be more difficult with a lower tooth count. Choosing this range of teeth sets F to 35. Circular pitch is the arclength between each tooth at a distance defined as the radius from the center to the midpoint in the tooth's face. This is equivalent to the circumference divided by number of teeth. The thickness of the ratchet gear L , was set to be a range of [0.25, 0.50, 0.75] inches. Based on the bending stress distance with a shaft of 0.25 inches: both 0.25 and 0.5 inches would be acceptable thicknesses for the ratchet and pawl system.

A thickness of 0.75 inches would work under the same conditions as the others but it would be near the bending failure distance from the shaft and could require a thicker pawl shaft to be safer; however, the importance of this analysis is to determine the impacts these values have on safe stress.

The resulting value that will be subjected to the alterations is safe stress. Safe stress is defined as stress that does not undergo failure. For this calculation, the safe stress is the stress that the tooth experiences because of the moment and the conditions described. The 0.5 in the equation is a result of the system having two pawls, meaning there would be half the load on each tooth contacted by the pawl.



Using MATLAB, the relationship between safe stress and combined alterations in thickness and teeth count was plotted in **Figure 4.5.3**. The corresponding safe stress data is placed in **Table 4.5.1**.

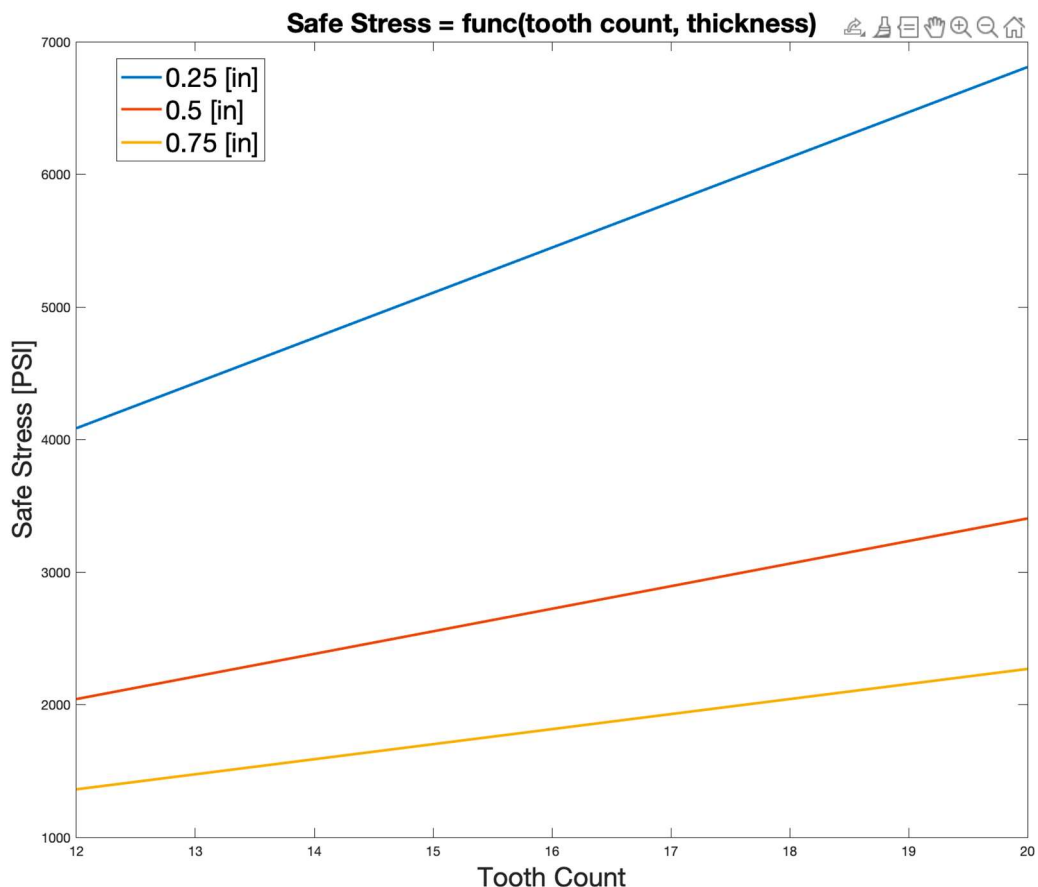


Figure 4.5.3: Safe stress as a function of tooth count and thickness.

Table 4.5.1 Safe Stress vs Thickness and Tooth Count

Safe Stress [ksi]										
Tooth Count		12	13	14	15	16	17	18	19	20
Ratchet Thickness	0.25 [in]	4.085	4.425	4.766	5.107	5.447	5.788	6.128	6.468	6.809
	0.50 [in]	2.043	2.213	2.383	2.553	2.734	2.894	3.064	3.234	3.404
	0.75 [in]	1.362	1.475	1.589	1.702	1.816	1.929	2.043	2.156	2.270

Over the span of 12 to 20 teeth with the varying thicknesses of 0.25, 0.5, and 0.75 inches, apparent trends appear, further supported by the numerical data in **Table 4.5.1**. As the thickness of the gear increases, the linear rate of change of safe stress decreases linearly. The difference between the 0.25-inch gear at 12 and 20 teeth was $2.724\text{e}3$ psi, whereas the thickest gear had a difference of $0.908\text{e}3$ psi. Thus, gear teeth play less of an effective role in safe stress as the thickness of the ratchet increases. Thickness also played a role in the safe stress at 12 teeth as the difference in starting points scaled exponentially as the difference between safe stress at 12 teeth for 0.5 and 0.75 inches was $0.681\text{e}3$ psi, whereas the difference between 0.5 and 0.25 inches was $2.042\text{e}3$ psi.

The most important conclusion that can be drawn from this plot is that the maximum safe stress values for all thicknesses, which all occur at a tooth count of 20, is well below the shear stress value of Aluminum 6061, 30000 psi. For the lunar flagpole's ratchet characteristics, all combinations are acceptable for this test. Due to its lighter weight and acceptable safe stress limits on the tooth of contact, a thickness of 0.25 for the ratchet and pawl can be utilized. Any tooth count within the specified range is acceptable. For this ratchet, 18 teeth is an acceptable number. This count would prevent the potential occurrence of a stress concentration that could cause failure with a high gear count, and enough teeth where the astronaut could make small rotations if the surface proves to be challenging to drill into.

The acceptable ratchet and pawl system will have a ratchet gear with a thickness of 0.25 inches and 16 teeth, a pawl shaft with a diameter of 0.25 [in], and the center plane of the pawl no greater than 0.341 inches from the base of the pawl shaft.



4.6 Spring Selection

The selection of a spring to pair with the pawl is essential to ensure that the system works seamlessly and ensures a clean retraction of the pawl back into the ratchet gear slot.

The kinetic friction coefficient between two pieces of aluminum is 1.4 and ranges between 1.05 and 1.35 for static friction [26]. For all calculations of friction, the higher value of the kinetic friction coefficient will be used.

To keep the aluminum pawl sliding seamlessly over the aluminum locking ring that holds it in place, the friction between both parts is determined using

$$F_k = \mu_k N,$$

where F_k is the force due to kinetic friction, μ_k is the kinetic friction coefficient, and N is the normal force. The frictional force from a 0.035 lb pawl is 0.049 lb. To find a spring that can be used in the lunar flagpole, the spring constant will be calculated using,

$$F_s = kx,$$

where F_s is the force experienced by spring, k is the spring constant, and x is the spring extension distance. With spring force being equal to the force due to kinetic friction in the worst-case scenario, and the spring stretching approximately 0.25 inches to reduce wasted space. The spring constant is determined to be 0.196 lb per inch.



5 Prototype

This section provides a summary of the layout, manufacturing, results, and operation procedure of the final prototype.

5.1 Prototype Design

The final prototype design incorporates three telescoping poles that seamlessly nest within each other for convenient storage, connecting internally through threaded collars as they extend. The bottom pole is affixed to an auger which digs into the ground using a ratchet mechanism. Additional supporting poles, which double as handles to operate the ratchet, provide additional support to the auger by balancing the flagpole and providing resistance to moment inducing forces. The pole that attaches to the top of the flag will be attached to a cap that is secured in place by a rubber O-ring, and a slot to slide into when fully extended. The design was tested using a prototype that outlines the main concepts.

The design can be split into three sections to detail the prototype, which are discussed below.

5.1.1 Top Pole Assembly

Three sections make up the Top Pole Assembly: the pole, Top Cap assembly, and the collar which allows the pole to thread to the rest of the flagpole assembly. The extended assembly is pictured in **Figure 5.1.1**.

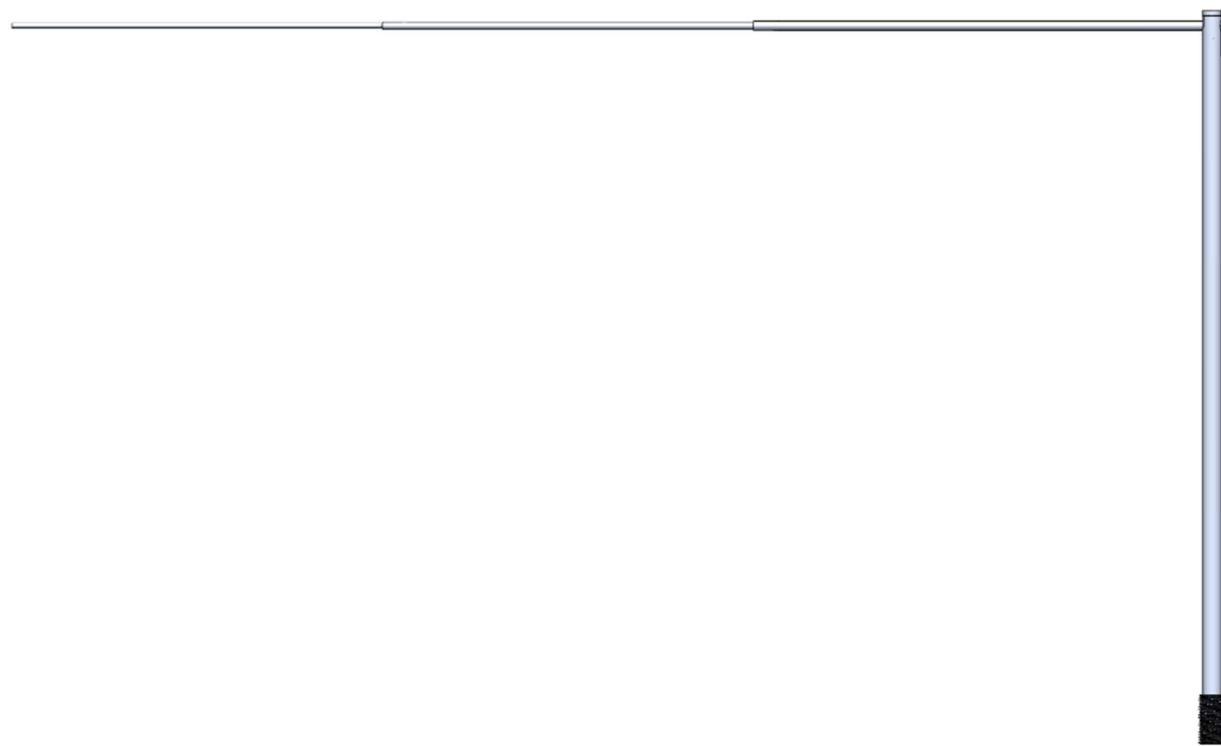


Figure 5.1.1: Top pole assembly in the extended configuration.

The top pole is the smallest of the three poles and features a circular cut near its top. One side of this cut has additional material removed, as illustrated in **Figure 5.1.2**. These cutouts allow for the smaller telescoping pole which holds the flag to stay fixed in place.

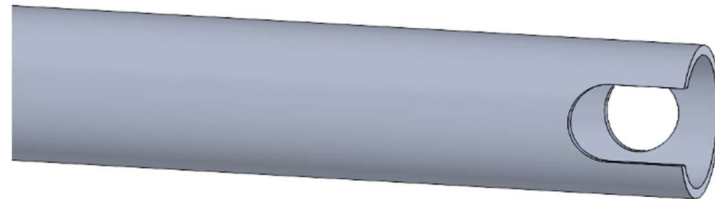


Figure 5.1.2: View of the top pole cutouts.

The Top Cap assembly is composed of an aluminum cap, a small dowel, and a thin extending pole. The slotted areas in the part facilitate the insertion of a dowel through both the cap and the extending pole, allowing for vertical transitional motion of the extending pole and rotational motion. The extending pole itself is also slotted, providing an even greater range of motion. In its stored configuration, the extending pole is contracted, and the cap remains in place through the friction of an O-ring. During flag display, the cap is pulled out, and the extending pole is rotated horizontally and extended. Upon placing the cap back on top of the pole, the rear of the extending pole can be pushed into the circular hole depicted **Figure 5.1.2** to secure the cap, as the O-ring is not designed to support the weight of the flag and the extended pole moment. The extended cap assembly is visualized in **Figure 5.1.3**, while the collapsed cap assembly is shown in **Figure 5.1.4**.

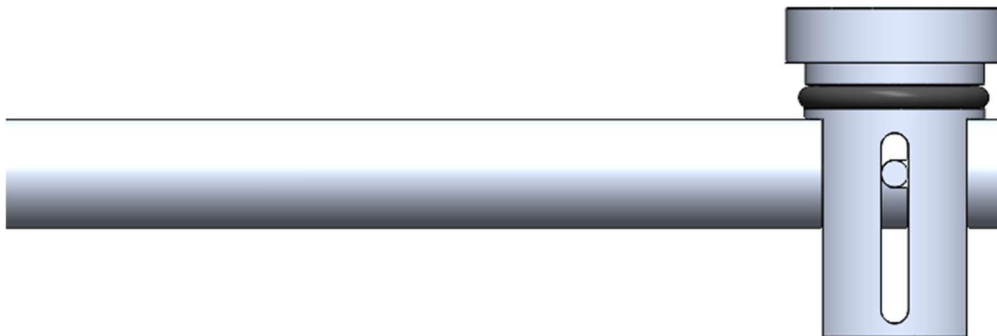


Figure 5.1.3: Top Cap assembly in the extended configuration.

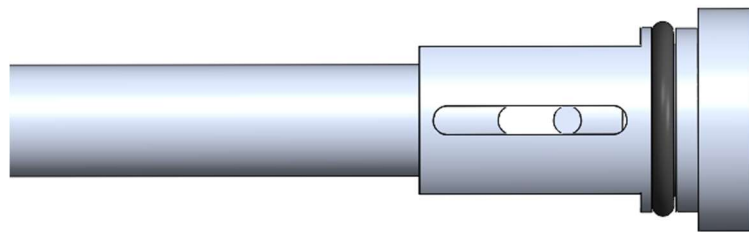


Figure 5.1.4: Top Cap assembly in the stored configuration.

Completing this assembly is a male threaded collar, enabling the assembly to be securely screwed into the lower sections of the full flagpole assembly and facilitating extension during flag display. The depiction of this collar is visible at the bottom of the pole in **Figure 5.1.1**.

5.1.2 Middle Pole Assembly

The middle pole, pictured in **Figure 5.1.5**, consists of a 1.5-inch diameter pipe featuring a threaded collar at each end. On the right side, the female section of the threaded collar pair is attached to the top of this section, connecting the middle pole to the top pole through a matching male collar. Simultaneously, a separate, larger male threaded collar, depicted on the left side, is affixed to the exterior bottom of the middle pole. This arrangement enables the middle pole assembly to be threaded into the bottom pole assembly in **Figure 5.1.6**.



Figure 5.1.5: Assembly of the middle pole.

5.1.3 Bottom Pole Assembly

The bottom pole assembly consists of the bottom pole with an auger and collar attached to opposing ends, and the ratchet system. This assembly is detailed in **Figure 5.1.6**.

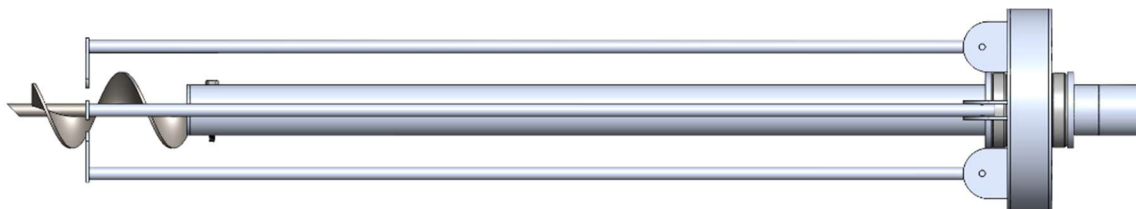


Figure 5.1.6: Assembly of the bottom pole.

The ratchet assembly comprises the ratchet system enclosed within the extruding collar, along with the holding plates and thrust bearings. Positioned atop the thrust bearings, the extruding collar is free to rotate. The pawls are affixed to the top plate of the collar, as depicted in **Figure 5.1.7**. The gear is welded to the bottom pole, resulting in the entire pole rotating when the ratchet system is engaged. To prevent translational movement along the shaft, the housing collar is securely held in place by fixed ring plates on each end.

In examining the ratchet assembly, particular attention will be directed toward the internals within the collar to illustrate the arrangement of the pawl, ratchet, and springs. The detailed depiction of this focused assembly is presented in **Figure 5.1.7**.

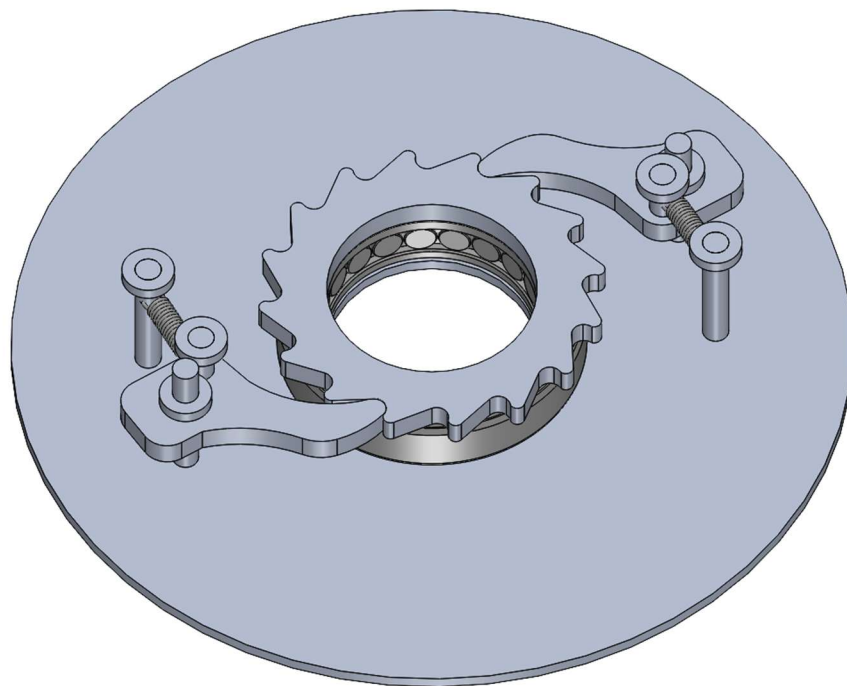


Figure 5.1.7: Internal assembly of the ratchet and pawls.

From **Figure 5.1.7**, the arrangement of how the pawls make contact with the ratchet gear is evident, connecting in an offset manner to the center of the assembly. The pawls are affixed to an aluminum shaft, and another aluminum shaft passes through the opposite side of the part of the pawl that interfaces with the ratchet. This shaft, attached to the pawl, secures one side of the spring, while the other side is connected to a different shaft located at a distance from the pawl, ensuring tension. This design allows the pawls to swiftly snap back into place as they rotate counterclockwise around the fixed gear. Small aluminum rings secure the springs and pawls in place, with the bottom ring on the pawl, when correctly oriented from top-down, supporting the weight of the pawl to ensure a flush connection with the gear. The top ring on the pawl is attached with a small gap, approximately 1/8 of an inch, to minimize friction while preventing the pawl from slipping upward and getting jammed above the teeth of the ratchet gear.

The ratchet gear is intended to be welded to the bottom pole, with a thrust bearing affixed to the top of the gear and the bottom of the top plate to facilitate the rotation of the pawls around the gear. In the completed configuration of the ratchet assembly, as depicted in **Figure 5.1.6**, the supporting poles connected to the bottom plate of the ratchet enclosure assembly serve as handles to rotate the collar and the attached components.

In conjunction with the ratchet assembly, the bottom pole incorporates additional attachments, namely the auger and its associated hardware, as well as the collar. The segment of the assembly featuring the auger is depicted in **Figure 5.1.8**. It is important to note that the auger is designed to be driven into the ground in a clockwise direction.

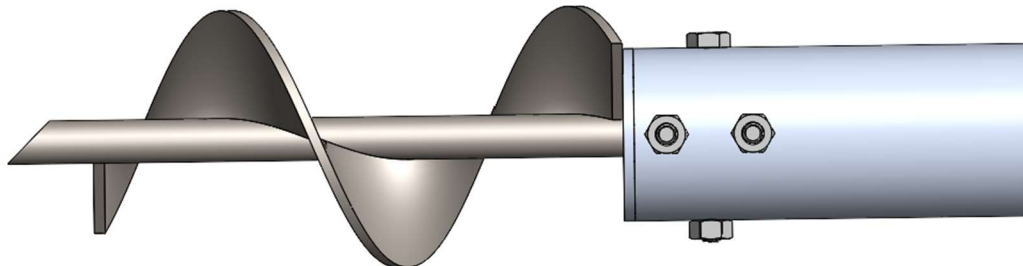


Figure 5.1.8: Auger attached to the bottom pole with necessary hardware.

The steel auger is precisely centered using an external plate affixed to the bottom pole, featuring a center hole to enable the passage of the auger shaft. To ensure stability, three bolts are strategically positioned through the auger shaft, with two arranged horizontally and one vertically, as illustrated in **Figure 5.1.8**. This bolt configuration is selected to minimize auger wobble under load, as the cross pattern eliminates side-to-side motion in one direction. The choice of bolts, as opposed to permanent mounting methods, is deliberate, considering the potential encounter with larger lunar rocks or bedrock near the lunar surface, which could damage the blades and reduce the auger's effectiveness. Opting for bolts allows for easy replacement of the auger, minimizing waste and weight associated with replacing the entire assembly.

5.1.4 Lunar Flagpole Full Assembly

The combination of all three subassemblies results in the full assembly depicted in **Figure 5.1.9** when fully extended as if it were planted on the lunar surface, and **Figure 5.1.10** when in its collapsed configuration.

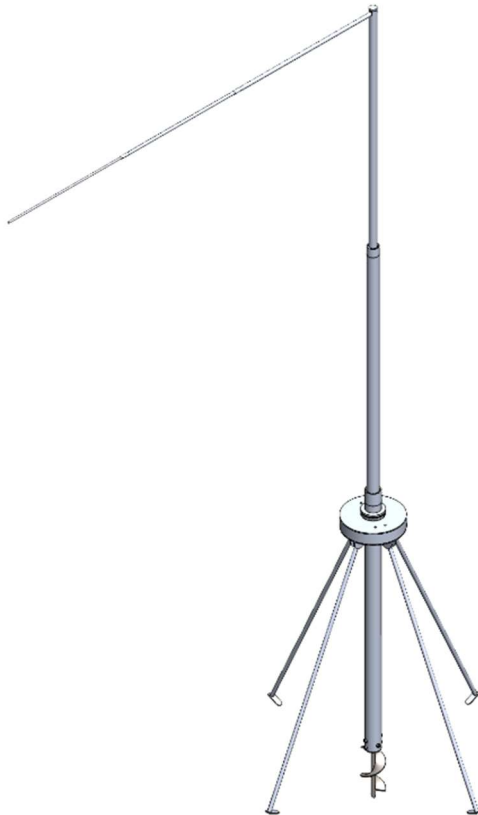


Figure 5.1.9: Full flagpole assembly in extended configuration.



Figure 5.1.10: Full flagpole assembly in its collapsed configuration.

In its contracted configuration, the assembly measures 47.5 inches in height, comfortably within the 48-inch maximum height, and 8 inches in width, fitting well within the 48x12x8 inch size constraint. When fully extended, the assembly reaches a height of 9 ft from the base above the auger to the top of the cap. Remarkably, the overall weight is 9.928 lb, staying under the specified maximum weight limit of 10 lb.

5.2 Manufacturing

This section covers the processes used to create the prototype.

5.2.1 Part Simplifications

Prototype sizing was based primarily on availability of parts and may not reflect the most optimal design. The sizes chosen for the poles used in the main telescoping section as well as the parts are outlined in **Table 5.2.1**.

Table 5.2.1 Prototype Poles and Support Sizes

	Outer Diameter [in]	Wall Thickness [in]	Length [ft]
Pipe 1	1	0.065	3
Pipe 2	1.5	0.065	3
Pipe 3	2	0.065	3
Supports (x4)	0.5	0.035	3

To expedite the manufacturing process, a premanufactured auger was acquired. The selected auger features one and a half threads with a thread width of 1.25 inches. Both the auger and the bottom pole underwent modifications, involving the drilling of a set of perpendicular holes through each component. Nuts and bolts were employed to securely attach the auger to the base pole. Additionally, a small plate was affixed to the base of the bottom pole to contain its internal components and prevent the rotation of the auger relative to the bottom pole.

As a result of ordering springs from an online provider and utilizing 0.25-inch diameter shafts for the end of the spring links, the only springs available from the chosen manufacturer were one inch in length under no load and had larger spring constants. The decision was made to select the spring with the 12.7 lb/in spring constant. The rationale behind this choice was the perceived benefit of a quicker contraction, particularly advantageous if lunar regolith enters the internal components, potentially inducing additional friction between the pawl and holding ring.

The extending pole, to which the flag attaches, was also ordered pre-made. The initial design specified a three-piece extending aluminum pole utilizing a pinch fit at the ends to ensure a snug fit for each sliding rod. However, due to limited experience in manufacturing such a part, a 5 ft extending pole made up of 7 sections was utilized. While 5 ft falls short of the required length, approximately 1.5 inches are occupied by its placement within the pole when extended. This simplification facilitated the completion of the prototype within the desired timeframe.



The primary approach for securing the extending poles together involved using solid aluminum male and female collars. However, due to the intricate machining processes needed for manufacturing these parts and considering the materials available, it was decided that FDM 3D printing the collars using tough PLA was the optimal choice to complete the prototype. The distinction between tough PLA and regular PLA adhered to the specifications outlined in the design requirements.

The initial plan was to waterjet the stakes and have them slide onto the support poles through cutouts, facilitating welding them together. However, to streamline the process and align with the design specifications, this approach was simplified to using prepackaged stakes, which were rounded off to eliminate sharp edges.



5.2.2 Part Manufacturing Methods

For the in-house manufacturing of components, three primary processes were employed: milling, turning on the lathe, and water jet cutting.

Flat pieces, including the pawls, ratchet gear, and plate components, were precision-cut from aluminum sheets with a specified thickness using a water jet. This method ensures clean and accurate cuts at a reasonable market cost, typically ranging from \$12 to \$30 per hour. Given the scale of the lunar flagpole's parts, less than 2 hours would be needed to cut all the pieces, assuming no simplifications were made to any part.

For the Top Cap in **Figure 5.2.1**, both the mill and lathe were utilized to achieve the required shape, including the center cutout, slots in the extended material, and the O-ring groove. The mill played a crucial role in all other applications that demanded precise placement of holes or slots.

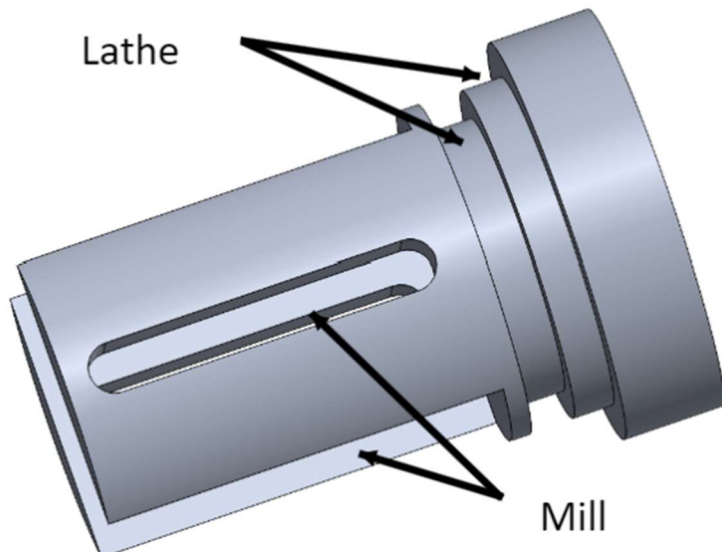


Figure 5.2.1: Top Cap with machining technique callouts.

5.2.3 Assembly Simplifications

Welding aluminum posed a significant challenge during the prototype assembly, as precise welds were crucial for the success of the lunar flagpole.

Limited welding experience led to the application of epoxy, specifically JB-Weld Metal, on various surfaces. Epoxy was strategically used on the inner radius face of the ratchet gear and the bottom. Holding rings were also epoxied to the largest pole, preventing potential issues such as heat warping and uneven welds that could affect smooth rotation, possibly leading to imbalance.

Epoxy was employed on the auger holding plate for simplicity and to prevent heat warping that might misalign holes. Support stakes were attached to the support poles using epoxy as well.

Addressing potential weaknesses in the prototype assembly, the aluminum dowels holding the pawls, springs, and locking ring were identified. To eliminate potential warping issues from improper welds, $\frac{1}{4}$ -20 bolts replaced the 0.25-inch diameter dowels. Pawls and springs were secured with bolts and washers. Smaller dowels holding the spring to the pawl were substituted with an 8/32-28 bolt. Short dowels, also serving to attach the support poles to the flanges, were replaced with $\frac{1}{4}$ -20 bolts, each secured with nuts and washers.



5.3 Results and Observations

This section displays the final prototype, lessons learned, and future work.

5.3.1 Prototype Results

The finalized prototype, in its collapsed configuration, is depicted **Figure 5.3.1**, showcasing the assembly simplifications. **Figure 5.3.2** displays the prototype securely anchored in the ground in its fully extended configuration.



Figure 5.3.1: Final prototype in collapsed configuration.



Figure 5.3.2: Final prototype in extended configuration.

A close up of the auger is shown in **Figure 5.3.3**, where the pattern of the bolts can be better seen.



Figure 5.3.3: Auger attached to bottom pole in the final prototype.

In **Figure 5.3.4**, the ratchet assembly is encapsulated within the collar, featuring the thrust bearings and holding rings that maintain its position. Additionally, it highlights the secure attachment of the support flanges to the bottom plate of the collar assembly.

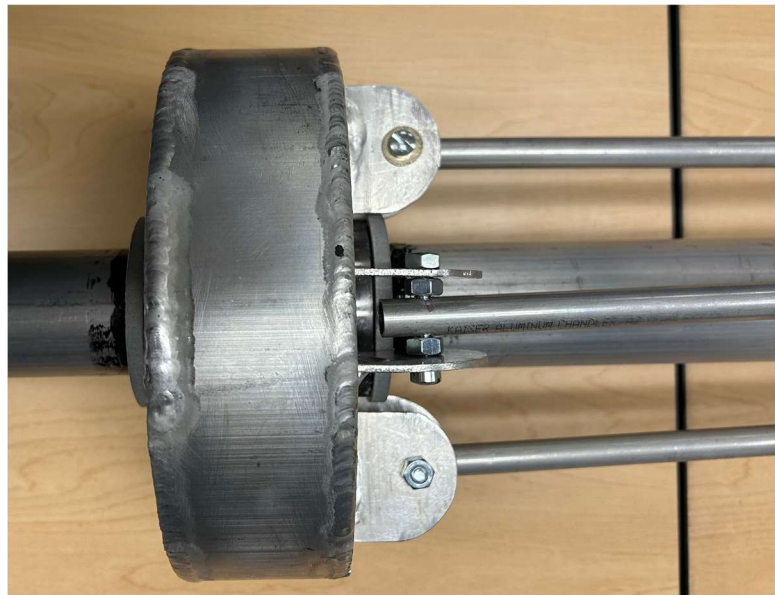


Figure 5.3.4: Close up of the ratchet assembly in the final prototype.

Figure 5.3.5 showcases a pivotal element of the lunar flagpole design: the 3D printed threaded collars. Although the male ends of the collars are not visible in the prototype, they screw in counterclockwise to secure the poles together in the assembly.



Figure 5.3.5: Female collar around the middle pole.

The prototype of the Top Cap is pictured in **Figure 5.3.6** and matches the desired dimensions. The black O-ring can be seen and is stretched to fit around the part.



Figure 5.3.6: Prototype Top Cap.

5.3.2 Observations and Refinements

Despite the prototype successfully meeting all the criteria for the design competition, adaptations and continuing research are necessary to enhance the functionality of the design for a revised version to remain competitive.

While analyzing the structure, it is advisable to explore the possibility of altering the material primarily used in the construction. Instead of the current utilization of aluminum, composite materials like carbon fiber or a combination of carbon fiber and aluminum mesh should be evaluated. This aims to reduce the weight of the structure, facilitating a quicker and more seamless assembly for astronauts during deployment.

The vulnerability of the cap that the telescoping pole is attached to has been identified as a weakness. The partially exposed O-ring is susceptible to brittleness caused by UV rays, degrading the material. Investigation of an approach that combines the current cap method with the one depicted in **Figure 3.1.11** may offer a more robust yet simpler method for deploying the telescoping pole.

The primary source of refinement is focused on the ratchet and pawl assembly, as well as the enclosing collar assembly. The collar assembly, with an outer diameter of 8 inches, contrasts with the 2-inch outer diameter of the bottom pole, resulting in an unappealing aesthetic. To address this issue, downsizing the pawls and adjusting their geometry can enhance the overall appearance as the collar and plates can be shrunk. Another aspect for improvement is how the supports attach to the collar. The existing design features four 3 ft poles hanging off the main assembly, with two used for turning the ratchet and the other two dragging across the ground. This configuration proves challenging on uneven surfaces and surfaces requiring greater ground pressure.

A proposed change involves transforming the support poles into telescoping poles, eliminating their role in driving the auger into the ground. With this modification, holdable handles fixed to either the top or the side of the collar would facilitate easier ratcheting. This adjustment not only streamlines the operation, but also enables the user to apply increased ground pressure for initial auger penetration into the ground.

The final alteration would be the addition of a mechanism that locks the collar and ratchet gear together to allow the handles to be used to back the auger out of the ground for easy removal or in the case that the auger is driven in crooked.



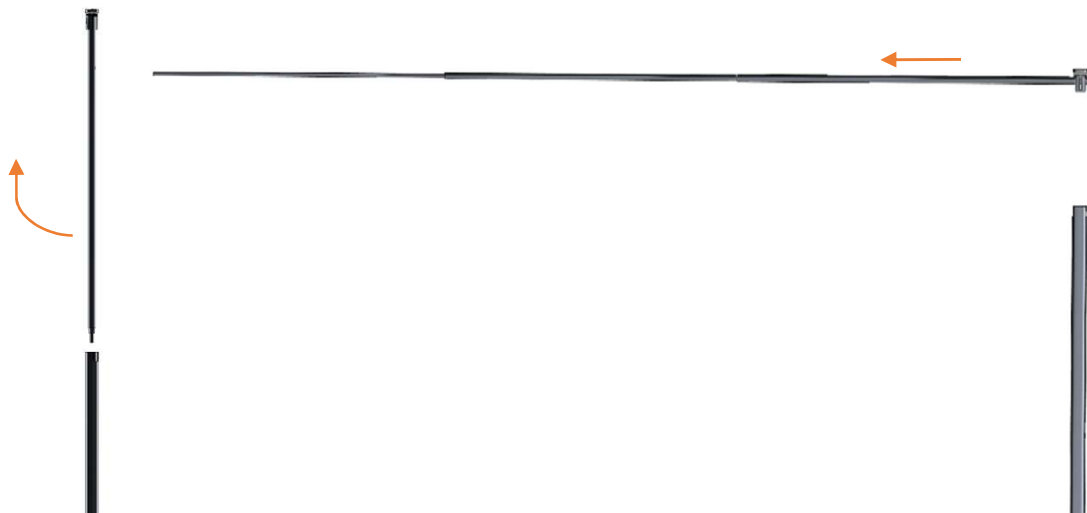
5.4 Operation Procedure

When not in use or if in transport, the design should be collapsed into the stowed configuration shown in **Figure 5.1.10** in steps opposite to those portrayed below. To deploy the design, the following instructions should be followed.

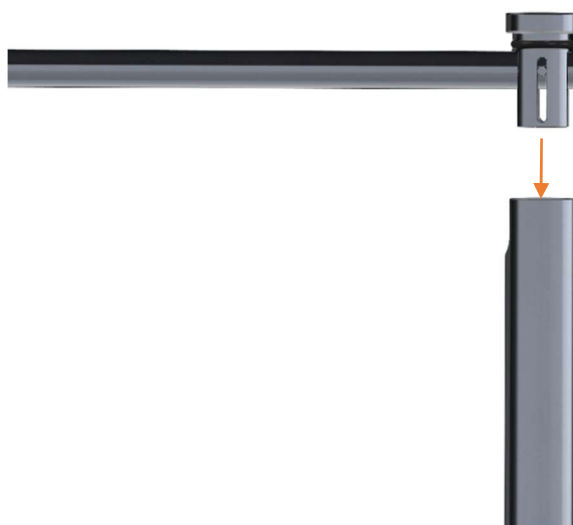
1. Place the design perpendicular to the ground with the auger making contact with the surface.
2. Manually turn the assembly to wedge the auger into the ground.
3. Engage the ratchet assembly by using the support poles to turn the housing clockwise and continue until the auger is firmly in the ground.
 - o If necessary, place one hand on the collar and the other on a support pole to generate more ground pressure when ratcheting.
4. Extend the support bars and hammer the stakes into the ground.
5. Lift the top pole out and turn it counterclockwise to lock it into the threads in the center pole.



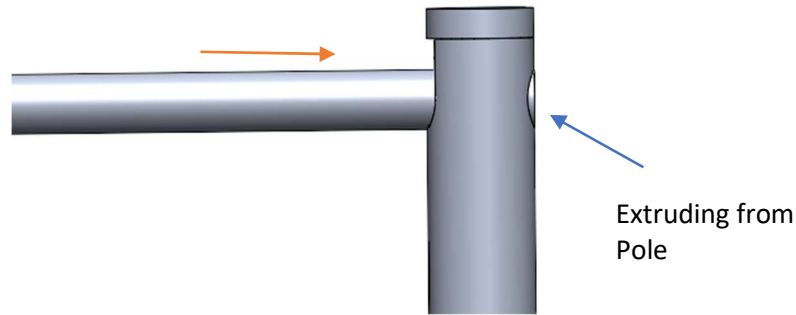
6. Take the cap out of the top pole and extend the small telescoping pole.



7. Slip the flag onto the telescoping pole.
8. Reinstall the cap to the top pole with the telescoping pole horizontal to the ground.



9. Push the telescoping pole back so the end of the shaft fits into the hole cutout on the backside of the top pole.



10. Lift the center pole out and turn it counterclockwise to thread it into the bottom pole.



6 Conclusion

Humans are headed back to the Moon, thanks to the daring and unprecedented Artemis missions. This mission's success relies heavily on new and innovative technologies, practices, and strategies and with this comes the opportunity to improve upon existing infrastructure. One such innovation lies in the design of the flag that is planted upon the Moon after astronauts have successfully landed. Planting and flying a flag signify the completion of a task, symbolizing the pride, strength, sacrifice, and resilience it took to achieve the task. NASA has presented this tremendous design opportunity to undergraduate students through their Micro-G NExT Lunar Flag competition. This competition tasks teams with designing a lunar flag, flagpole, and anchoring system that can be deployed on the lunar surface [4]. The design must be able to withstand 10 lb. forces occurring horizontally and vertically at the top of the flagpole. It must also weigh under 10 lb. and be able to be stowed within a volume of 48 in by 12 in by 8 in for transport on the space shuttle. The goal of this project was to design and develop a dependable, stable, and ergonomically friendly flag for deployment on the lunar surface during the Artemis III missions.

The implemented design features an auger with a ratchet system for initial deployment. Support bars attached to the gear box can then be lowered and hammered into the ground for additional support of the horizontal load. The flagpole consists of three poles in varying sizes that nest within each other for transport. Each pole lifts out and screws into the pole beneath it to lock it in place. The top pole has a cap on the top that connects to an additional smaller telescoping pole. When in transport, this pole remains in a collapsed configuration and fits inside the top pole. During deployment, the cap is lifted out of the top pole and the telescoping pole is extended and slipped into the loops of the flag. Then, with the telescoping pole now horizontal to the ground, the cap can be returned to the top pole and the telescoping pole rests in a cutout. The final product is 9 ft tall and can fly up to a 3 ft by 5 ft flag in the absence of wind. The design is collapsible within a space of 48 in by 8 in by 8 in.

The competition required the design to be able to withstand two 10 lb loads at the top of the flagpole, applied horizontally and vertically. To ensure the design would not fail under these loads, an auger was chosen as a solid base and then additional support poles were configured onto the ratchet housing collar. The additional supports were chosen to resist the moment created by the horizontal 10 lb force as whether or not the auger could withstand the pull-out force on its own was a concern. Multiple analyses were done to verify that this configuration would work. The primary goal was to show that the design could withstand the loads. To do this, thread width and counts for the auger were varied to determine the minimum amounts required to withstand the pull-out force. It was determined that the required values were smaller than anticipated and an auger was able to be chosen freely. An auger of 1.25 in thread width and 1.5 threads were used to ensure that the auger would not fail under the pull-out force. The thickness of the pipes used in the supports were also analyzed to ensure that they wouldn't fail under the given loads. It was determined that for the proposed half inch pipe, any standard thickness would be able to support the loads. Thus, in using these two anchoring systems, the design can withstand the two 10 lb loads.



The size of the design was a large consideration throughout the process. The stowed configuration was required to fit into a volume of 48 in by 12 in by 8 in. In order to accomplish this, the three main poles of the design nest inside each other when collapsed and the supports fold in. The telescoping pole that holds the flag can also be stowed in the top pole using the cap. The prototype ended up fitting within a 48 in by 8 in by 8 in volume, which is smaller than the required amount. This could be reduced further by reducing the housing collar size. The deployed configuration was required to be within 8 to 10 ft tall and hold a 3 ft x 5 ft flag. The prototype ended up being 9 ft tall with a 5 ft telescoping pole to hold the flag up.

Weight is a large consideration on space flights and reducing it wherever possible is important. The design was required to be a maximum of 10 lb in Earth's gravity. Because of this, Aluminum alloys were primarily used in the design. The auger, however, was made of steel as that was what was available. The material of the auger could be changed to something lighter in the future to reduce weight further. The prototype weighed just under 10 lb, which meets competition requirements; however, exploring other materials for the design would be beneficial. Composite materials could reduce the weight of the structure while maintaining its strength. Although the design fits within the required 10 lb, reducing this could be beneficial for the mission as a whole.

On the moon, the terrain is very sandy, and dust is a large concern for assemblies used there. Dust can get into small places and affect the operation of machinery. Because of this, NASA required the design to be fully dust tolerant. In order to accomplish this, the housing collar and plates were welded shut to prevent dust from entering the ratchet system. Dust does not pose a risk to any other aspect of the design as they can operate as they are.

As astronauts need to complete important research tasks, they should not be spending a lot of time deploying the flag. Because of this, NASA outlined a 10-minute deployment timeframe using strictly manual power. The prototype was tested to ensure this however the support bars did get in the way of ratcheting the system at times. It was found that it was best to enlist two people to rotate the ratcheting system, each holding two support bars, rather than the intended one person. While the competition doesn't explicitly say that the design must be able to be deployed by one person, this is considered a design flaw, and it would be beneficial to reapproach this aspect of the design in the future. Ideally, the flag should be able to be deployed with one person.

The physical design was also analyzed for potential modifications. The proposed modification for the support poles is to have them telescope out, similar to the pole that holds the flag. This would ensure that they are out of the way during deployment but can then be extended to add additional support. This would require additional analysis to ensure that they could still withstand the loads. It was also proposed to remove their role in the ratchet system entirely. They would remain attached to the bottom plate of the housing collar however the ratchet system would be rotated using handles fixed to either the top or side of the housing collar. This would simplify the deployment process and potentially make it easier for a single astronaut to deploy the design.



Further modifications can be done to fine tune the design. While building the prototype, it was also obvious that the housing collar in the design was much larger than necessary and has a harsh contrast with the 2-inch outer diameter of the bottom pole. In the future, the geometry of the pawls can be adjusted to decrease the size of the housing collar and plates. This would make the design more visually appealing. The cap also poses as a weakness as the partially exposed O-ring is susceptible to brittleness caused by UV rays. Combining the current cap design with the bracket method from the preliminary concepts may prove to be a simpler and more robust design. The addition of a mechanism that locks the collar and ratchet gear together was also proposed. This would provide easier removal of the auger and would be beneficial in cases of misalignment during ground penetration.

Throughout this design process, feedback and collaboration were very important in creating a design that successfully met design specifications. It was crucial to meet with more knowledgeable people to discuss design specifics. Meeting with these people, especially to discuss manufacturing feasibility, ideally should have been done earlier. While building the prototype, it was discovered that some parts of the design, like the threaded collars, are not easily manufactured by hand. The threaded collars were 3D printed using tough PLA for the prototype, which meets material requirements, however they were originally designed to be aluminum. To achieve this, these parts would need to be cold formed or sand cast instead. The design process also required real life application of various mechanics of materials equations to fully analyze the design. This led to an extensive amount of research in textbooks and continued learning to ensure the flagpole would operate as intended.



7 References

- [1] Space Foundation Editorial Team, "The Space Report 2022 Q2," Space Foundation, 27 July 2022. [Online]. Available: <https://www.spacefoundation.org/2022/07/27/the-space-report-2022-q2/>. [Accessed 28 September 2023].
- [2] R. D. Launius, "Monographs In Aerospace History Number 9," August 1998. [Online]. Available: <https://history.nasa.gov/SP-4225/documentation/hsf-record/hsf.htm#apollo>. [Accessed 28 September 2023].
- [3] National Aeronautics and Space Administration, "About: NASA Artemis," 18 April 2023. [Online]. Available: <https://www.nasa.gov/specials/artemis>.
- [4] "2024 Micro-g NExT Challenges," NASA, 8 2023. [Online]. Available: https://microgravityuniversity.jsc.nasa.gov/docs/micro-g/FY24%20Micro-g%20NExT%20All%20Challenges_Updated%2009182023_merged.pdf.
- [5] A. M. Platoff, "Where No Flag Has Gone Before;" NASA Johnson Space Center, 1993. [Online]. Available: <https://historycollection.jsc.nasa.gov/JSCHistoryPortal/history/flag/flag.htm>.
- [6] "Flag Pole, Apollo," Smithsonian, [Online]. Available: https://airandspace.si.edu/collection-objects/flag-pole-apollo/nasm_A19770570000#:~:text=The%20Apollo%20flag%20pole%20was%20specifically%20designed%20enable.
- [7] S. L. Johnson, "Red, White, & Blue: U.S. Flag at Home on the Moon," Houston Histoy Magazine, 2008. [Online]. Available: <https://houstonhistorymagazine.org/wp-content/uploads/2014/03/red-white-and-blue-US-flag.pdf>.
- [8] J. Fincannon, "Six Flags on the Moon: What is there Current Condition?," Eric M. Jones, [Online]. Available: <https://history.nasa.gov/alsj/ApolloFlags-Condition.html>.
- [9] "China becomes second nation to plant flag on the moon," BBC News Services, 4 12 2020. [Online]. Available: <https://www.bbc.com/news/world-asia-china-55192692>.
- [10] S. T. a. B. University, "Foldable portable flagpole". China Patent CN210422107U, 28 4 2020.
- [11] American Institute of Aeronautics and Astronautics, "Aerospace Research Central," 2023. [Online]. Available: https://arc.aiaa.org/action/showPublications?pubType=standards&_ga=2.96609434.428746957.1695940828-111044456.1678218747&_gl=1*ydnup6*_ga*MTExMDQ0NDQ1Ni4xNjc4MjE4NzQ3*_ga_BFMKMMY72*MTY5NTk0MDgyOC4xMi4wLjE2OTU5NDA4MjguNjAuMC4w. [Accessed September 2023].
- [12] "Additional Requirements for Student Projects," NASA Micro-G Next, [Online]. Available: <https://www.nasa.gov/wp-content/uploads/2023/08/fy24-micro-g-next-nbl-engineering-and-safety>



requirements.pdf#:~:text=Acceptable%20Materials%20for%20use%20in%20the%20NBL%20Allo
wable,foam%2C%20or%20adhesives%20are%20shown%20in%20Appendix%20A..

- [13] R. M. J. N. aoul Caimi, "ROCKET LAUNCH-INDUCED VIBRATION AND IGNITION OVERPRESSURE RESPONSE," NASA, Merritt Island, 2001.
- [14] P. L., "4 USC Ch. 1: THE FLAG," in *FLAG AND SEAL, SEAT OF GOVERNMENT, AND THE STATES*, 112 Stat. 1498, 1998, pp. 105-225.
- [15] Grainger, "General Purpose Aluminum Tubing," Grainger, 2023. [Online]. Available: <https://www.grainger.com/search/pipe-hose-tube-fittings/tube-tube-fittings/tubing/metal-tubing/lightweight-aluminum-tubing?attrs=Tubing+Material%7C6061+Aluminum&filters=attrs>.
- [16] MatWeb, "Aluminum 6061-T6; 6061-T651," MatWeb, 1999. [Online]. Available: <https://matweb.com/search/DataSheet.aspx?MatGUID=b8d536e0b9b54bd7b69e4124d8f1d20a&ckck=1>.
- [17] V. A. L. Marko V. Lubarda, Intermediate Solid Mechanics, Cambridge: Cambridge University Press, 2020.
- [18] E. A. Avallone and T. Baumeister III, Marks' Standard Handbook for Mechanical Engineers, 10th ed, New York: McGraw-Hill, 1916.
- [19] V. K. Srinivasula Reddy, "Dry sliding friction and wear of Al 6061 and Al 6082 alloys under different normal loads," *Materials Today: Proceedings*, vol. 27, pp. 2631-2634, 2020.
- [20] A. D. Deutchman, W. J. Michels and C. E. Wilson, Machine Design: Theory and Practice, New York: Macmillan Publishing Co., Inc., 1975.
- [21] Engineers Edge, LLC, "Self Tapping Screws Installation Design," Engineers Edge, 2023. [Online]. Available: https://www.engineersedge.com/hardware/self_tapping_screws_installation_design_9998.htm. [Accessed 26 October 2023].
- [22] S. W. Johnson and K. Meng Chua, "Properties and Mechanics of the Lunar Regolith," in *Applied Mechanics of a Lunar Base*, Albuquerque, 1993 American Society of Mechanical Engineers, 1993, pp. 285-300.
- [23] W. C. Young and B. R. G, "13.7 Pipe on Supports at Intervals," in *Roark's Formulas for Stress and Strain*, New York, McGraw-Hill, 2002, p. 590.
- [24] D. Hageman, "PUMPS & SYSTEMS," 30 May 2013. [Online]. Available: <https://www.pumpsandsystems.com/improved-torque-tension>. [Accessed 12 12 2023].
- [25] E. Oberg, F. D. Jones, H. L. Horton and H. H. Ryffell, Machinery's Handbood 26th ed, New York: Industrial Press Inc., 2000.
- [26] E. Edge, "Coefficient of Friction Equation and Table Chart," 2023. [Online]. Available: https://www.engineersedge.com/coeffients_of_friction.htm#google_vignette.



- [27] J. Fincannon, "Six Flags on the Moon: What is there Current Condition?," Eric M. Jones, [Online]. Available: <https://history.nasa.gov/alsj/ApolloFlags-Condition.html>.



8 Appendix A – Product Design Specifications

EMA 469

Product Design Specifications

Product: **Artemis Mission Lunar Flagpole**

Date: **9/14/2023**

Revision: **3**

Group Members: **Brian Jerominski, Emmett Peters, Chase Orvis, Olivia Janson, Kaden Reybrock**

Specification Element	Team Design	Competition
Performance	<p>Withstanding 10 lb axial pole force, prevent from yielding or buckling.</p> <p>Withstanding 10 lb horizontal force from top of flag pole tip prevents from yielding or buckling.</p> <p>Material Properties to prevent structural failure</p> <ul style="list-style-type: none"> -Stress/Strain -Buckling -Impact -Vibrations -Safety factor 1.25 <p>For any mechanism used</p> <ul style="list-style-type: none"> -less or equal to 20 lbf for linear actuating mechanism -less or equal to 30 in-lb for rotational mechanism <p>Must go from stowed to assembled in 10 minutes. Only deployed once.</p> <p>Flag must remain unfurled in absence of wind</p>	<p>US Apollo Missions: Assembled in 10 minutes</p> <p>Withstood forces applied on the moon</p> <p>Fell over after takeoff due to engine blast on Apollo 11 mission</p> <p>Crews had trouble extending the telescoping poles</p> <p>Lower portion of the pole could only be driven 6 to 9 inches in the ground</p> <p>China's lunar mission: Flag fabric can maintain color within +/- 270F</p> <p>Deployed from lander's body not planted in dirt</p>
Environment	<ul style="list-style-type: none"> -Temperature swings from sunlight to in the dark on moon, -298F to 260F -Moon dust erosion -Dust tolerant -Testing pool, 86F, 40 ft deep -Radiation from space/sun -Sterilization for spacecraft -Outgassing in space -Vibration from rocket launch 	<p>US: Mounted outside of Lunar Module which experienced temperatures of up to 2,000 F. 180 F was experienced by the flag inside the protective casing.</p> <p>Moon specs:</p> <ul style="list-style-type: none"> - Temperature: -298F to 260F - Gravity: 1.2 m/s^2 - Surface pressure: 3x10^-15 bar
Maintenance	Remain vertical for long periods of time. Only deployed once.	Regular maintenance was not a consideration on Apollo missions
Size	Collapsed assembly must fit within a volume of 48 in. x 12 in. x 8 in.	US: 3 ft x 5 ft flag, 7 ft tall China: 2 m wide, 90 cm tall



	Flagpole must be between 96 and 120 inches in height when fully deployed Flag size must be 3 ft x 5 ft	
Weight	Weight max is 10 lb on Earth	US: 9 lb 7 oz China: 2.2 lb
Materials	Must use NBL approved materials Must be compatible for use underwater for testing No regular PLA, tough PLA okay. As specified by NASA.	US: Gold anodized aluminum tubing, 1 inch diameter, 1/32 inch thick Hardened steel point
Product Life Span	Looking for the flag to fly for as long as possible. Fatigue analyses will be done to determine how long the flag/pole will last.	All but one of the flags from the Apollo missions are still standing as of 2012, 41-43 years later, however the flags are all bleached white by sun.
Standards and Specifications	<u>Tentative standards</u> NASA-STD-6001 -> Flammability, Off gassing, and Compatibility requirements and test procedures NASA-STD-1008 -> Testing against dust NASA-STD-5006 -> General welding requirements for aerospace materials NASA-STD-5017 -> Design and development requirements for mechanisms NASA-HDBK-7009 -> NASA handbook for models and simulations NASA-STD-7001 -> Payload vibracoustic test criteria NASA-STD-7002 -> Payload test criteria NASA-STD-7009 -> Standard for models and simulations AIAA S-110-2005 -> Standard for the design, analysis, material selection and characterization, fabrication, test, and inspection of structural items in space systems	All competitors must reach or surpass the tentative standards.
Ergonomics and Human Factors	Flagpole must be able to be EVA compatible All parts must be able to be used by EVA gloved hands, no sharp edges Deploying the flagpole must use only manual power No holes/openings that allow entrapment of fingers	US: Had to be assembled within astronauts' reach constraints due to spacesuit (28"-60") Amount of force astronauts could apply was limited, spacesuits pressurized to 3.7 psi



Customer / Market	NASA is the only true customer. Focus is on a working prototype that could be replicated for other lunar missions. It isn't necessary for this product to have mass production capabilities. It is highly important that the flag remain visible at all times.	NASA contracted it for use
Testing	Tests are done at the bottom of a 40 ft deep NBL pool at 86F in a barrel of sand 3 ft in diameter and 3 ft deep Can use an EVA hammer to deploy if desired	Meet NASA specifications Other submissions are unavailable to opposing parties. (Especially in the given time frame)
Safety, Public Health, and Human Welfare	Cannot have sharp pieces that can puncture astronaut's spacesuit No holes or openings that can trap fingers Sterilization of the material in order to keep organic matter from Earth from touching the lunar surface	Meet NASA specifications listed in tentative standards and specifications section Other submissions are unavailable to opposing parties. (Especially in the given time frame)
Economic, Cultural, Social Factors	Storage and presentation of flag must comply with United States Flag Code. Flag cannot touch ground during deployment or once deployed Flag and its appearance is a direct representation of NASA and the United States as a whole, meaning the success of this mission could greatly impact the future of NASA and space exploration as a whole.	Symbolic gesture of national pride There were no formal complaints from other nations after planting flags on the moon.
Environmental Impact	Must not degrade while on the moon Must be able to be sterilized/resist harsh chemicals As the material has not yet been chosen for this project, there may be an environmental impact from the acquisition of the raw material used to create the flag pole.	Product is not intended to be removed from the moon, even after its end of life



9 Appendix B – Pole Analysis

```
% November 2023
% EMA 469 Badger Engineers - Lunar Flagpole
% Group Members: Emmett Peters, Chase Orvis, Brian Jerominski, Kaden Reybrock, Olivia
Janson
% Code by Emmett Peters

% This code analyzes the loads applied to the pole section of the assembly

clear all;

% Material Properties

% Aluminum 2024-0
%
https://www.matweb.com/search/datasheet.aspx?matguid=642e240585794f0ab91428aa78c27b4e
% E = 10600e3; % modulus of elasticity [psi]
% G = 4060e3; % shear modulus [psi]
% v = 0.33; % Poisson's ratio
% rho = 0.100; % density [lb/in3]
% sigma_Y = 11000; % yield strength [psi]
% tau_max = 18000; % shear strength [psi]

% Grainger 3003 Aluminum Tubing
%
https://www.matweb.com/search/datasheet\_print.aspx?matguid=91c99440833341fc8fbe1d26149bc35e
% E = 10000e3; % modulus of elasticity [psi]
% G = 3630e3; % shear modulus [psi]
% v = 0.33; % Poisson's ratio
% rho = 0.0986; % density [lb/in3]
% sigma_Y = 27000; % yield strength [psi]
% tau_max = 16000; % shear strength [psi]

% Grainger 6061 Aluminum Tubing
%
https://matweb.com/search/DataSheet.aspx?MatGUID=b8d536e0b9b54bd7b69e4124d8f1d20a&ckck=1
E = 10000e3; % modulus of elasticity [psi]
G = 3770e3; % shear modulus [psi]
v = 0.33; % Poisson's ratio
rho = 0.0975; % density [lb/in3]
sigma_Y = 40000; % yield strength [psi]
tau_max = 30000; % shear strength [psi]

% Pipe sizing
L = 12.*[3 3 3]; % pole section length [in]
t = 0.065; % wall thickness [in]
n = 100;
% D = linspace(0.5,2,n); % outer diameters [in]
D = linspace(0.5, 0.907, n);
```



```

% Define Loads
P = 10; % horizontal and vertical static test loads [lbf]
F = 20; % maximum load to install [lbf]
T = 18*15*2; % maximum torque to apply [in-lb]
SF = 1.25; % factor of safety [-]

% Pipe geometry
d = D-2*t; % inner diameter [in]
A = pi/4*(D.^2-d.^2); % cross section area [in^2]
I = pi/64*(D.^4-d.^4); % moment of inertia [in^4]
J = 2.*I; % polar moment of inertia [in^4]

% Test stresses
% Section 1
sigma_test1 = zeros(n,1);
for i = 1:1:n
    sigma_a = P./A(i); % tensile vertical stress
    M = P*L(1); % moment from horizontal force
    sigma_b = M*D(i)./2./I(i); % bending stress
    sigma_test1(i) = sigma_a + sigma_b; % total test stress
end
% Section 2
sigma_test2 = zeros(n,1);
for i = 1:1:n
    sigma_a = P./A(i);
    M = P*(L(1)+L(2));
    sigma_b = M*D(i)./2./I(i);
    sigma_test2(i) = sigma_a + sigma_b;
end
% Section 3
sigma_test3 = zeros(n,1);
for i = 1:1:n
    sigma_a = P./A(i);
    M = P*(L(1)+L(2)+L(3));
    sigma_b = M*D(i)./2./I(i);
    sigma_test3(i) = sigma_a + sigma_b;
end

figure(1)
hold on;
plot(D,sigma_test1,displayname='Section 1')
plot(D,sigma_test2,displayname='Section 2')
plot(D,sigma_test3,displayname='Section 3')
yline(sigma_Y/SF,displayname=['Maximum Stress with SF = ',num2str(SF)])
xlabel('Outer Diameter [in]')
ylabel('\sigma [psi]')
grid on;
xticks([0.75 1 1.25 1.5 1.75 2])
ylim([0 5e4])
legend()
title('Total Test Stress')
hold off;

```



```

% Application Stresses
sigma_A = F/A(end);
Tau_A = T*D(end)/2./J(end);
figure(2)
subplot(2,1,1)
hold on;
yline(sigma_Y/SF, 'b--', DisplayName=['Maximum Normal Stress with SF = '
    , num2str(round(sigma_Y/SF,0)), ' psi'])
yline(sigma_A, 'b', DisplayName=['Application Normal Compression Stress = '
    , num2str(round(sigma_A,0)), ' psi'])
legend()
xticks([])
ylim([0 3.5e4])
subplot(2,1,2)
yline(tau_max/SF, 'r--', DisplayName=['Maximum Shear Stress with SF = '
    , num2str(round(tau_max/SF,0)), ' psi'])
yline(Tau_A, 'r', DisplayName=['Application Shear Stress = ', num2str(round(Tau_A,0)), ' '
    psi])
legend()
xticks([])
ylim([0 3.5e4])
hold off;

% Make D Selections

% Weight of pole
D = [0.561 0.757 0.907]; % optimal D's
% D = [1 1.5 2];
d = D-2*t;
A = pi*t.* (D-t);
W = rho*sum(L.*A);
if W > 15
    disp(['Pole is too heavy! ', num2str(W), ' lbs.'])
else
    disp(['Weight of pole is ', num2str(W), ' lbs.'])
end

% Plot geometry
theta = linspace(0,2*pi,n);
x = cos(theta);
y = sin(theta);
figure(3)
for i = 1:1:
    subplot(2,2,i)
    hold on; grid on; axis square;
    plot(d(i)/2*x,d(i)/2*y,'k', linewidth=1)
    plot(D(i)/2*x,D(i)/2*y,'k', linewidth=1)
    plot(0,0,'b.', 'MarkerSize',10)
    xlim([-1 1])
    ylim([-1 1])
    title(['Outer D = ', num2str(D(i)), ' in'])
    subplot(2,2,4)
    hold on; grid on; axis square;

```



```

plot(d(i)/2*x,d(i)/2*y,'k', linewidth=1)
plot(D(i)/2*x,D(i)/2*y,'k', linewidth=1)
plot(0,0,'b.', 'MarkerSize',10)
xlim([-1 1])
ylim([-1 1])
title('All Pipes')
hold off;
end

% November 2023
% EMA 469 Badger Engineers - Lunar Flagpole
% Group Members: Emmett Peters, Chase Orvis, Brian Jerominski, Kaden Reybrock, Olivia
Janson
% Code by Emmett Peters

% This code aids with analytical solutions for the analysis of the loads applied to
the pole section of the assembly

clear all;

syms E G D t L sigma_Y P F T i

% Define Geometry
d = D - 2*t;
A = pi/4*(D^2-d^2);
A = simplify(A);
I = pi/64*(D^4-d^4);
J = 2*I;

% Test Loads
sigma_a = P/A;
M = P*L;
sigma_b = M*D/2/I;

sigma = sigma_a+sigma_b;
sigma = subs(sigma,[P t L],[10 0.065 3*12*i]);
sigma = vpa(sigma);

failure = sigma == 40000/1.25;

% Solve for maximum outer diameters for each section
failure1 = subs(failure,i,1);
D1 = max(vpasolve(failure1,D))
failure2 = subs(failure,i,2);
D2 = max(vpasolve(failure2,D))
failure3 = subs(failure,i,3);
D3 = max(vpasolve(failure3,D))

% Application loads and stresses
sigma_A = F/A;
sigma_A = subs(sigma_A,[F t D],[20 0.035 2]);
sigma_A = vpa(sigma_A);
sigma_A <= 40000/1.25

```



```
Tau_A = T*D/2/J;
Tau_A = subs(Tau_A,[D T t],[2 540 0.035]);
Tau_A = vpa(Tau_A);
Tau_A <= 30000/1.25

% Weight
syms rho D_i
W = rho*3*L*A;
W = subs(W,[rho L t D],[0.0975 3*12 0.065 D_i]);
```



10 Appendix C – Support Pole, Support Pin, and Collar Analysis

```
% Define Constants
% Aluminum 6061
clearvars;

E = 100000000; %Young's Modulus in psi
v = 0.33; %Poisson's
rho = 0.0975; %Density lb/in^3
mus = 0.5; %Static coefficient of friction
sig_y = 40000; %Axial yield Stress in psi
tau_y = 30000; %Shear yield stress in psi
FS = 1.25;
sig_a = sig_y/FS; %Max allowable normal stress
tau_a = tau_y/FS; %Max allowable shear stress

%Set outer radii and thickness vectors
r = 0:1/2^6:1/2;
t = 0.01:0.0005:0.1;
[r1, t1] = meshgrid(r',t);

%Calculate moments of inertia and area for each tube
I = 0.25*pi*((r1).^4-(r1-t1).^4);
A = pi*((r1).^2-(r1-t1).^2);

%Set the angle of the support and the equivalent forces it experiences
th = acos(2.5/3);
P = 36*sin(th);
L = 36*cos(th);

%% Beam Buckling
%Check the critical axial load and compare it to the actual load
Pcr = (pi^2*E*I)/(0.8*36)^2;
figure(1); plot(r1(1,:), Pcr(1,:),r1(51,:), Pcr(51,:),r1(79,:), Pcr(79,:),r1(111,:), Pcr(111,:)),r1(1,:),P*ones(size(r1(1,:))));

xlabel('Outer Radius of Support [in]')
ylabel('Critical Force [lbs]')
ylim([0,100])
leg1 = legend([string([t1(1,1),t1(51,1),t1(79,1),t1(111,1)]), 'Applied Force'], 'location', 'best');
title(leg1,'Thicknesses [in]')

%% Maximum Axial Stress
%Check the normal stress caused by the moment and axial force

S_b = P./A+L*3*(r1)./I;

figure(2); semilogy(r1(1,:), S_b(1,:),r1(51,:), S_b(51,:),r1(79,:), S_b(79,:),r1(111,:), S_b(111,:)),r1(1,:),sig_a*ones(size(r1(1,:))));

xlabel('Outer Radius of Support [in]')
ylabel('Equivalent Stress [psi]')
```



```

ylim([10^3,10^6])
leg2 = legend([string([t1(1,1),t1(51,1),t1(79,1),t1(111,1)]),"Max Stress"]);
title(leg2,'Thicknesses [in]')

%% Bearing Stress
% Define a range of pin sizes to use
pt = 1/2^6:0.005:1/2; % Variety of pin thicknesses
[pt2,t2]=meshgrid(pt',t);

%Calculate the projected area for each pin and pipe thickness
A_br = 2*pt2.*t2;

%Calculate the bearing stress for each pin and pipe thickness
S_br = P./A_br;

%Plot results
figure(3); semilogy(pt2(1,:), S_br(1,:),pt2(51,:), S_br(51,:),pt2(79,:), ...
S_br(79,:),pt2(111,:), S_br(111,:),r1(1,:),sig_a*ones(size(r1(1,:))));

xlabel('Pin Diameter [in]')
ylabel('Bearing Stress [psi]')
leg3 = legend([string([t1(1,1),t1(51,1),t1(79,1),t1(111,1)]),'Max Stress']);
title(leg3,'Pole Thickness [in]')

%% Pin Shear
tau = (0.5*36)./(0.25*pi.*pt.^2);

%Plot results
figure(4); semilogy(pt, tau,pt,24000*ones(size(pt)));

xlabel('Pin Thickness [in]')
ylabel('Shear Stress [psi]')
legend('Pin Shear Stress','Max Shear Stress')

%% Collar Analysis
c1 = 0.44:0.0005:0.620;
a1 = 0.625;
b1 = 0.435;

del1 = (0.3:1/2^5:1.3)'*0.001;
pc1 = (E*del1)./(2*c1.^3).*((a1.^2-c1.^2).*(c1.^2-b1.^2)./(a1.^2-b1.^2)); %Contact Pressure
Ppo1 = mus*pc1*2*pi.*c1; %Pullout force required per unit length of collar

figure(5); plot(c1,pc1(1,:),c1,pc1(10,:),c1,pc1(20,:),c1,pc1(30,:));
xlabel('Radius of Contact [in]')
ylabel('Contact Pressure [psi]')
leg5 = legend(string([del1(1,1),del1(10,1),del1(20,1),del1(30,1)]));
title(leg5,'Interference [in]')

figure(6); plot(c1,Ppo1(1,:),c1,Ppo1(10,:),c1,Ppo1(20,:),c1,Ppo1(30,:));
xlabel('Radius of Contact [in]')

```



```

ylabel('Pullout Force per unit length [lbs/in]')
leg6 = legend(string([del1(1,1),del1(10,1),del1(20,1),del1(30,1)]));
title(leg6,'Interference [in]')

c2 = 0.69:0.0005:0.87;
a2 = 0.875;
b2 = 0.685;

del2 = (0.4:1/2^5:1.4)'*0.001;
pc2 = (E*del2)./(2*c2.^3).* (a2.^2-c2.^2).*(c2.^2-b2.^2)./(a2.^2-b2.^2); %Contact Pressure
Ppo2 = mus*pc2*2*pi.*c2; %Pullout force required per unit length of collar

figure(7); plot(c2,pc2(1,:)),c2,pc2(10,:)),c2,pc2(20,:)),c2,pc2(30,:));
xlabel('Radius of Contact [in]')
ylabel('Contact Pressure [psi]')
leg7 = legend(string([del2(1,1),del2(10,1),del2(20,1),del2(30,1)]));
title(leg7,'Interference [in]')

figure(8); plot(c2,Ppo2(1,:)),c2,Ppo2(10,:)),c2,Ppo2(20,:)),c2,Ppo2(30,:));
xlabel('Radius of Contact [in]')
ylabel('Pullout Force per unit length [lbs/in]')
leg8 = legend(string([del2(1,1),del2(10,1),del2(20,1),del2(30,1)]));
title(leg8,'Interference [in]')

c3 = 0.88:0.0005:0.995;
a3 = 1;
b3 = 0.875;

del3 = (0.6:1/2^5:1.8)'*0.001;
pc3 = (E*del3)./(2*c3.^3).* (a3.^2-c3.^2).*(c3.^2-b3.^2)./(a3.^2-b3.^2); %Contact Pressure
Ppo3 = mus*pc3*2*pi.*c3; %Pullout force required per unit length of collar

figure(9); plot(c3,pc3(1,:)),c3,pc3(10,:)),c3,pc3(20,:)),c3,pc3(30,:));
xlabel('Radius of Contact [in]')
ylabel('Contact Pressure [psi]')
leg9 = legend(string([del3(1,1),del3(10,1),del3(20,1),del3(30,1)]));
title(leg9,'Interference [in]')

figure(10); plot(c3,Ppo3(1,:)),c3,Ppo3(10,:)),c3,Ppo3(20,:)),c3,Ppo3(30,:));
xlabel('Radius of Contact [in]')
ylabel('Pullout Force per unit length [lbs/in]')
leg10 = legend(string([del3(1,1),del3(10,1),del3(20,1),del3(30,1)]));
title(leg10,'Interference [in]')

```



11 Appendix D – Auger Analysis

% function Auger Analysis

```
clear all; close all; clc
```

```
%% Surveyor Values
```

```
% 0.35 <= c <= 0.7 kPa
```

```
% 35 deg <= phi <= 37 deg
```

```
d_r = [0.0127 0.0254]; % Root diameter [m]
```

```
n_t = [1 1.5 2 2.5 3 3.5 4 4.5 5 5.5 6 6.5 7 7.5 8 8.5 9 9.5 10]; % # of engaged threads [-]
```

```
t = [0.0015875 0.003175 0.0047625 0.00635]; % thickness [m] = [1/16 1/8 3/16 1/4] [in]
```

```
L = 0.3048; % Axial length of thread engagement [m] = 12 [in]
```

```
% w = 0.0889 is the max value; % width of thread (single side only) [m]
```

```
c_min_S = 0.35; % Minimum cohesive component [kPa]
```

```
c_max_S = 0.7; % Maximum cohesive component [kPa]
```

```
rho_reg = 1701; % density of lunar regolith [kg/m^3]
```

```
SF = 1.25; % Safety Factor [-]
```

```
F = 10*SF; % Pullout force [N]
```

```
phi_min_S = 35 * pi / 180; % Minimum soil friction angle [rad]
```

```
phi_max_S = 37 * pi / 180; % Maximum soil friction angle [rad]
```

```
g = 1.62; % Gravitational Acceleration on Moon [m/s^2]
```

```
%w = 0:0.0015875:0.0889;
```

```
count = 0;
```

```
Thickness1 = zeros(1);
```

```
Root_Diameter1 = zeros(1);
```

```
N_threads1 = zeros(1);
```

```
Width_thread1 = zeros(1);
```

```
Thickness2 = zeros(1);
```

```
Root_Diameter2 = zeros(1);
```

```
N_threads2 = zeros(1);
```

```
Width_thread2 = zeros(1);
```

```
for i = 1:length(n_t)
```

```
    n=n_t(i);
```

```
    for j = 1:length(d_r)
```

```
        dr = d_r(j);
```

```
        for k = 1:length(t)
```

```
            count = count + 1;
```

```
            th = t(k);
```

```
            func_min = @(w) (c_min_S + (3.*rho_reg.*(((dr./2)+w).^2)
```

```
.*L.*w.*g))./(dr.*n.*th.^2).*tan(phi_min_S).*(pi*(dr+w).*L) - F;
```

```
            w_min = fzero(func_min,0.003);
```

```
            width_min = dr + 2.*w_min;
```



```

if(width_min<0.2032)
    %disp([th,dr,n,w_min])
    Thickness1(count,1) = th;
    Root_Diameter1(count,1) = dr;
    N_threads1(count,1) = n;
    Width_thread1(count,1) = w_min;
end
func_max = @(w) (c_max_S + (3.*rho_reg.*(((dr./2)+w).^2)
.*L.*w))./(dr.*n.*th.^2).*tan(phi_max_S).*((pi*(dr+w).*L) - F);
w_max = fzero(func_max,0.003);
width_max = dr + 2.*w_max;
if(width_max<0.2032)
    %disp([th,dr,n,w_max])
    Thickness2(count,1) = th;
    Root_Diameter2(count,1) = dr;
    N_threads2(count,1) = n;
    Width_thread2(count,1) = w_max;
end
end
end
end

```

```

Summary_Min = table(Thickness1,Root_Diameter1,N_threads1,Width_thread1)
Summary_Max = table(Thickness2,Root_Diameter2,N_threads2,Width_thread2)

```

